EXPERIMENTAL EVIDENCE OF HYPERFILTRATION INDUCED PRECIPITATION OF HEAVY METALS

by

Gina DeRosa

Submitted in partial fulfillment of the requirements for the degree of Master of Science in Hydrology

New Mexico Institute of Mining and Technology
Earth and Environmental Sciences
Socorro, New Mexico

August, 1999

ABSTRACT

It has long been known that clays and shales have membrane properties. A semi-permeable membrane is defined as a material that will permit the passage of some molecules, but not others. When a shale membrane partially rejects solute, a concentration polarization layer (CPL) forms at the higher-pressure membrane face. Non-equilibrium thermodynamic calculations, for conditions of reasonable hydraulic gradient, aquitard hydraulic conductivity, and pollutant heavy metal concentration, suggest that it should be possible for concentrations of heavy metal solute in the CPL to reach supersaturation, resulting in the precipitation of heavy metals. The purpose of this research was to test this concept. Eight hyperfiltration experiments were conducted with undersaturated heavy metal solutions of varying composition. Of these eight, six succeeded in precipitation of heavy metal on the high-pressure face of the membrane. The heavy metals of interest included lead, copper, and cobalt.

In order for solute sieving to occur, there must be a head difference across the shale aquitard. Such head differences can occur as the result of rapid sedimentation of fine-grained materials or lateral tectonic compression. Head differences observed in perched and artesian aquifer systems are sufficient to drive the phenomenon. Additional theoretical calculations indicate that much lower pressure-head gradients that those used in these experiments will drive hyperfiltration in natural systems resulting in the precipitation of heavy metals as described in this study.

The experiments demonstrate that clay-membrane induced precipitation of heavy metals can occur when undersaturated solutions pass through membranes. Mathematical analysis coupled with the findings of this study suggest that hyperfiltration may induce

heavy metal precipitation in the subsurface where contaminated aquifers are bounded by membrane-functioning shales.

TABLE OF CONTENTS

LIST OF FIGURES

LIST OF FIGURES (Concluded)

LIST OF TABLES

LIST OF SYMBOLS

J_v = solution flux through the membrane (cm/s)
L_p = water permeation coefficient (cm^3/dyne·s)
ΔP = pressure difference across the membrane (dyne/cm^2)
σ = reflection coefficient (dimensionless)
$\Delta\pi$ = theoretical osmotic pressure difference across the membrane (dyne/cm^2)
J_s = solute flux through the membrane (moles/cm^2·s)
ω = solute permeation coefficient (mole/dyne·s)
C_s = average solute concentration across the membrane in mole/cm^3
C_o = concentration at the high-pressure membrane face (mole/cm^3)
C_e = effluent concentration (mole/cm^3)
R = gas constant, 8.314×10^{-7} dyne·cm/mole·°K
T = temperature reported in degrees Kelvin
v = stiochiometric coefficient that corrects for the number of particles due to ion formation
L_p = water permeation coefficient
K = the hydraulic conductivity (cm/s)
ρ = the fluid density (g/cm^3)
g is the gravitational constant (cm/s^2), and x is the thickness of the membrane (cm)
C_x = concentration in moles/cm^3 at a distance x cm from the membrane
x_i = distance from the membrane where $C_x = C_I$
D = diffusion coefficient of the solute in the x direction
w = unitless empirical constant determined from laboratory studies
Δx = the membrane thickness (cm)
ζ = the tortuosity of the flow path through the membrane

1.0 Introduction

Fritz and Eady (1985) experimentally demonstrated that membrane-induced solute concentration results in calcite precipitation and postulated that clay membranes play a meaningful role in such processes as calcite cementation at or adjacent to shale/sandstone boundaries. In addition, theoretical, non-equilibrium thermodynamic calculations by Whitworth and Lueth (1994) suggested that membrane-induced precipitation of heavy metals, as a result of hyperfiltration processes, might be important in heavy-metal contaminated zones.

Prior to this study, there has been no experimental verification of membrane-induced precipitation of heavy metals. The objective of this research was to experimentally investigate the hypothesis that membranes may induce precipitation of heavy metals, and provide initial mathematical descriptions of the conditions under which the process might be applied with respect to contaminated aquifers.

1.1 Membrane processes

Noggle (1984) defined a semi-permeable membrane as a material that will permit the passage of some molecules, but not others. A membrane which prevents the passage of all solute would be considered a perfect membrane. Perfect membranes probably do not exist in nature (Fritz, 1986), so a more accurate working definition for a semi-permeable geologic membrane would be any lithology that retards one solution component more effectively than another.

Membranes reject solutes on the basis of size and/or electrical restrictions (Gregor and Gregor, 1978). Smectite clays, the type of clay used in these experiments, carry a net

negative surface charge. This negative charge is caused by broken bonds at the mineral surface and by substitution of low-valence cations within the mineral lattice (Grim, 1968). When smectite is exposed to an electrolytic solution, the negatively charged mineral surface attracts cations, forming an outer layer of predominately positive charges. The density of cations decreases away from the mineral surface, until at some distance the charge density is the same as the ambient solution. The resultant positive-negative layer nearest the membrane surface is termed a double layer. When clays are compacted, these double layers overlap, resulting in increased impedance of both positively and negatively charged species as they attempt to pass through the membrane. Anions are repelled from entering the clay pores by the overall negative charge in the pore. To maintain electoneutrality, the associated cation must move with the repelled anion, thus positively charged cations are also repelled. Uncharged ion pairs or non-electrolytes are not influenced by the electrical restrictions within the membrane. Separation of these uncharged solutes is attained because the non-electrolyte species enter and traverse the membrane more slowly than the aqueous solvent.

Membrane processes include both osmosis and reverse osmosis (hyperfiltration). The occurrence of osmosis in any particular system depends on the existence of a semi-permeable membrane. If a membrane separates solutions of differing concentration (activity), the species of interest will diffuse through the membrane from the high concentration side to the side where the concentration is lower. Because the water concentration is lower where the solute concentration is greatest, water will diffuse through the membrane into the higher solute concentration. Transport will cease when the solution activities on either side of the membrane are equal.

Reverse osmosis, or hyperfiltration, occurs when a pressure differential in excess of the osmotic pressure is applied across the membrane. When applied to the high solute concentration side of the membrane, this pressure has the effect of reversing the direction of water flow through the membrane such that now both solute and water flow in the same direction. In the subsurface, hyperfiltration can be described by two end-member scenarios. In the one dimensional flow scenario, all of the flux is constrained to pass through the membrane (Figure 1). A theoretical description of this situation begins with identical solute concentrations on either side of the membrane at time $t = 0$, and C_i is the concentration of the input solution (Figure 1A). Because water passes more easily through the membrane than the solute (water is electrically neutral and therefore not subject to electrical restrictions), as time passes, solute begins to accrue at the high-pressure membrane face, where the concentration of the effluent is represented by C_e and the concentration of the solution adjacent to the membrane face is represented by C_o (Figure 1B). In this early stage of hyperfiltration, the capacity of a membrane to reject solutes is high due to the low ionic strength with which it is in contact (Marine and Fritz, 1981). Preliminary high rejection rates of ions results in a build-up of solute at the high-pressure membrane face. This zone of increased concentration at the high-pressure membrane face is termed a concentration polarization layer (CPL). As the CPL grows, ever more solute is available to enter the membrane at the high-pressure face. A characteristic of clay membranes is decreased membrane efficiency with increasing concentration at the CPL (Fritz and Marine, 1983; Fritz, 1986; Fritz and Whitworth, 1994). As time passes, the width of the CPL and the concentration of the solutes within it

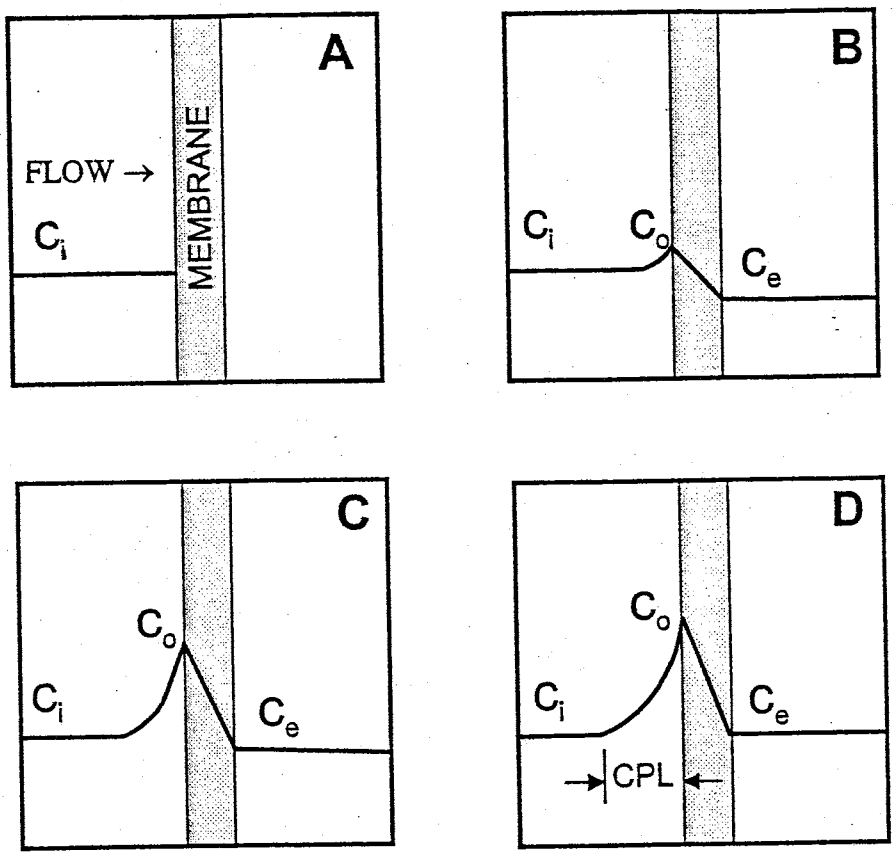

Figure 1. Conceptual development of the concentration polarization layer in a static cell. A theoretical description of this situation begins with identical solute concentrations on either side of the membrane at time $t = 0$, and C_i is the concentration of the input solution (A). Solute begins to accrue at the high-pressure membrane face, where the concentration of the effluent is represented by C_e and the concentration of the solution adjacent to the membrane face is represented by C_o (B). Increased solute concentration at the membrane face, and the effluent concentration approaches that of the influent (C). An equilibrium is eventually reached such that the effluent concentration is equal to that of the input (D).

also continues to increase. Ever more solute accrues at the membrane face, and the effluent concentration approaches that of the influent as the membrane efficiency begins to decrease due to increasing solute concentration at the higher-pressure membrane interface (Figure 1C). An equilibrium may eventually be reached such that the effluent concentration is equal to that of the input (Figure 1D). It is important to recognize that when the system is at steady-state, described here as effluent concentration equal to input concentration, the CPL still exists, even though the membrane efficiency is zero. Note that the definition of steady-state as just presented is not the only basis for a condition of steady-state. For consistency however, the interpretation of steady-state as described above will be assumed for the purpose of discussion in this text.

The concentration gradient as illustrated in Figure 1 is maintained as long as the diffusive forces of the species within the CPL are less than the advective forces of the system in the direction of the high-pressure face. If concentrations within the CPL reach and exceed saturation, precipitation of the solutes can result. When precipitation occurs within the CPL, the conditions of steady-state are somewhat different in that effluent concentration will not quite reach influent (some solute is being lost in precipitation). If, however, saturation within the CPL is not attained, membranes functioning in a 1-dimensional flow mode eventually reach an equilibrium where the effluent concentration is equal to that of the input.

The second end-member scenario is that of a cross-flow cell (Figure 2). This flow scenario describes the process used in commercial reverse osmosis desalinization with synthetic membranes. CPL development is minimized in commercial reverse osmosis desalinization by a high velocity flux that sweeps across the high-pressure membrane

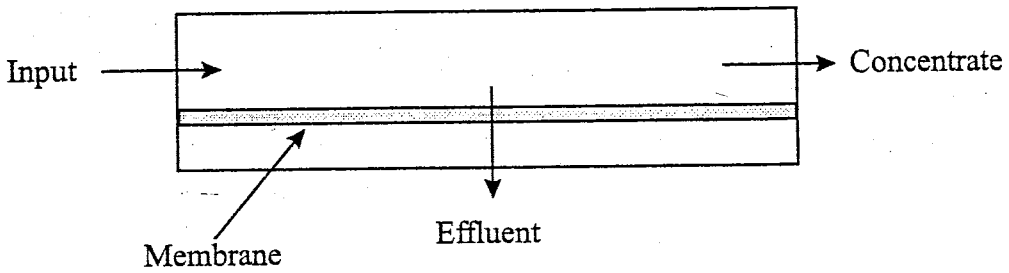

Figure 2. Schematic of the cross-flow cell.

face. Only a portion of the total flux passes through the membrane. In the subsurface, this would occur when the majority of groundwater flow is directed parallel to the membrane, and a much smaller flux is directed perpendicularly through the geologic membrane. Because of the diminished CPL, a quasi-equilibrium is reached such that the membrane efficiency is greater than zero. Synthetic membranes operated in this mode have reported membrane efficiencies for removal of NaCl as high as 99.8%. In the subsurface, due to typically slow groundwater flow velocities, the existence of a cross-flow component of flux great enough to diminish the CPL on the high-pressure membrane face as extensively as in commercial processes is unlikely. Instead, the effect in the subsurface should be to limit CPL development. The experiments in this study were designed to investigate flow systems operating in the 1-dimensional mode.

1.2 Previous Work

Previous work with geologic membranes, specifically clays and shales, has ranged from laboratory-based experimentation to field scale observations. Numerous laboratory investigations have experimentally confirmed that clays have the capacity to act as semi-permeable membranes (Briggs, 1902; Marshall, 1948; Wyllie, 1948, 1949; Kemper, 1960, 1961; McKelvey and Milne, 1963; Bernstein, 1960; Coplen and Hanshaw, 1973; Fritz and Marine, 1983; Benzel and Graf, 1984; Fritz et al, 1987; Fritz and Whitworth, 1994; Whitworth and Fritz, 1994). Fritz and Eady (1985), demonstrated that calcite could precipitate from undersaturated solutions as a result of hyperfiltration through clay membranes. Young and Low (1965) passed saline solutions through actual discs of shale and siltstone; their results indicated that these materials are capable of acting as semi-permeable membranes.

In addition to laboratory studies on membrane behavior, several field-scale investigations have cited membrane phenomena as an explanation for the observed data. For example, field and experimental work performed on Holocene marine muds have suggested that mudrock membranes have a significant effect on the chemical composition of brines that formed as a result of the compaction of shales (Siever et al, 1965). A study of the Milk River aquifer system, Alberta Canada (Phillips et al, 1986), cited ion filtration by shales as a possible explanation for the observed increased concentration of Cl^- ions in a down-dip direction documented at the site. In addition, Phillips et al (1986) suggested that membrane processes could also explain the observed increase in heavy isotopes (specifically δD and $\delta^{18}O$) recorded at the site.

Whitworth and Lueth (1994), Lueth and Whitworth (1994a), and Lueth and Whitworth (1994b) studied two copper deposits in New Mexico and found that copper mineralization occurred at sand-shale boundaries, with mineralization most concentrated nearest the shale, and diminishing with distance from it. There was no case in which significant mineralization extended into unfractured shales. It was also noted that the most abundant mineralization occurred adjacent to thinner shales.

Based on these observations, the authors proposed that the copper deposits may have been the result of solute-sieving by the shales. A brief description of their proposed model is as follows. Groundwater flows through rocks that are high in copper, dissolving the heavy metal into solution. The majority of the copper-enriched groundwater then flows along an aquifer that is bounded by confining shales. A portion of the heavy metal solute is rejected as the copper-enriched groundwater passes through the shale membrane.

A CPL forms if the velocity toward the membrane is sufficient to prevent the rejected solute from completely diffusing back into the source waters. The concentrations within the CPL near the membrane can reach supersaturation, resulting in the precipitation of copper minerals in the sandstones that are adjacent to the confining shale units. Whitworth and Lueth (1994) noted that copper mineral precipitation might be enhanced by the presence of sulfate-reducing bacteria that may be concentrated within the CPL.

No CPL will form if the flux toward the membrane cannot prevent the rejected solute from diffusing back into the aquifer. The CPL development in this case is restricted because the advective forces of flux are not great enough overcome the diffusive forces of the solutes. Mineralization will result only when the CPL develops to such an extent that the solute concentration at the higher-pressure membrane face is greater than solubility for a given mineral species. The copper mineralization noted at the sites studied by Whitworth and Lueth (1994), Lueth and Whitworth (1994a), and Lueth and Whitworth (1994b) can be explained by this interpretation. It was speculated that, for a given set of conditions, the solution flux through the thinner shales is the highest, allowing for relatively more solution to pass through the shale, ultimately resulting in relatively more copper mineralization at these locations. The conclusion that sedimentary copper deposits may form as a consequence of solute-sieving processes (Whitworth and Lueth, 1994; Lueth and Whitworth, 1994a; Lueth and Whitworth 1994b) has significant implications for the potential fate and transport characteristics of heavy metal contaminants in the subsurface.

The following studies have concluded that geologic membrane processes are active in natural systems: the Imperial Valley in California (Berry 1966, 1967), the

Oxnard coastal basin, Ventura County, California (Greeenberg et al, 1973), the San Juan basin in Northeastern New Mexico and southwestern Colorado (Berry, 1959), the Paradox basin in Utah, Colorado, and New Mexico (Hanshaw and Hill, 1969), the Wheeler Ridge anticline, San Joaquin Valley, California (Berry, 1960) and finally the Saginaw aquifer system, in the upper Grand River Basin, Michigan (Wood, 1976).

One of the unanswered questions concerning geologic membranes involves the debate over how thick a clay must be in order to function as a membrane in the natural environment. Greenberg et al (1973) implied that thicker membranes have a greater capacity of reducing solute movement. Conversely, Fritz (1986) states that membrane thickness has no effect on the solute sieving properties. The debate on this matter is not yet resolved, although Fritz and Eady's (1985) experiments with 50 μm-thick clay membranes demonstrate that very thin clays can have significant membrane properties. Generally speaking, membrane thickness in the natural environment is often in excess of those used in laboratory investigations. These investigations primarily make use of disks of natural or fabricated clays ranging from <1 mm to 3 cm in thickness. Table 1 summarizes some investigations relating lithology composition, thickness, and physiochemical membrane phenomena in the natural environment (amended from Alexander, 1990).

1.3 Subsurface Pressures

Previous studies have provided both a range of experimental evidence in support of osmotic processes, as well as mathematical models in attempts at defining them. Several studies have cited osmotic processes as an explanation of two main observations in the

Table 1. Site-specific geologic membrane studies (Modified from Alexander, 1990).

Age Lithology Sediment Thickness (m)	Membrane Thickness (m)	Recognized Process	Location	Observed Features	References
Pliocene and Miocene age Marine sandstone's and clays 8000 m	10-15 m	osmosis	Gulf of Mexico, USA	High fluid Pressures	Jones, 1968
Miocene McLure Shales 182 m	182 m	reverse osmosis	North Dome oil field California, USA	High water pressures and anomalous chemical compositions	Kharaka et al, 1973
Cretaceous silts 518 m	518 m	reverse osmosis	Alberta Basin, Canada	Anomalous pore pressures	Toth and Millar, 1983
Tertiary and Cretaceous materials coastal plain sediments/ mudstones and sand lenses 330 m/1615 m	30-300 m	osmosis	Dunbarton basin, Savannah river plant, South Carolina, USA	anomalously high hydraulic head	Marine, 1974; Marine and Fritz, 1981
Carboniferous sandstones and shales of the Saginaw formation 125 m	7 m	reverse osmosis	Grand River Basin, Michigan, Canada	Chemical concentrations above shale beds higher than input waters from glacial materials	Wood, 1976
Middle Jurassic Opalinus Clay 70 - 120 m	70 - 120 m?	reverse osmosis or osmosis?	Homberger Tal Region, Wiesenberg Tunnel Project, Switzerland	Anomalously low heads	Horseman, 1982
Cretaceous Marine Shales and Milk River Sandstone 350 m	50-300m	ion filtration	Milk River Aquifer. Alberta, Canada	Increased concentration in Cl^- ion .	Phillips et al, 1986

subsurface, specifically in sedimentary basins. These are the occurrence of anomalously high and low hydraulic heads (Jones, 1968; Marine and Fritz, 1981), and the existence of fluids of anomalous chemical composition (Bredehoeft et al, 1963; Graf, 1982).

Generally speaking, in the natural environment, in order for hyperfiltration to occur, some non-osmotic process must generate an overpressuring greater than osmotic pressure. Graf (1982) identified several mechanisms capable of producing subsurface overpressuring great enough to drive reverse osmosis. These mechanisms include, but are not limited to, rapid sedimentation of fine-grained materials, lateral tectonic compression, aquathermal pressuring, and dehydration of gypsum and/or clay materials. Because the subject matter is of particular interest in this study, rapid sedimentation of fine-grained materials will be discussed in more detail.

It has been reported that the development of pore pressure in excess of hydrostatic is guaranteed if the deposition rate of clay-rich sediments exceeds a specific value, which is dependant upon sediment permeability and the total thickness deposited by continuous sedimentation (Graf, 1982). Present-day deltas are good examples of this process in action. Furthermore, Bredehoft and Hanshaw (1968) reported from model calculations that fluid pressures approaching lithostatic can be attained with a continuous sedimentation rate of 500 m/10^6 years, a value reasonable for the Gulf Coast. This deposition rate is capable of forming a sediment column with a hydraulic conductivity of 10^{-8} cm/sec, which is close to the median observed values for shales. It should be noted that other researchers (Plumley, 1980) have argued that overpressured zones may be a result of several mechanisms, including mineral dehydration and aquathermal pressuring, working in tandem.

Limitations on the effects of rapid sedimentation of fine-grained materials become evident in the form of dissipated overpressuring at rapid rates when (1) the sedimentation rate decreases below a value critical for the particular depositional area, (2) sedimentation stops, and (3) the area is uplifted and eroded.

Calculations presented by Graf (1982) illustrate that overpressuring of fine-grained sediments can produce sufficient hydraulic head gradients to drive reverse osmosis in the subsurface. Phillips (1983) made an important note to these conclusions. He identified that the calculations presented by Graf (1982) are most likely highly conservative in nature, and the osmotic pressures which must actually be overcome before reverse osmosis can occur in the subsurface is expected to be less than those calculated by Graf (1982). Phillips (1983) explains that most geologic membranes are not 100% efficient, which means that these membranes cannot maintain osmotic pressure differences as large as ideal semi-permeable membranes. Secondly, the osmotic pressure difference across a membrane of finite thickness is not equal to the difference which would be maintained if the two solutions were separated by an infinitely thin membrane of the same efficiency; rather it is the difference resulting from variation in concentration between each side of the membrane and the solutions which the membrane separates. Phillips (1983) concludes that the analysis by Graf (1982) is conservative, and ion filtration by reverse osmosis may take place under hydraulic head differences ranging down to less than one-tenth the ideal calculated osmotic head differences. The significance of Phillips' (1983) comment is that reverse osmosis processes can occur under normal (i.e. elevation induced) conditions, as well as from overpressuring, identifying that no special mechanism is required to drive the process.

Hyperfiltration in the subsurface requires a head difference across a shale or clay membrane. This means that the head (or pressure) must be greater on one side of the shale than the other. Such head differences commonly occur in artesian aquifers. Tolman (1937) reported a well drilled in the Paris Basin to a depth of 548 meters into an artesian aquifer produced a column of water many feet into the air. Other wells in the lower portions of the alluvial fans in the southwestern U.S. alluvial basins produce artesian flows that extended from less than a meter to as much as 115 meters above the ground (Tolman, 1937; Paulsen, 1949). Furthermore, analysis of reservoir-pressure data indicates that relatively high subsurface pressures in sedimentary basins commonly exist (OSU, 1998).

Significant head differences also exist across the aquitards that support perched aquifers. The head difference across the lower aquifer boundary of a perched aquifer is equal to the depth of water, assuming very high initial hydraulic conductivity in the aquifer. Thus head differences across perched aquifer boundaries can be from less than a meter to several or even tens of meters, pressures which Whitworth (1998) calculated produce significant membrane effects.

1.4 Membrane Mathematics

Kedem and Katchalsky (1962) and Katchalsky and Curran (1965) developed a non-equilibrium thermodynamic approach to describe membrane processes. The first to systematically apply this mathematical treatment to geologic membranes were Fritz and Marine (1983) in a paper in which they stated that it is possible to experimentally determine the osmotic efficiencies of clay membranes by hyperfiltration, provided that

solution flux and effluent concentrations are measured at steady-state. Further studies, including ones performed by Fritz and Eady (1985), Fritz (1986), Fritz et al (1987), Fritz (1992), Fritz and Whitworth (1993, 1994), advanced the development and application of the system of equations derived by Kedem and Katchalsky (1962) and Katchalsky and Curran (1965). The approach developed by Kedem and Katchalsky (1962) and Katchalsky and Curran (1965) is also commonly used in work with synthetic reverse osmosis desalinization membranes (Spiegler and Kedem, 1966; Harris et al., 1976; Mariñas and Selleck, 1992; Whitworth et al, 1994).

De Groot and Mazur (1962) note that non-equilibrium thermodynamics is a continuum theory that treats the state parameters as continuous functions of space coordinates and time. Thus, this thermodynamic approach applies to both steady-state and smoothly changing transient conditions. Therefore, the use of these equations to describe subsurface hydrological situations is appropriate. Other mathematical descriptions of membranes exist, including kinetic models, the application of impedance, cable theory, and Hodgkin-Huxley equations (Lakshminarayanaiah, 1984), as well as transient solutions by Greenberg et al (1973), and Fritz and Whitworth (1994).

The flow of solution and solute through membranes can be described by two equations developed by Kedem and Katchalsky (1962). Although these equations were derived for non-electrolytes, they have been successfully applied to electrolytes (Spiegler and Kedem, 1966; Harris et al, 1976; Mariñas and Selleck, 1992; Whitworth et al, 1994). The two equations presented below describe a single solute system with no precipitation from solution within the CPL. These equations are:

$$J_v = L_p(\Delta P - \sigma\Delta\pi) \quad (1)$$

and

$$J_v = C_s(1-\sigma)J_v + \omega\Delta\pi \quad (2)$$

Where J_v = solution flux through the membrane (cm/s), L_p = water permeation coefficient (cm^3/dyne·s), ΔP = pressure difference across the membrane (dyne/cm^2), σ = reflection coefficient (dimensionless), $\Delta\pi$ = theoretical osmotic pressure difference across the membrane (dyne/cm^2), J_s = solute flux through the membrane (moles/cm^2·s), ω = solute permeation coefficient (mole/dyne·s), and C_s = average solute concentration across the membrane in mole/cm^3 and is defined as:

$$C_s = \frac{(C_o + C_e)}{2} \quad (3)$$

where C_o = concentration at the high-pressure membrane face (mole/cm^3), and C_e = effluent concentration (mole/cm^3).

Furthermore, the theoretical osmotic pressure difference, $\Delta\pi$, can be defined as

$$\Delta\pi = vRT(C_o - C_e) \quad (4)$$

where R is the gas constant (8.314 x 10^{-7} dyne·cm/mole·°K), and T is the temperature reported in degrees Kelvin. Lastly, v is a stiochiometric coefficient that corrects for the number of particles due to ion formation. For example, NaCl disassociates to two ions in solution, Na^+ and Cl^-, resulting in v = 2. Likewise, a $CaCl_2$ ion disassociates to one Ca^+ ion and two Cl^- ions, and v = 3.

The three phenomenological coefficients, σ, ω, and L_p, are useful in describing the behavior of non-ideal geologic membrane systems (Fritz, 1986). Staverman (1952) first defined the reflection coefficient, σ, as the ratio of the observed osmotically induced hydraulic pressure (ΔP) to that calculated solely from solution properties ($\Delta\pi$). The measurement of σ is customarily performed when $J_v = 0$, but it is possible to measure σ in a hyperfiltration system that has reached steady-state (Fritz and Marine, 1983).

Permissible values of σ range from zero to 1.0. If $\sigma = 0$, there is no membrane effect, conversely, if the value is equal to 1.0, the membrane is ideal, and all solute is prohibited from passing through the membrane. Considering a system in which the reflection coefficient is equal to zero, the solution flux equation, $J_v = L_p(\Delta P - \sigma\Delta\pi)$, is reduced to $J_v = L_p \cdot \Delta P$, which is the equivalent to a one-dimensional form of Darcy's law. The value of σ for natural geologic membrane systems must be greater than zero, but less than one. Values of σ calculated in a study performed by Fritz and Marine (1983) ranged from 0.04 to 0.89. A membrane with a $\sigma = 0.89$ will exhibit 89 percent of the theoretically predicted osmotic pressure.

The diffusion of solute through a membrane is depicted by ω, the solute permeation coefficient. The value of ω for ideal membranes is zero, indicating that no solute can pass through the membrane. For typical non-ideal membranes this value is greater than zero. Elrick et al. (1976) measured ω for a Na-bentonite slurry with 90% porosity, and obtained a value of $\omega = 3 \times 10^{-15}$ mole/dyne·s. Fritz and Marine (1983) suggested that this value should be considerably lower for more compacted bentonites.

There is a direct relationship between the water permeation coefficient, L_p, and hydraulic conductivity, as described by

$$L_p = \frac{K}{\rho g x} \tag{5}$$

where K is the hydraulic conductivity (cm/s), ρ is the fluid density (g/cm^3), g is the gravitational constant (cm/s^2), and x is the thickness of the membrane (cm) (Fritz, 1986). As a general rule, as L_p decreases, membrane efficiency increases.

The steady-state CPL profile in free solution adjacent to the membrane face can be described by the following equation (Fritz and Marine, 1983):

$$C_x = (C_o - C_e)\left[\exp\left(\frac{-J_v x}{D}\right) - \exp\left(\frac{-J_v x_i}{D}\right)\right] + C_i \tag{6}$$

where C_x is the concentration in moles/cm^3 at a distance x cm from the membrane, x_i is the distance from the membrane where $C_x = C_i$, and D is the diffusion coefficient of the solute in the x direction.

It has been determined that the term $-\exp(-J_v x_i/D)$ can be ignored in the above equation if the length of the test cell is large relative to the ratio D/J_v (Fritz and Whitworth, 1994). However, diffusion in free solution occurs more readily than diffusion in porous media. So a more appropriate representation of the diffusive component of flux would make use of an effective solute diffusion coefficient for porous media (Fritz and Whitworth, 1994), typically represented by D* (Freeze and Cherry, 1988; Fetter, 1988). D* is defined as follows:

$$D^* = wD \tag{7}$$

Where w is a unitless empirical constant determined from laboratory studies. Values of w range from 0.01 to 0.5, as reported by Freeze and Cherry (1988). Clay sediments fall in the lower end of this range (Berner, 1971). Nonetheless, the second term in the brackets of Equation 6 can be ignored in situations where the aquifer thickness is large relative to the ratio D^*/J_v. Hence, for a porous medium, the CPL concentration profile equation can be reduced to (Fritz and Whitworth, 1994):

$$C_x = (C_o - C_e)\left[\exp\left(\frac{-J_v x}{D^*}\right)\right] + C_i \tag{8}$$

It was determined by Fritz and Marine (1983) that the $\omega\Delta\pi$ term in Equation 2 can often be ignored, as ω tends to be very small. By omitting this term, and substituting Equation 3 into Equation 2, the following relationship was derived:

$$\sigma \approx \frac{C_o - C_e}{C_o + C_e} \tag{9}$$

Recall that $C_e = C_i$ in a condition of equilibrium in a static cell scenario. By substituting C_i for C_e into the above relationship and solving for C_o, the following relationship can be established :

$$C_o \approx \frac{(\sigma C_i + C_i)}{\sigma - 1} \tag{10}$$

Applying equation 9, and plotting the values of σ versus C_i, yields a graph of σ versus C_o/C_i (Figure 3). As an example, Fritz and Whitworth (1994) calculated a value of σ = 0.55 in their steady-state hyperfiltration experiment. In Figure 3, the value of C_o/C_i for

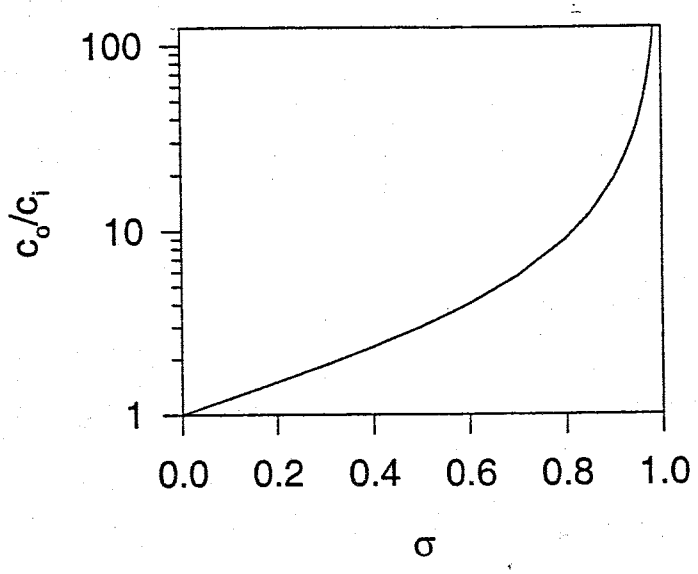

Figure 3. Relationship between the ratio of solute concentration at the high pressure membrane face and the background solute concentration within the aquifer (C_o/C_i) and the reflection coefficient σ.

$\sigma = 0.55$ is about 3.45, very close to the value of 3.48 obtained by Fritz and Whitworth (1994). This suggests that Equation 10 is reasonably accurate.

1.5 Heavy Metals

Heavy metal contamination may result from municipal solid waste, sewage sludge deposits, industrial by-product disposal sites, waste piles from mining and smelting operations, and disposal areas of filter residues from waste water treatment (Merian, 1990). Nonetheless, to fully comprehend the scope of the potential problems involving the fate and transport of heavy metals, it is necessary understand how and why these metals reach the groundwater.

Physiochemical consequences of heavy metal pollution depend strongly on chemical speciation, which in turn is a function of the kinds and amounts of Lewis bases present, the redox status (pE), and the acidity-alkalinity (pH) of the particular environment (Merian, 1990). It has been found that heavy metal mobility may increase as a function of the following four parameters, note that these parameters are guidelines, and exceptions to these guidelines may exist:

- lowering of pH.
- increased salt concentration — this results in the effect of competition on sorption sites on solid surfaces as well as the formation of soluble complexes with some trace metals.
- increasing the occurrence of natural or synthetic complexing agents — this can result in the formation of soluble metal complexes with trace metals that would otherwise be adsorbed to the solid surface.

- changing redox conditions — under oxidized conditions, a pollutant heavy metal plume in groundwater may be retarded relative to the water flow due to adsorption, while little retardation may occur under reduced conditions as the dissolved metal concentration may be in equilibrium with a precipitate (Merian, 1990).

Heavy metal concentrations approaching, or in excess of maximum allowable concentrations are common at contaminated sites (Tables 2 and 3).

1.5.1 Heavy Metals of Interest - Lead, Copper, and Cobalt

Heavy metals studied in this project included lead, copper, and cobalt. The following sections describe the role that these metals play in the natural environment.

1.5.1.1 Lead

In nature, lead concentrations in the biosphere are quite low (it is ranked 36th in abundance in the earth's crust) (Merian, 1990). In the past fifty years, however, the use of lead by humans has introduced this metal into our ecosystem in sometimes unsafe amounts. Because this element does not decompose naturally in the environment, it carries potential health risks, especially for young children (Merian, 1990). In guidelines set forth by the Safe Water Drinking Act, the U.S. EPA has set lead and copper apart when quantifying the amount of these elements considered safe for human consumption. Treatment techniques, rather than Maximum Contaminant Levels (MCLs) have been established for lead and copper. The "action level" for lead is 0.015 mg/l at the 90th percentile. A detailed description of the method used in calculating an action level can be found in the U.S. EPA Safe Water Drinking Act booklet, 1996.

1.5.1.2 Copper

Copper is a ubiquitous element that is almost always extracted from ores in underground or open mine pits. Commonly found in mining wastes, copper (as copper sulfate) is also widely used to supplement agricultural soils deficient in this element (Merian, 1990). Further applications include use as an algaecide and molluscide in water, with lime as a plant fungicide, as well as use in electroplating operations. Cupric oxide has been used in paints, and as an additive to swine and poultry food. It is clear from this abbreviated list that the use of copper in agriculture and industry is widespread. The action level for copper set by the US EPA is 1.3 mg/l at the 90^{th} percentile.

1.5.1.3 Cobalt

Cobalt is not as common as lead and copper in the natural environment. The major cobalt ore deposits are located in Zaire, Africa (found in sulfuric copper ores), Ontario, Canada (found in pyrites), as well as Morocco and northern Zimbabwe (Merian, 1990). Although deposits of cobalt-containing ores are found in the United States, they have not been mined commercially as of 1991 (Merian, 1990). Rather, imported ores or ore concentrates are processed in the United States.

The major technological applications of cobalt, which between them account for two thirds of its use, are as a base for hard magnet alloys and as a major constituent of the cobalt base 'Superalloys' used primarily in high temperature components for gas turbines (MIT, 1998). Other applications are: for soft magnet alloys, for metallurgical and glass making furnaces, for cutting and wear resistant alloys, for hard facing alloy consumables, for dental and bone surgery materials, for alloys with special thermal expansion characteristics and as a material for stainless, constant rate springs (MIT, 1998). Cobalt

also forms a base for permanent magnet alloys, and is sometimes alloyed with iron (MIT, 1998).

Mining activities and the extensive industrial uses of cobalt pose potential dangers to the natural environment, as waste products of cobalt ore processes can easily accumulate to toxic levels (Merian, 1990).

2.0 Experimental Methods

The hyperfiltration experiments of this study involved forcing undersaturated heavy metal solutions through relatively thin smectite membranes, and collecting effluent samples for analysis. The smectite membranes used in the experiments were sedimented and housed in an experimental hyperfiltration cell, and an ISCO™ 500-ml syringe pump was used to provide the hydraulic pressure. The pump has the capacity to discharge solutions at constant rates ranging from 1.0 µl/min to 80 ml/min, or at a constant pressure up to 258 bars. The ISCO™ unit used in these experiments was equipped with a pressure transducer at the factory, and has a precision rating of approximately ± 1.0%. The hyperfiltration cell is composed of a transparent acrylic cylinder with an internal diameter of 5.02 cm with a wall thickness of 0.64 cm. Two o-ringed Garlite™ caps were fitted to the cell and the apparatus was held in place by eight threaded rods that pass through caps parallel to the cylinder. A flat gasket provided the seal between the cylinder and the membrane. This cell has a maximum operating pressure of 68 bars or 1000 psi.

As previously stated, smectite clay (bentonite) was used in the preliminary experiments. The commercial bentonite that was selected for these procedures was an upper Cretaceous clay, mined in Crook county, near Colony, Wyoming. The clay was

examined by X-ray analysis prior to this study, and was found to be a relatively pure Na-smectite, with only trace amounts of quartz (Fritz and Whitworth, 1994). Typical properties of sodium bentonite clays are as follows (Wyo-Ben, 1998):

- Specific gravity: 2.55 ± 0.1
- Surface Area: External surface 82 m^2/g
- All surfaces 800 m^2/g
- Bulk density: 5.5 lbs/ft^3
- Typical particle size: 98% passing 80 mesh standard U.S. sieve (180 μ)
- pH: 9.1 ± 0.4
- Moisture content: 6-9%
- Cation Exchange Capacity, CEC meq (100 g): 70-90
- Free swell: 11 ± 1 cm^3/g

An air separator was used to segregate the bentonite clay used in this study to an average 30 mm size (Whitworth.et. al, 1993). The fine fraction was slurried in a one molar NaCl solution and dialyzed to remove the surplus solute, and then freeze-dried.

Pyrophyllite clay, composition $Al_2Si_4O_{10}(OH)_2$, was used in the final experiment, WRRI-11. Unlike smectite, pyrophyllite has no suficial charge imbalance. This clay displays monoclinic crystallography that is not formed in distinct crystals. Pyrophyllite is commonly foliated in radiating lamellar aggregates. It has perfect {001} cleavage with flexible folia, but is not elastic. Pyrophyllite is white to gray-brown in color with a pearly to greasy luster. This aluminum silicate hydroxide is characterized by a micaceous habit, cleavage, and greasy feel. Its physical properties are nearly identical to talc, but distinguished from it by positive test for Al, and it will yield water at high temperatures. Pyrophyllite is a relatively rare mineral found in low- and medium-grade metamorphic rocks rich in aluminum, and is often associated with kyanite. Its industrial applications are similar to those of talc. The purpose of using pyrophyllite in this series of

hyperfiltration experiments was to attempt to determine the relative importance of surface charges on clay with respect to precipitation processes within the CPL.

The smectite experiments were numbered WRRI-1 through WRRI-10. Each membrane for experiments WRRI-1 through WRRI-9 was constructed by gravimetrically weighing out 0.60 grams of the freeze-dried smectite clay, and making a slurry with approximately 200 ml of ultra-pure deionized water. Experiment WRRI-10 utilized 2.0 grams of the smectite, prepared in the same manner. The process of setting up the experiments began by placing filter paper into the bottom of the hyperfiltration cell, which was cleansed in a 5% HNO_3 wash before each experiment to ensure no residual solution remained from any previous experiments. The entire smectite clay slurry was then placed into the hyperfiltration cell, and the cell was filled to volume with ultra-pure deionized water. The syringe pump was also washed with a 5% HNO_3 solution and filled with deionized water, which was then used to sediment the membrane in the hyperfiltration cell. A constant flow rate between 25 and 100 ml/min was set on the pump, and the clay was allowed to collect on the filter paper at the base of the experimental cell. Following sedimentation, the membrane was compacted by raising the pressure in the hyperfiltration cell. This was accomplished by incrementally increasing the flow rate of the deionized water to the cell using the ISCO™ pump, and noting the resultant pressure increase with time. Pressures inside the cell approached 1000 psi during compaction, a process which took between six and eighteen hours. The filtration coefficient, L_p, was calculated from measurements of time, flowrate of deionized water, and fluid pressure after the compaction procedure was completed.

The deionized water was emptied from the pump, and decanted from the hyperfiltration cell. The undersaturated heavy metal stock solution was then placed in the cell, and flushed through the pump several times before final fill, once again to ensure against contamination from earlier runs. For reference, the undersaturated solutions included solutions of copper carbonate, copper chloride, lead chloride and cobalt chloride. Information regarding the specific solution concentration for each experiment is provided later in the text. These undersaturated solutions were prepared by saturating ultra-pure deionized water with reagent grade heavy metal chemicals and stirring the solution continuously for no less than 24 hours. This saturated solution was subsequently filtered through 22 μm pore size filter paper to remove any remaining chemical solids. The filtered solution was then diluted using ultra-pure deionized water. This diluted solution served as the stock solution to be used in the experiments. Two samples of the stock solution were taken from the pump, one stored in a clean 60 or 125 ml Nalgene® container, the other in a 125 ml Nalgene® container with 1-2 ml of HNO_3, to prevent plating out of the heavy metal. This storage sequence was followed in the collection of all effluent samples for each experiment.

After the stock solution sample was collected from the pump, the experimental set-up was assembled as described below (Figure 4). The syringe pump has two ports, one connected to the stock solution holding tank, the other to the top of the hyperfiltration cell. An additional port on the effluent end of the hyperfiltration cell was connected to the sample collection bottle, sizes of which ranged from 125 ml to 250 ml. Each of these connections were made using PEEK (polyetheretherketone) tubing, which had an internal

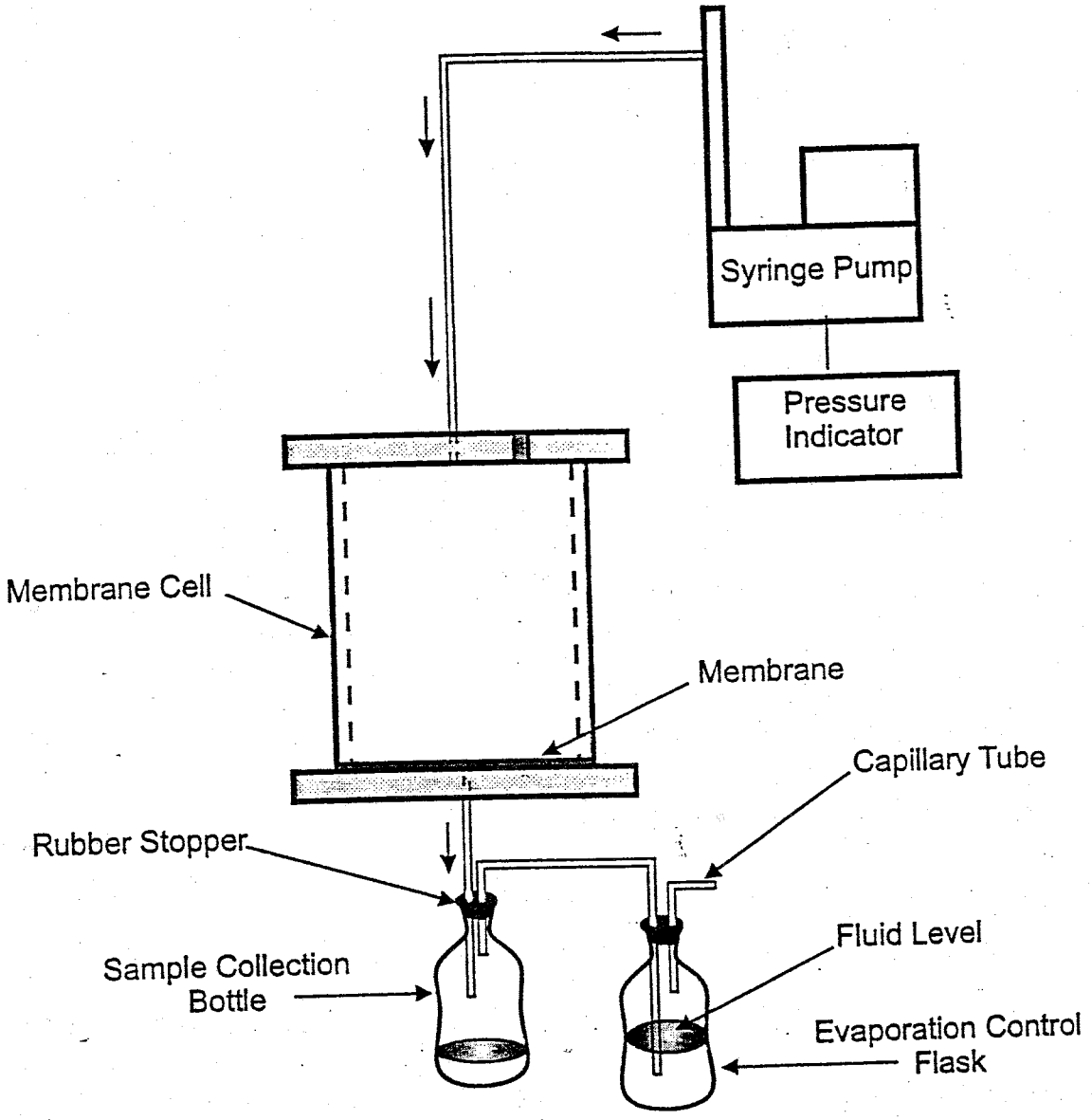

Figure 4. Experimental set-up for the hyperfiltration experiments in this study.

diameter of 0.159 cm, and a burst strength of 345 bars. In order to avoid corrosion, stainless steel Swagelock® fittings and valves were used. However, a single monel fitting was inadvertently used in the first successfully completed experiment (WRRI-2). It was replaced with a stainless steel fitting for the subsequent runs.

The final experimental set-up involved the use of an evaporation suppressant system because the dry climate and the length of the experiments posed a potential evaporation problem. This issue was circumvented by inserting a rubber stopper with two holes into the acidified sample collection bottle, and the 125 ml bottle that would serve as the evaporation control. The effluent sample collection bottle had one connection to the hyperfiltration cell (using the PEEK tubing), and one connection to the evaporation control unit, made with capillary tubing. The capillary tubing in this last connection ran to the control bottle and remained below the liquid level. Finally, another short length of capillary tubing, which was open to the atmosphere, was inserted in the remaining hole of the rubber stopper in the evaporation control unit.

Once the system was arranged, the pump was turned on, and parameters such as collection time, ambient temperature of the surroundings, and fluid pressure as measured by the ISCO™ syringe pump were recorded. The weight of the collection bottles (without the caps) was noted before and after sample acquisition. The acidified storage bottles were weighed before and after acid addition, as well as after the sample was deposited.

Because the ISCO pump had only a 500 ml capacity, it was necessary to periodically refill the pump. This was done by valving off the line from the cell to the pump, in order to maintain the pressure in the cell. The pump was then refilled with

stock solution, and built back up to pressure, after which the valve from the call was reopened. This process typically took less than three minutes.

Any noticeable changes that took place on the surface of the membrane during the experiment were noted. At the end of each run, the cell was disassembled, and the solution inside the hyperfiltration unit was stirred to homogenize it, and collected. The membrane itself was washed repeatedly in ethanol in order to displace any remaining solution, and prevent any precipitation due to evaporation. A final pump stock solution sample was collected for comparative analysis.

Two approaches were used to prepare the pyrophyllite clay for the experiments. First, the clay was ground by hand to a powder with a mortar and pestle. The ground pyrophyllite was then sedimented in the hyperfiltration cell in the same manner as the smectite experiments. Pressure failed to build in the hyperfiltration cell during the sedimentation procedure, and the sedimented pyrophyllite repeatedly cracked. After several efforts, this approach was abandoned.

The second approach to utilize pyrophyllite in this series of experiments began by grinding the pyrophyllite in a hockey puck grinder in an attempt to further minimize the particle size. The ground clay was then stirred in a water bath and allowed to settle for 59 hours and 20 minutes, separating the < 1 micron particles to the top 5 centimeters of the bath. Sedimentation of these particles failed to form a significant membrane, as the pressure did not reach greater than 8 psi with flow rates up to 650 ml/hr. This trial was abandoned as well. A different compaction method or preliminary freeze-drying of the clay may be necessary to complete a successful run.

2.1 Analysis

The membranes from each completed hyperfiltration experiment were stored in custom-sealed acrylic cylinders to avoid contamination. These containers were composed of two four-inch diameter by one-inch turned disks, one with a 4-mm deep recess to house the membrane and attached filter paper. The seal for the disks was formed with stopcock grease. The analysis of the precipitates present on the membrane was performed in a JEOL 733 Electron Microprobe at the University of New Mexico, Department of Earth and Planetary Science/Institute of Meteorics. This probe has five tunable wavelength dispersive spectrometers (WDS) and a Link Analytical thin-window energy dispersive spectrometer (EDS), controlled by an Oxford eXL II x-ray analytical system.

The acidified effluent samples were analyzed by both graphite furnace atomic adsorption and flame atomic adsorption. The standards used in all of the analyses were prepared from recently purchased, high purity NBS-traceable standards. The Cl^- anions in experiments WRRI-5 and WRRI-6 were measured by titration; measurements were made with a Hach digital titrator. The remaining anion measurement were made on a Dionix Ion Chromatograph, model 2000iSP. Periodic triplicate analyses were used to determine the precision for all of the analytical methods (Table 4).

2.2 Experimental Results

2.2.1 Introduction

We were not aware of any previous studies involving hyperfiltration of heavy metal solutions through clay membranes at the time of this report. Eight hyperfiltration

Table 4. Analytical precision for the analyses performed in this study.

Graphite Furnace Atomic Adsorption
Copper, ± 23% at 2 standard deviations
Chrome, ± 10.6% at 2 standard deviations
Manganese, ± 8.1% at 2 standard deviations
Iron, ± 25% at 2 standard deviations
Nickel, ± 37% at 2 standard deviations
Chloride titrations are ± 1.0% at 2 standard deviations
Alkalinity titrations are ± 2% at 2 standard deviations
Lead by flame AA (Experiment WRRI-6) is ± 0.8 % at 2 standard deviations
Lead by flame AA (Experiment WRRI-5) is ± 2.7 % at 2 standard deviations
Copper by flame AA is ± 3.3 % at 2 standard deviations
Copper by flame AA (Experiment WRRI-8) is ± 0.34% at 2 standard deviations
Cobalt by flame (Experiment WRRI-9) AA is ± 1.23 % at 2 standard deviations

Note: Sample pH was measured at collection time using a Hach pH meter.

experiments were conducted using undersaturated solutions and smectite clays; three with copper carbonate, two with lead chloride, one with copper chloride, and two with cobalt chloride. Of these eight experiments, six produced heavy metal precipitation from undersaturated solutions at the high pressure side of the membrane. Several attempts were made to utilize pyrophyllite clay in this series of hyperfiltration experiments without success. Table 5 provides a quick summary of the findings of the hyperfiltration experiments in this study. The solution concentrations expressed as a percentage represent the approximate concentration as estimated by dilution (see Experimental Methods). Heavy metal molarities in solution are calculated from pump solution concentrations. Please note that graphical representation of data from each experiment follows the associated tabulated data sets.

Table 5. Summary of the hyperfiltration experiments

EXPERIMENT	SOLUTION USED	MOLARITY OF HEAVEY METAL IN SOLUTION	RESULTS
WRRI-2	80% $CuCO_3$	7.16×10^{-3} mmol/L	Mineral precipitation observed on scanning electron microscope
WRRI-4	80% $CuCO_3$	3.12×10^{-3} mmol/L	Mineral precipitation observed on scanning electron microscope
WRRI-5	80% $PbCl_2$	23.04 mmol/L	Mineral precipitation visually observed during experimental run
WRRI-6	23% $PbCl_2$	7.37×10^{-3} mmol/L	Mineral precipitation visually observed during experimental run
WRRI-7	80% $CuCO_3$	1.96×10^{-3} mmol/L	No precipitation detected
WRRI-8	80% $CuCl_2$	30.17 mmol/L	Mineral precipitation visually observed during experimental run. Floating precipitate on membrane face observed at completion of run.
WRRI-9	80% $CoCl_2$	66.59 mmol/L	Precipitation visible on membrane surface at the end of the run
WRRI-10	70% $CoCl_2$	362.11 mmol/L	Membrane not analyzed.
WRRI-11	Pyrophyllite attempt	NA	Membrane formation was not successful

For purposes of review the term "stock solution" is the prepared undersaturated solution that is delivered to the pump for use in the experiments. The term "pump solution" represents the composition of the solution from the pump that is provided to the experimental cell. The term "cell solution" represents the composition of the solution decanted from the experimental cell at the conclusion of each experimental run.

2.2.2 Copper Experiments

2.2.2.1 WRRI-1

This first experiment utilized a Na-montmorillonite (smectite) pre-treated with a copper chloride solution. This pre-treatment was performed as an attempt to load the exchange sites with copper to minimize ion exchange during the experiment. This pre-treated clay was dialyzed to remove the excess copper ions and oven dried at 105° C. This clay proved difficult to rehydrate, and no membrane formed during sedimentation. The clay may have been difficult to rehydrate for several reasons, including that the clay was allowed to dry for too long, which may have altered the structure of the clay. The fluid pressure in this run did not rise above 0 psi, and the run was aborted. No further attempts to pre-treat the clay were made in succeeding experiments.

2.2.2.2 WRRI-2

The stock solution for this test was approximately 80% saturated copper carbonate, and the membrane (constructed with 0.06 grams of the bentonite clay) was compacted to 68 bars (1000 psi). The flow rate through the membrane was initially set to 150 ml/hour, but the fluid pressure in the cell rose quickly to 47 bars approximately four hours into the experiment, so the flow rate was decreased to 100 ml/hour for the remainder of the experiment. The total run time for this test was slightly over 19 hours, and the final fluid pressure was 31.37 bars (Table 6a, Figure 5). The temperature of the room varied between 20.3° C and 21.9° C during the experiment. The alkalinity of the input solution was 0.122 mN compared to an alkalinity of 0.195 mN of the cell solution that was collected and analyzed at the completion of the run (Table 6b, Figure 6). This is an alkalinity increase of 37.4% in the cell, suggesting that the sedimented clay was acting

Table 6a. Data for experiment WRRI-2. All data for effluent samples, unless otherwise noted in the comment column.

Sample #	Sample Interval (hours)	Time Elapsed Total (hours)	Sample Volume (cm^3)	Pressure (bars)	pH	Comment Solution flux = 150 ml/hr
1	--	--	--	--	5.95	pump solution
2	0.767	0.767	107.0	17.86	5.96	
3	0.700	1.467	110.1	21.65	5.96	
4	0.767	2.234	115.3	25.44	6.00	
5	0.850	3.084	124.3	29.23	5.79	
6	0.800	3.884	119.2	47.44	5.61	
7	1.067	4.951	120.8	30.13	5.59	flow rate 100ml/hr
8	1.283	6.234	129.2	30.27	5.49	
9	1.133	7.637	113.5	30.89	5.55	
10	1.300	8.667	127.8	26.89	5.37	
11	1.117	9.784	112.3	27.65	5.67	
12	1.183	10.967	118.0	28.34	5.69	
13	1.067	12.034	105.5	28.48	5.77	
14	1.167	13.201	112.7	28.34	5.68	
15	1.167	14.368	117.0	29.03	5.89	
16	1.167	15.535	116.2	29.51	5.33	
17	1.167	16.702	115.8	29.99	5.80	
18	1.200	17.902	117.7	30.75	5.67	
19	1.167	19.069	116.4	31.37	5.56	
20	--	--	--	--	6.47	pump solution
21	--	--	--	--	6.16	cell solution

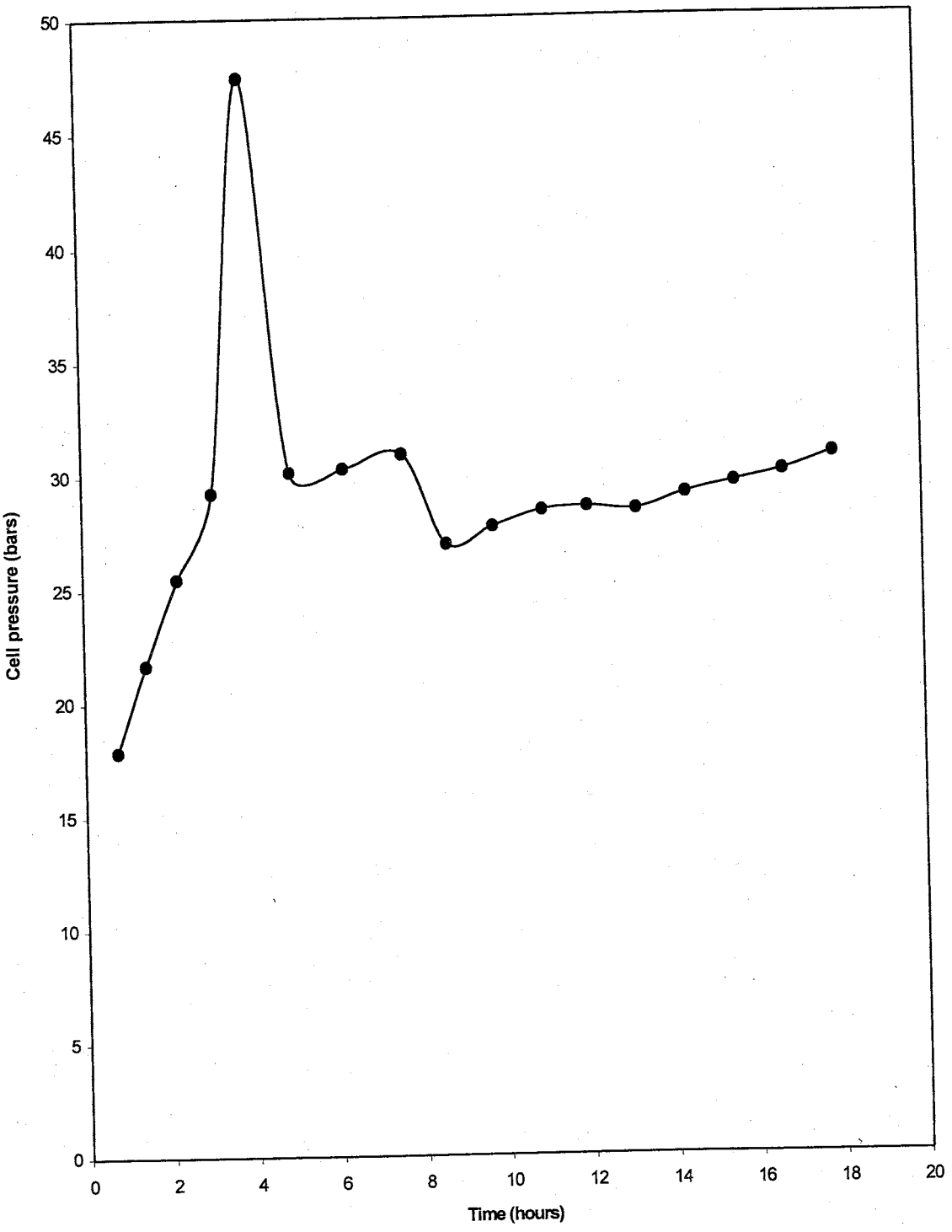

Figure 5. Time versus cell pressure for WRRI-2.

Table 6b. Chemical analyses for WRRI-2 (Performed by graphite furnace analysis unless otherwise noted). All data for effluent samples, unless otherwise noted in the comment column.

Sample #	HCO3 [1] (mN)	Cu (ppb)	Cr (ppb)	Ni (ppb)	Fe (ppb)	Mn (ppb)	Na[1]	Ca[1]	Comments
1	0.122	457[1]	0.8	2.8	19	1.6	0	0	pump solution
2	0.097	5.5	0.6	5.9	15	0	0	0	
3	0.090	3.6	0.5	0.6	20	0	0	0	
4	0.089	5.5	0.5	0.5	11	0	0	0	
5	0.086	4.8	0.4	1	14	0	0	0	
6	0.077	4.6	0.5	0.5	8	0	0	0	
7	0.069	4.8	0.6	0.7	14	0	0	0	
8	0.068	5	1	1	7	0	0	0	
9	0.067	5.5	0.5	0.6	11	0	0	0	
10	0.060	5.3	0.4	0.5	8	0	0	0	
11	0.067	9.3	0.5	0.6	6	0.3	0	0	
12	0.059	7.1	0.4	0.5	5	0.2	0	0	
13	0.059	8.4	0.6	0.6	6	0.4	0	0	
14	0.058	8	0.5	0.6	7	0.7	0	0	
15	0.059	9	0.6	0.7	15	2.4	0	0	
16	0.075	9.3	0.5	0.6	17	2.7	0	0	
17	0.081	20.8	2.9	0.7	13	3	0	0	
18	0.063	11.5	0.5	0.7	7	3.8	0	0	
19	0.051	20	0.8	1.3	8	3.4	0	0	
20	0.107	433[1]	0.2	2.8	6	0.7	0	0	pump solution
21	0.195	472[1]	1.5	11.1	42	1.6	0	0	cell solution

[1] analyses by flame atomic adsorption

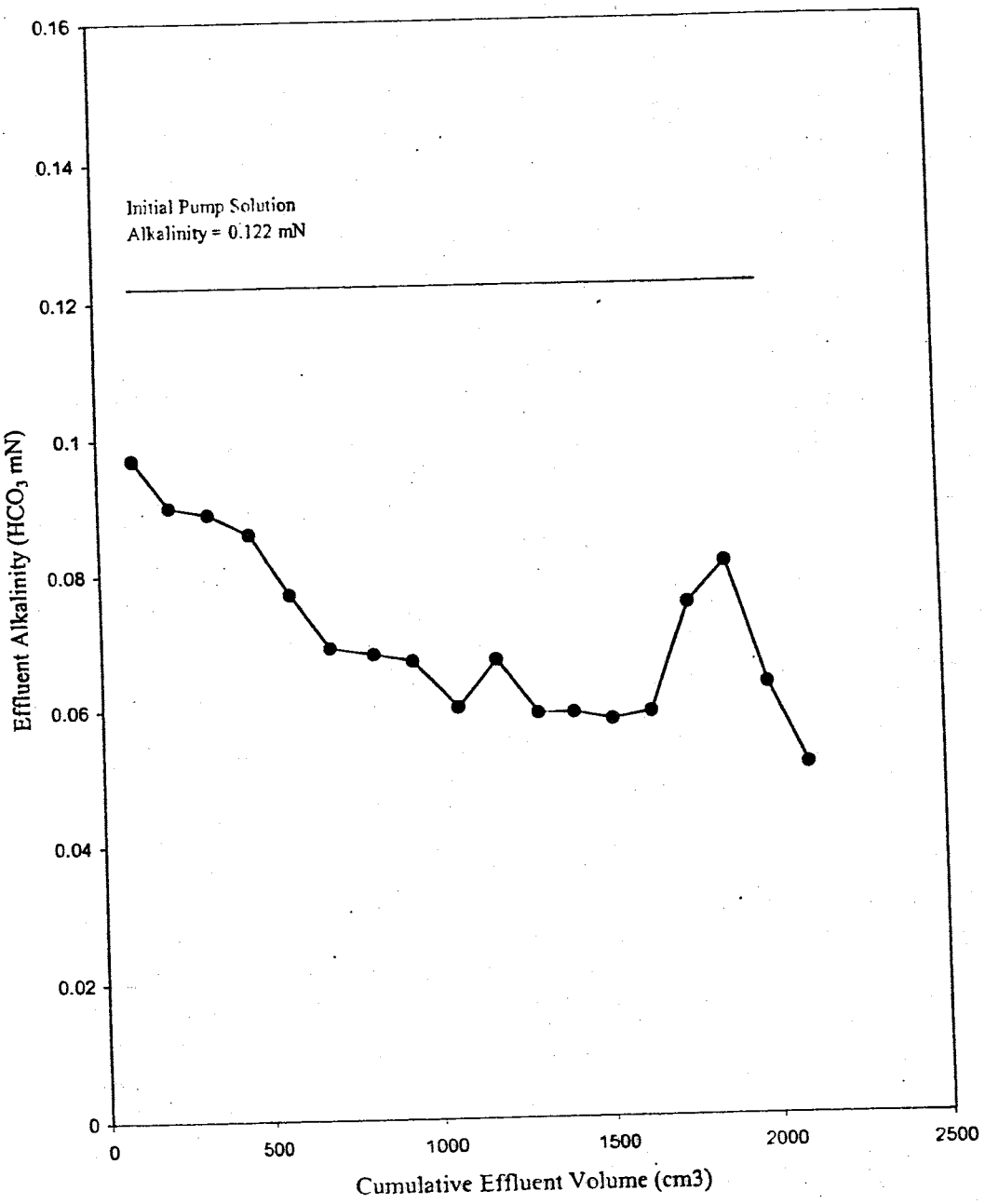

Figure 6. Cumulative effluent volume versus effluent sample alkalinity for WRRI-2.

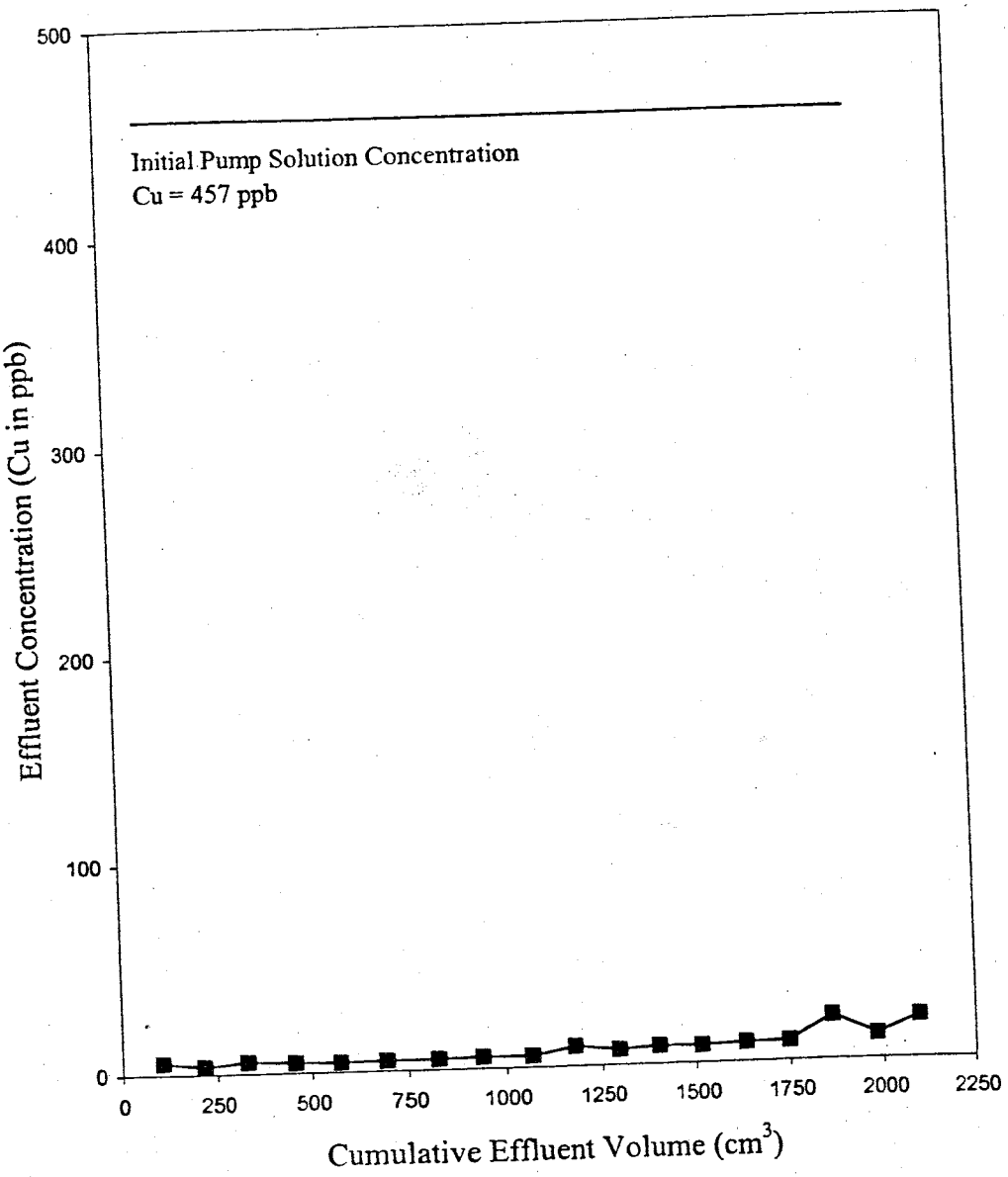

Figure 7. Cumulative effluent volume versus effluent sample copper concentration in ppb for WRRI-2.

as a membrane. The copper concentration of the input solution (457 ppb) was not significantly greater than that of the solution collected from the hyperfiltration cell at the termination of the run (472 ppb). Considering an analytical precision of 3.3% that was calculated for this experiment, there is no measurable difference in the copper concentrations between the input and cell solutions. The copper concentration of the first effluent sample was measured to be 5.5 ppb, and this value slowly rose to only 20 ppb measured in the last effluent sample collected (Figure 7, above). Less than three percent of the copper that was advected towards the membrane exited the experimental cell in the effluent.

Theoretically, at steady-state with no precipitation or ion exchange, the copper concentration of the effluent should be equal to that of the input solution, as described in this text. Therefore, either steady-state was not reached, precipitation of copper was occurring on the high-pressure side of the membrane, significant ion exchange was occurring within the clay membrane, or some combination of these effects occurred. On the same note, the results of the cell solution analysis can be explained simply. The CPL that would have formed during this experiment would be relatively thin, based on the chronological length of the experiment, probably less than 0.01 cm; the width of the CPL $\approx 10D/J_v$ (Fritz and Whitworth, 1994). When the cell solution is homogenized, this zone of increased concentration would have been diluted in the cell solution, so any CPL effect that may have been present would now be unrecognizable in the analyses of the cell solution. However, ion exchange or adsorption by the clay can not be discounted, as smectites are noted for their high CEC.

To determine which mechanism is most likely responsible for the low effluent concentrations, other ion analyses were performed. It was determined through flame atomic adsorption analyses that there was no sodium in any of the effluent samples. This rules out the possibility of significant exchange of Na^{+} for Cu^{++}. However, these samples were also analyzed for calcium, and although the results showed no measurable calcium in the samples, the detection limit for this ion was 0.75 ppm. So it is possible that the calcium ion may have played a role in ion exchange.

The membrane surface was examined on a scanning electron microscope and by qualitative energy dispersive analysis on an ion microprobe after the experimental run. Precipitation of heavy metals on the high-pressure membrane face was confirmed. The most unexpected finding in these analyses was the detection of particles on the membrane face composed of elements not present in the stock solution (a nickel-copper co-precipitate (containing minor amounts of Mn), iron sulfate, iron oxide, and calcium carbonate). Energy dispersive analyses of some of these particles are presented in Figures 8, 9, 10, and 11. The morphology of these precipitates displayed some crystallinity, with the majority of the precipitate amorphous in nature.

The copper carbonate used to make the stock solution contained no nickel (Table 7), so it was surprising to find nickel present as a precipitate on the membrane. These metals may have leached from the walls of the pump (see Table 8 for pump cylinder composition). Subsequent analysis of solution collected from the pump showed 0.8 ppb chrome, 2.8 ppb nickel, 19 ppb iron and 1.6 ppb manganese in solution. Furthermore, unlike the subsequent trials, this experimental set-up contained a single Monel fitting, so

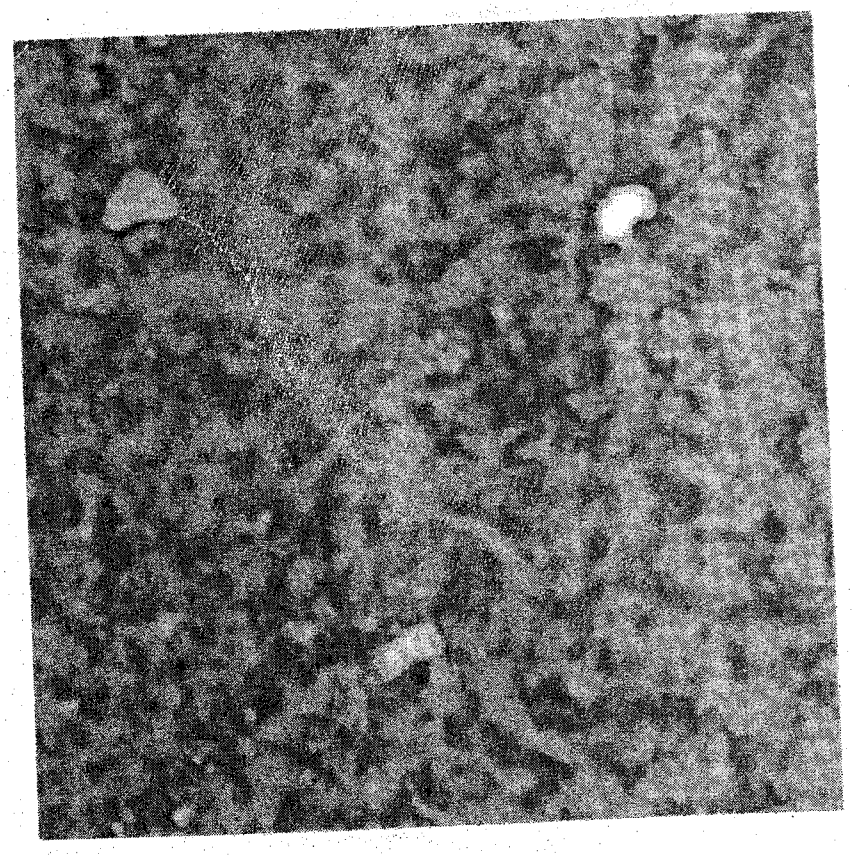

Figure 8. Scanning electron microprobe photograph of copper-nickel phase identified on the high pressure membrane face of experiment WRRI-2.

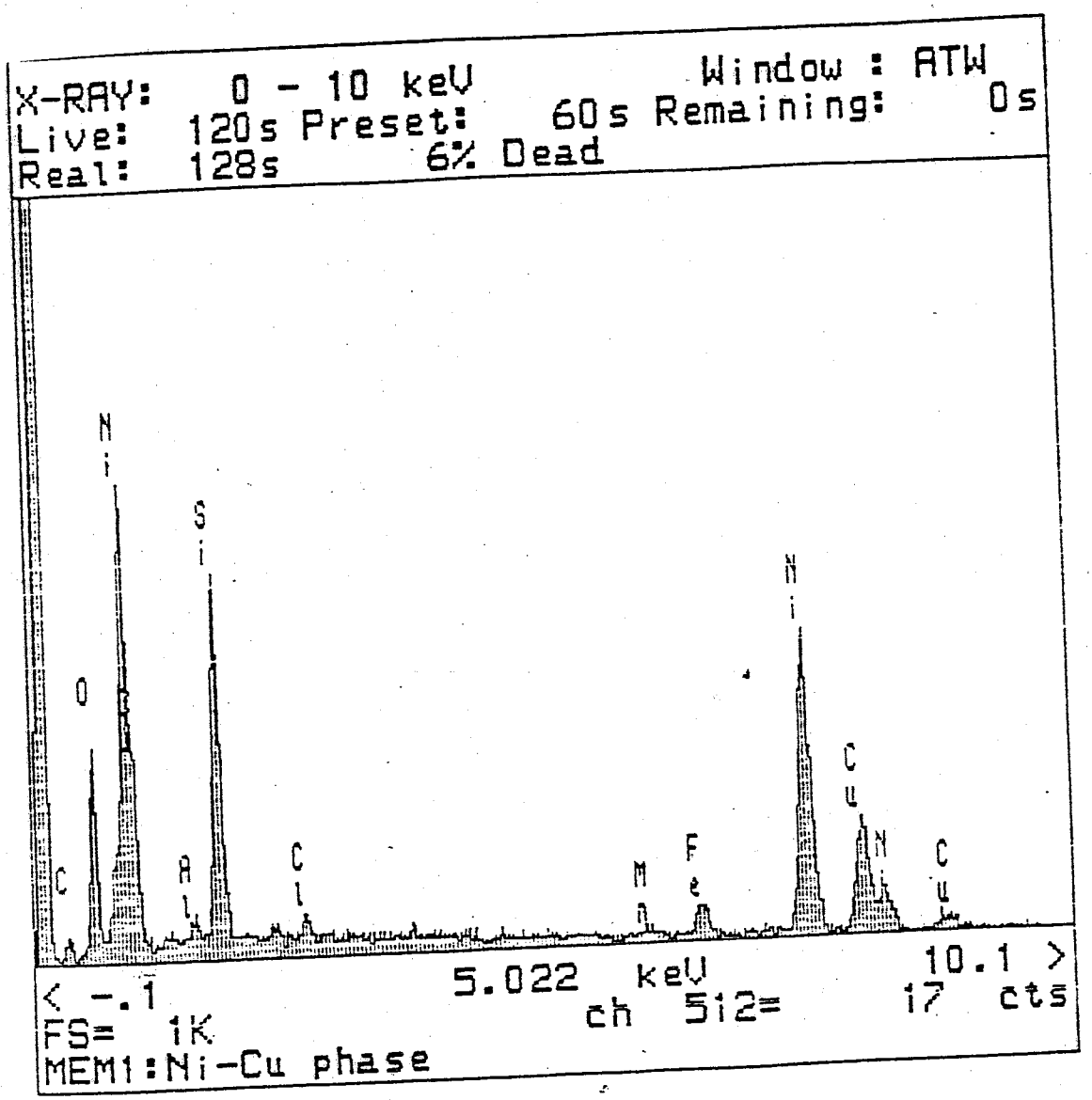

Figure 9. Energy dispersive spectra of Ni-Cu particle present on the surface of the membrane after experiment WRRI-2. Many of these Ni-Cu particles were observed.

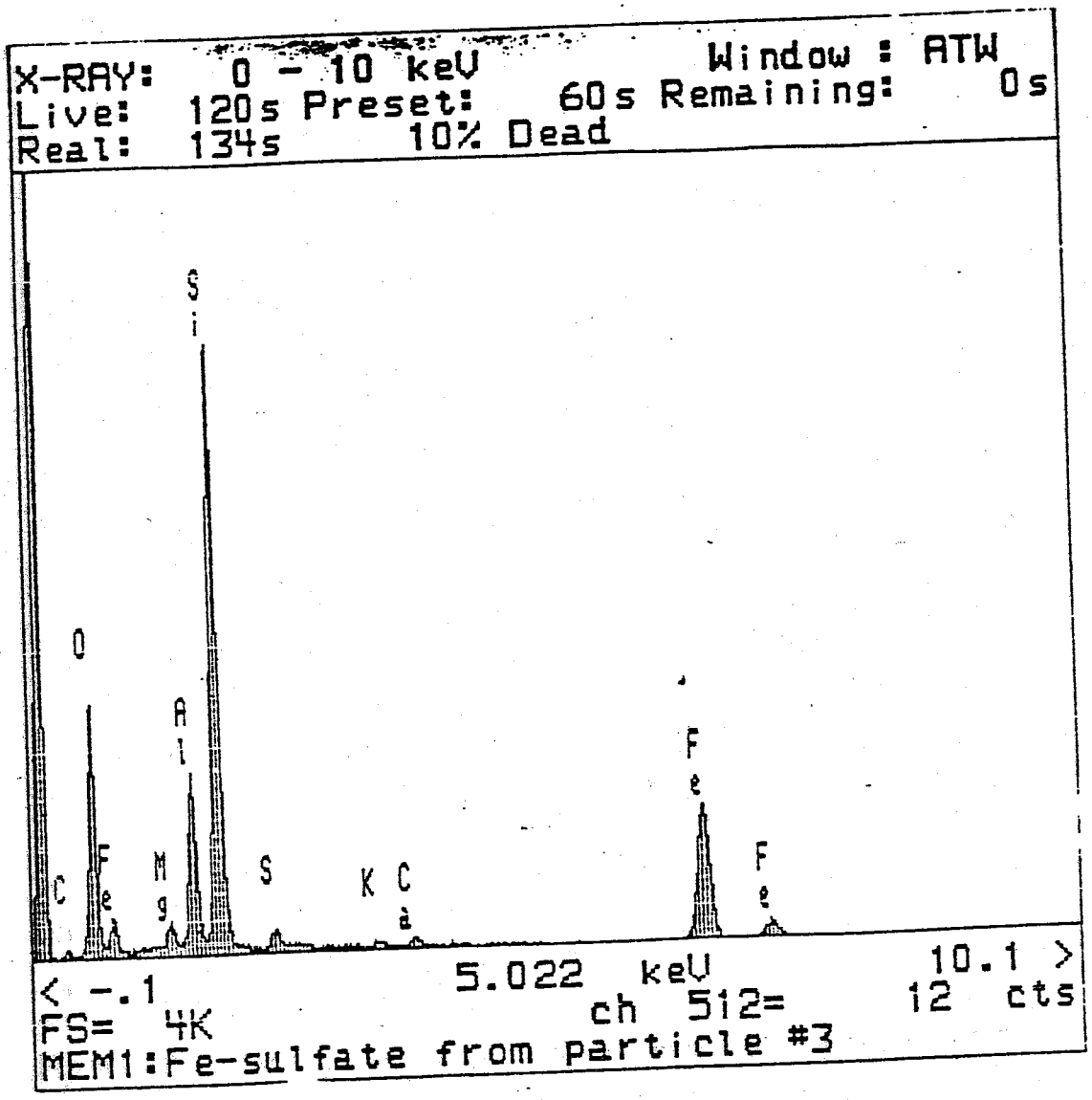

Figure 10. Energy dispersive spectra of iron sulfate particle present on the surface of the membrane after experiment WRRI-2. This is the only iron sulfate phase observed.

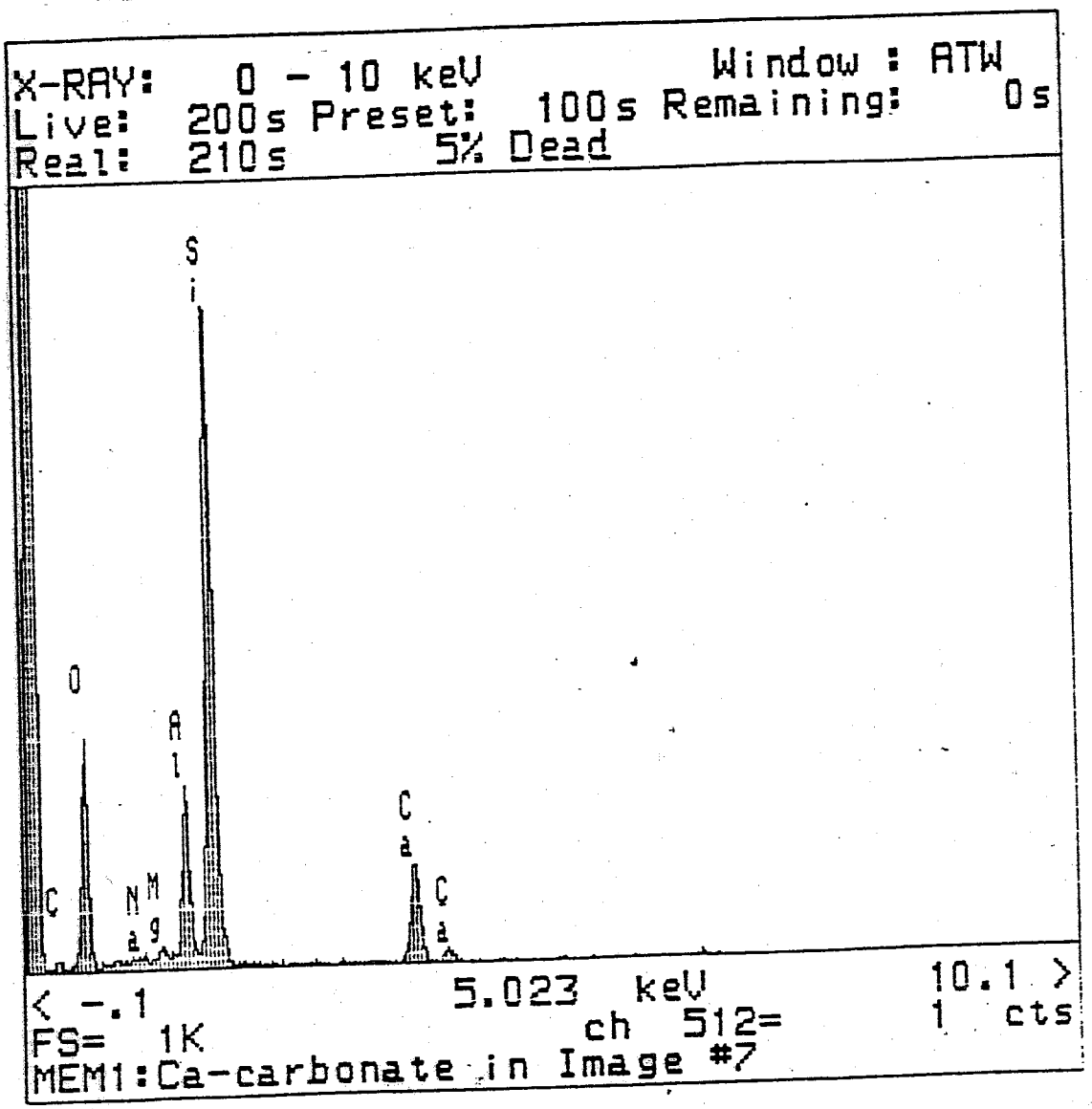

Figure 11. Energy dispersive spectra of calcium carbonate particle present on the surface of the membrane after experiment WRRI-2. This is the only calcium carbonate phase observed.

Table 7. Analysis of lot F52333, J.T. Baker copper carbonate used in this study.

COMPONENT	AMOUNT PRESENT
Assay (as Cu)	56.2%
Insoluble in HCL	<0.005%
Chloride (Cl)	<0.001%
Nitrate (NO_3)	0.03%
Sulfate (SO_4)	<0.005%
Barium (Ba)	<0.01%
Calcium (Ca)	0.01%
Iron (Fe)	0.001%
Lead (Pb)	<0.0005%
Potassium (K)	<0.005%
Silicon (Si)	0.002%
Sodium (Na)	0.3 %
Cadmium	<2 ppm

Table 8. Composition of syringe pump cylinder as provided by the manufacturer.

COMPONENT	AMOUNT*
Carbon	0.06% maximum
Manganese	4.0/6.0%
Phosphorus	0.04% maximum
Sulfur	0.03% maximum
Silicon	1.0% maximum
Chromium	20.5 / 23.5%
Nickel	11.5 / 13.5%
Molybdenum	1.5 / 3.0%
Columbium	0.1 / 0.3%
Vanadium	0.1 / 0.3%
Nitrogen	0.2 / 0.4%

*Note: Iron comprises the remainder of this alloy

3% Al + Ti (Oberg et al., 1992). The Ni-Cu ratio for monel is approximately 2.0, and the Ni-Cu ratio of the precipitates on the membrane was approximately 2.8. Based on the reported and collected ratios, it is most likely that the source of the other metals was dissolution from the pump. This dissolution process was most likely aided by the relatively low pH of the stock solution. The fact that precipitation was prevalent on the membrane surface, combined with the low copper concentrations in the effluent, and a lack of evidence for significant participation of sodium ion exchange, suggests that this experiment was successful in precipitating copper minerals on the surface of the membrane from an initially undersaturated copper carbonate solution.

2.2.2.3 WRRI-4

This experiment hyperfiltrated an approximately 80% saturated copper carbonate solution through a sedimented clay membrane. The final flow rate through the membrane was 100 ml/hour, and the final ΔP was 4.96 bars (72 psi) (Table 9a, Figure 12). The input alkalinity for this experiment was 0.177 mN, and by the end of the experiment, the alkalinity of the cell solution had risen to 0.201 mN, a 13.6% increase (Table 9b, Figure 13). The analytical precision for the alkalinity titrations for this run was ±2% at two standard deviations, which suggests that there was a significant membrane effect for alkalinity during the experiment. However, the copper concentration in the cell was determined as slightly lower than the copper concentration in the pump solution at the close of the experiment (Figure 14, above). This anomalous result could be due to either ion exchange, precipitation, or analysis error. Similar to experiment WRRI-2, the

Table 9a. Data for Experiment WRRI-4. All data for effluent samples, unless otherwise noted in the comment column.

Sample #	Sample Interval Interval (hours)	Time Elapsed Total (hours)	Sample Volume (cm^3)	Pressure (bars)	pH	Comment Solution flux 100 ml/hr
1	--	--	106.12	--	6.35	pump solution
2	1.000	1.000	100.00	2.55	5.93	
3	1.000	2.000	125.44	2.69	5.89	
4	1.000	3.000	100.83	2.76	5.89	
5	1.017	4.017	100.72	2.83	6.09	
6	0.950	4.967	99.57	2.83	6.09	
7	0.950	5.917	100.85	3.20	6.24	
8	0.950	6.867	94.27	3.20	6.20	
9	1.017	7.884	100.73	3.17	6.22	
20	1.000	8.884	117.69	3.24	5.96	
11	0.950	9.834	97.57	3.24	6.72	
12	0.950	10.784	92.00	3.24	7.20	
13	4.333	15.117	436.4	3.59	6.08	
14	4.400	19.517	437.7	3.72	6.53	
15	4.617	24.134	458.5	3.86	6.37	
16	4.300	28.434	430.6	4.14	6.33	
17	4.533	32.967	456.4	4.27	6.29	
18	4.366	37.333	435.6	4.41	6.32	
19	4.433	41.766	444.6	4.62	6.21	
20	4.433	46.199	444.3	4.62	6.05	
21	4.600	50.799	461.2	4.83	6.28	
22	4.300	55.099	427.6	4.90	6.36	
23	3.600	58.699	360.6	4.96	6.05	
24	--	--	--	--	6.55	pump solution
25	--	--	--	--	6.11	cell solution
26	--	--	--	--	--	blank

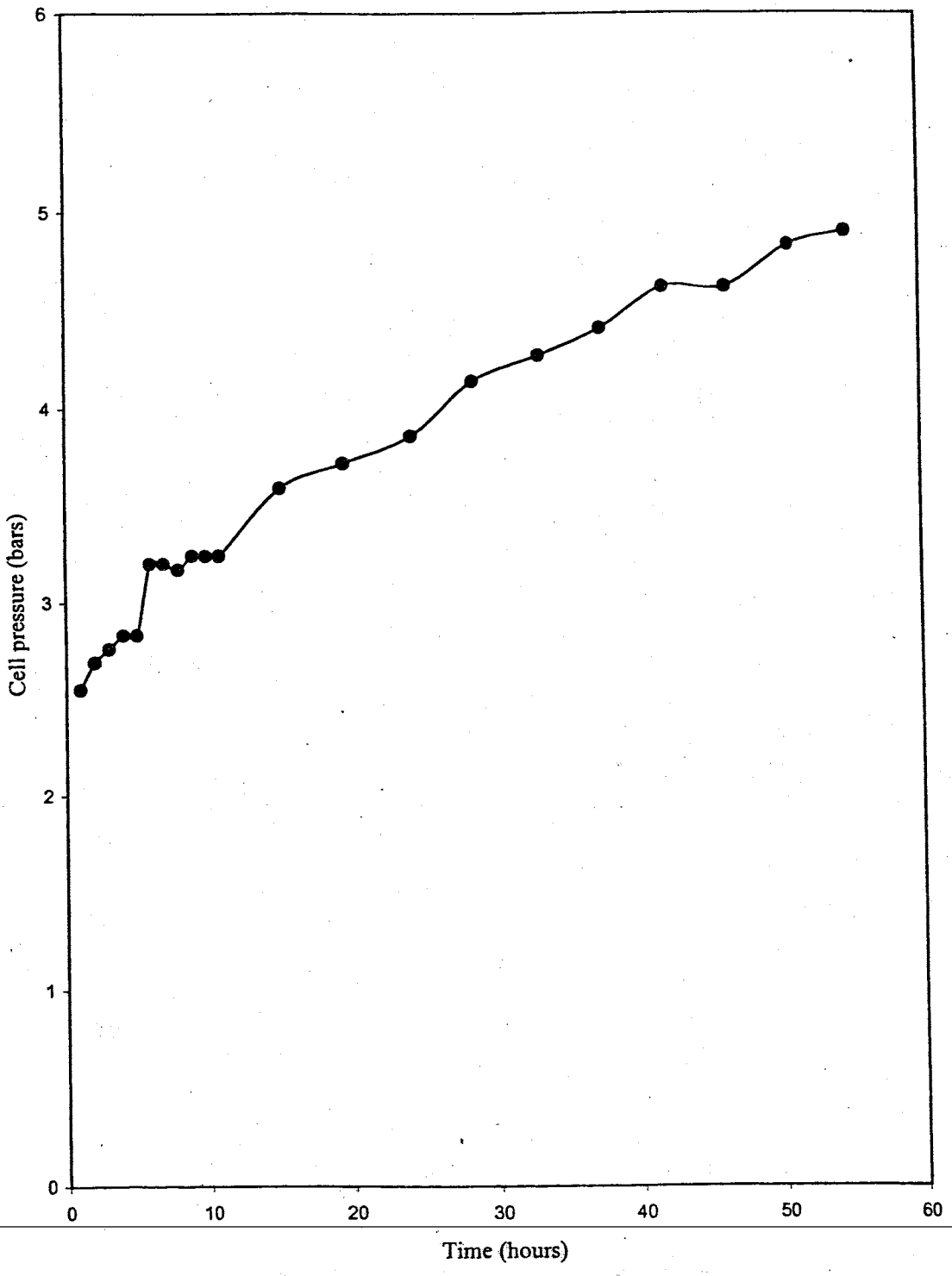

Figure 12. Time versus cell pressure for WRRI-4.

Table 9b. Chemical analyses for WRRI-4 (Performed by graphite furnace analysis unless otherwise noted). All data for effluent samples, unless otherwise noted in the comment column.

Sample #	HCO_3 (mN)	Cu (ppb)	Cr (ppb)	Ni (ppb)	Na[1] (ppb)	Ca[1] (ppm)	Comments
1	0.177	169	0.6	2.4	858	0	pump solution
2	0.110	16.7	0.6	8.0	788	0	
3	0.135	8.9	1.3	0.9	782	0	
4	0.115	11.7	0.3	2.1	790	0	
5	0.101	9.1	0.7	1.2	846	0	
6	0.110	7.6	0.6	0.5	886	0	
7	0.159	7.6	0.5	1.8	968	0	
8	0.147	5.7	1.3	0.5	935	0	
9	0.135	7.6	0.5	0.9	959	0	
10	0.152	7.9	0.4	0.8	1051	0	
11	0.149	20.2	0.9	1.0	986	0	
12	0.151	17.8	0.8	0.9	962	0	
13	0.163	27.2	0.2	1.1	965	0	
14	0.154	9.4	0.2	0.9	969	0	
15	0.167	11.2	0.3	2.9	987	0	
16	0.168	19.0	0.5	4.5	1009	0	
17	0.177	14.0	0.4	1.8	9971	0	
18	0.172	12.4	0.5	1.4	959	0	
19	0.172	32.9	0.2	0.8	915	0	
20	0.182	41.9	0.3	1.4	947	0	
21	0.190	52.2	1.2	1.2	941	0	
22	0.207	64.9	0.5	2.0	1135	0	
23	0.225	60.5	1.8	1.8	1053	0	
24	0.201	227	0.5	5.5	889	0	pump solution
25	0.245	179	0.3	2.8	1818	0	cell solution
26	--	1.6	0.3	1.2	0	0	blank

[1] analyses by flame atomic adsorption

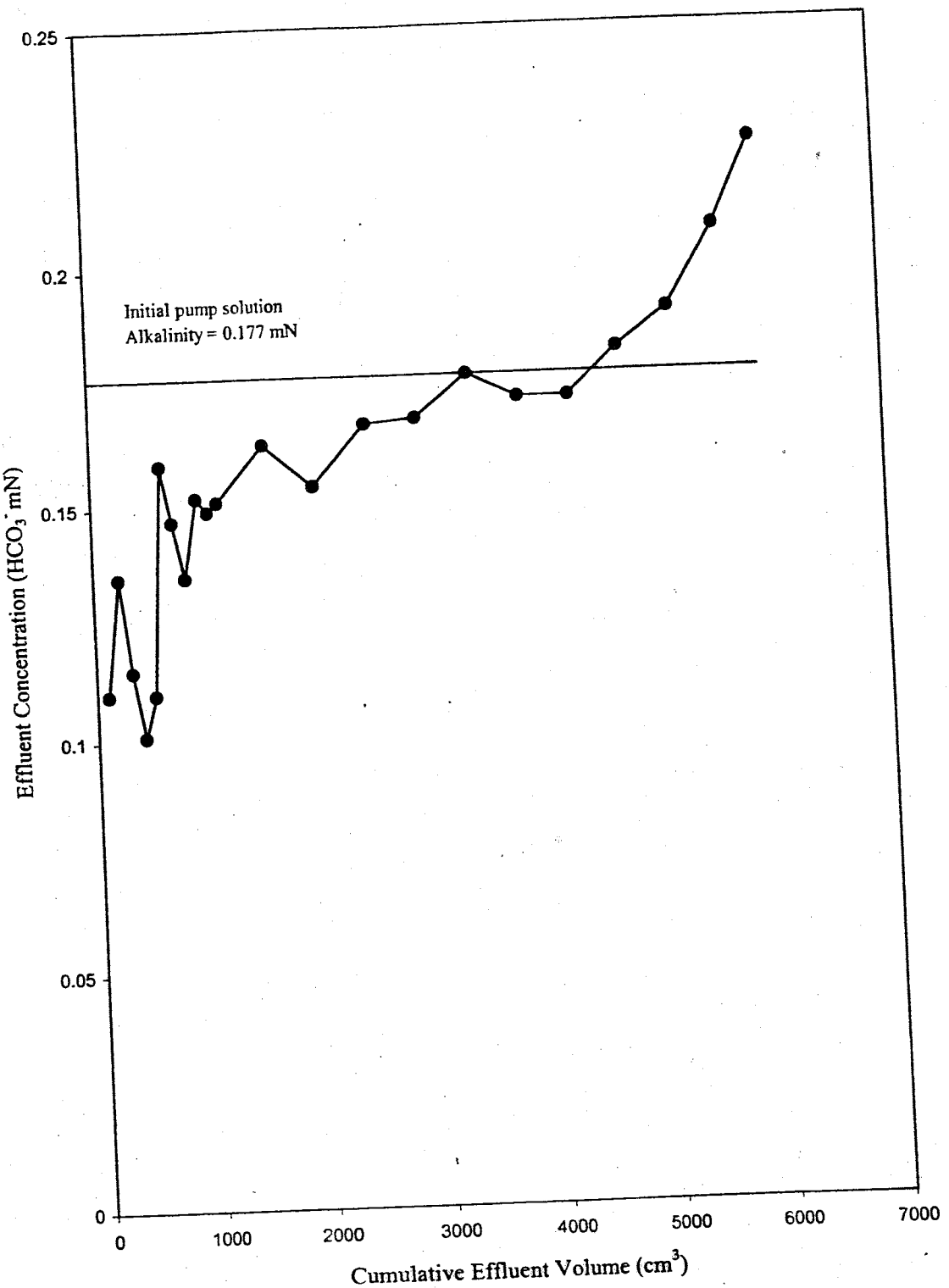

Figure 13. Cumulative effluent volume versus effluent sample alkalinity concentration for WRRI-4.

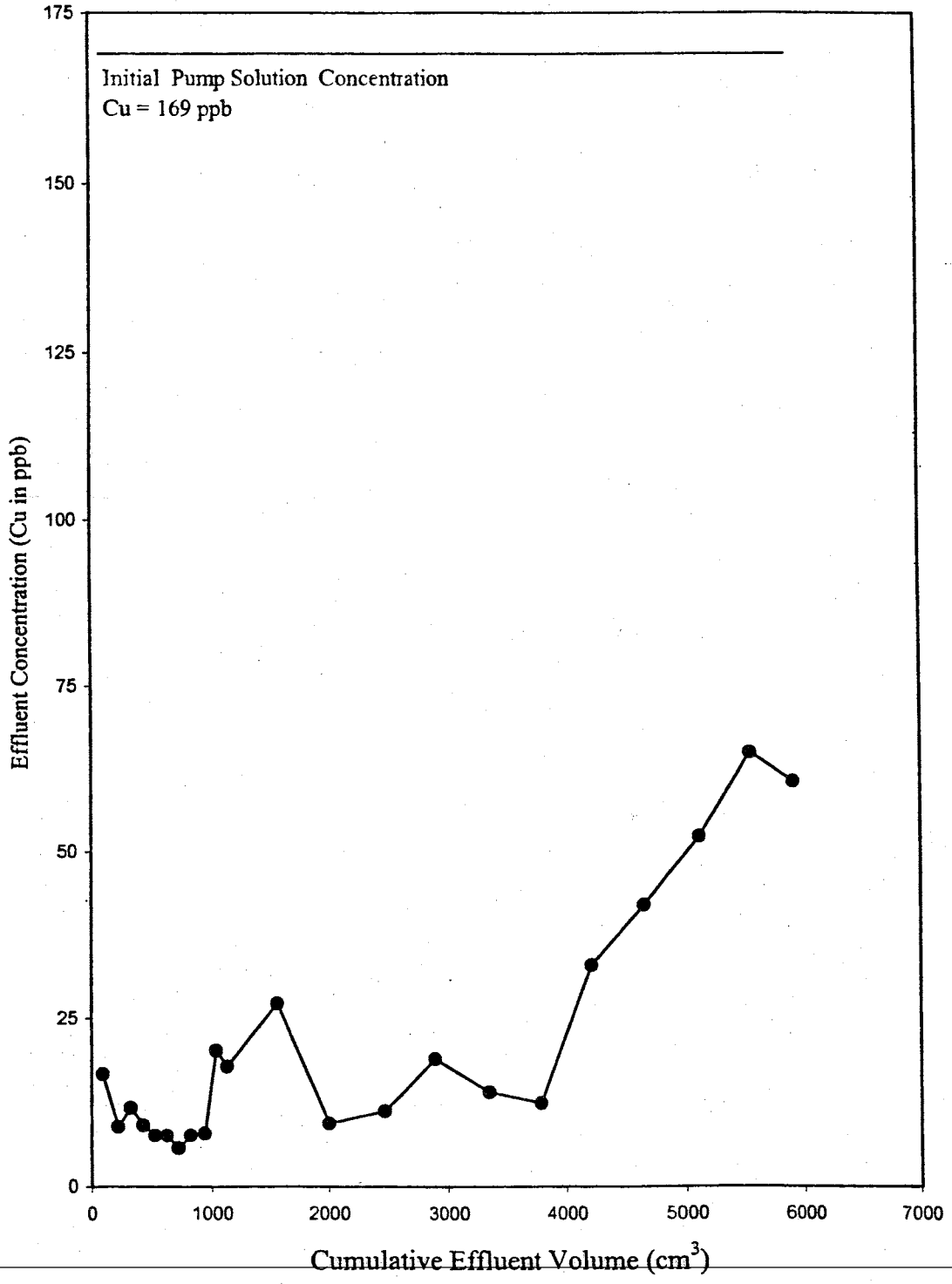

Figure 14. Cumulative effluent volume versus effluent sample copper concentration in ppb for WRRI-4.

effluent copper concentrations were low for the duration of the experiments. However, the effluent copper concentrations increased significantly toward the end of the run.

Scanning electron photomicrographs as well as electron microprobe energy dispersive analysis of the membrane confirmed the presence of copper precipitation on the high pressure membrane face. It is suspected that this copper mineralization is in the form of copper carbonate, but because carbon was used as a coating agent in the sample preparation for microprobe analysis, this is impossible to confirm. Unlike experiment WRRI-2, no nickel or iron phases were present on the membrane surface, although the concentrations of these metals in the effluent samples are similar to those found in run WRRI-2. The precipitates observed on the membrane face were common in nature, but not abundant. A number of the precipitates on the membrane face displayed good crystallinity, while others appeared to be amorphous in nature (Figures 15 and 16).

2.2.2.4 WRRI-7

An approximately 80% saturated copper carbonate solution was hyperfiltrated through a sedimented clay membrane at 10 ml/hr in this experiment, a much lower solution flux rate than in any of the previous experiments. The system reached a final ΔP of 6.19 bars (90 psi) (Table 10a, Figure 17). Both the alkalinity and the copper concentration of the cell solution were significantly lower than that measured for the input, by 43% and 18% respectively (Table 10b, Figure 18). Furthermore, the bicarbonate alkalinity of the final effluent sample was significantly lower than the final aliquot sampled from the pump (Figure 19). It is suspected that the stock solution for this experiment was poorly buffered, and interaction with atmospheric CO_2 within the stock

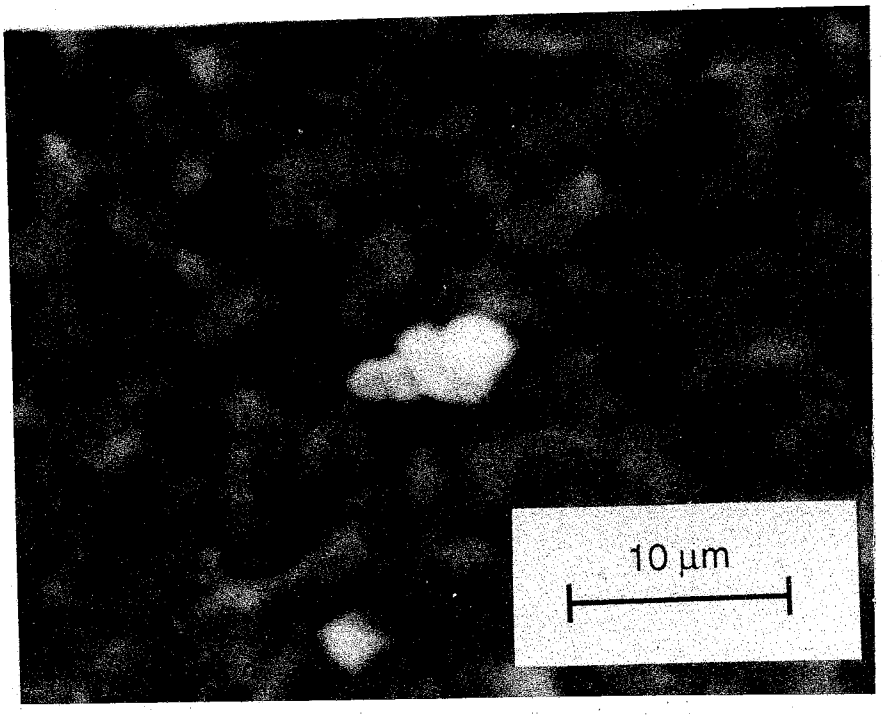

Figure 15. Scanning electron photomicrograph of copper particle on high-pressure membrane face from experiment WRRI-4.

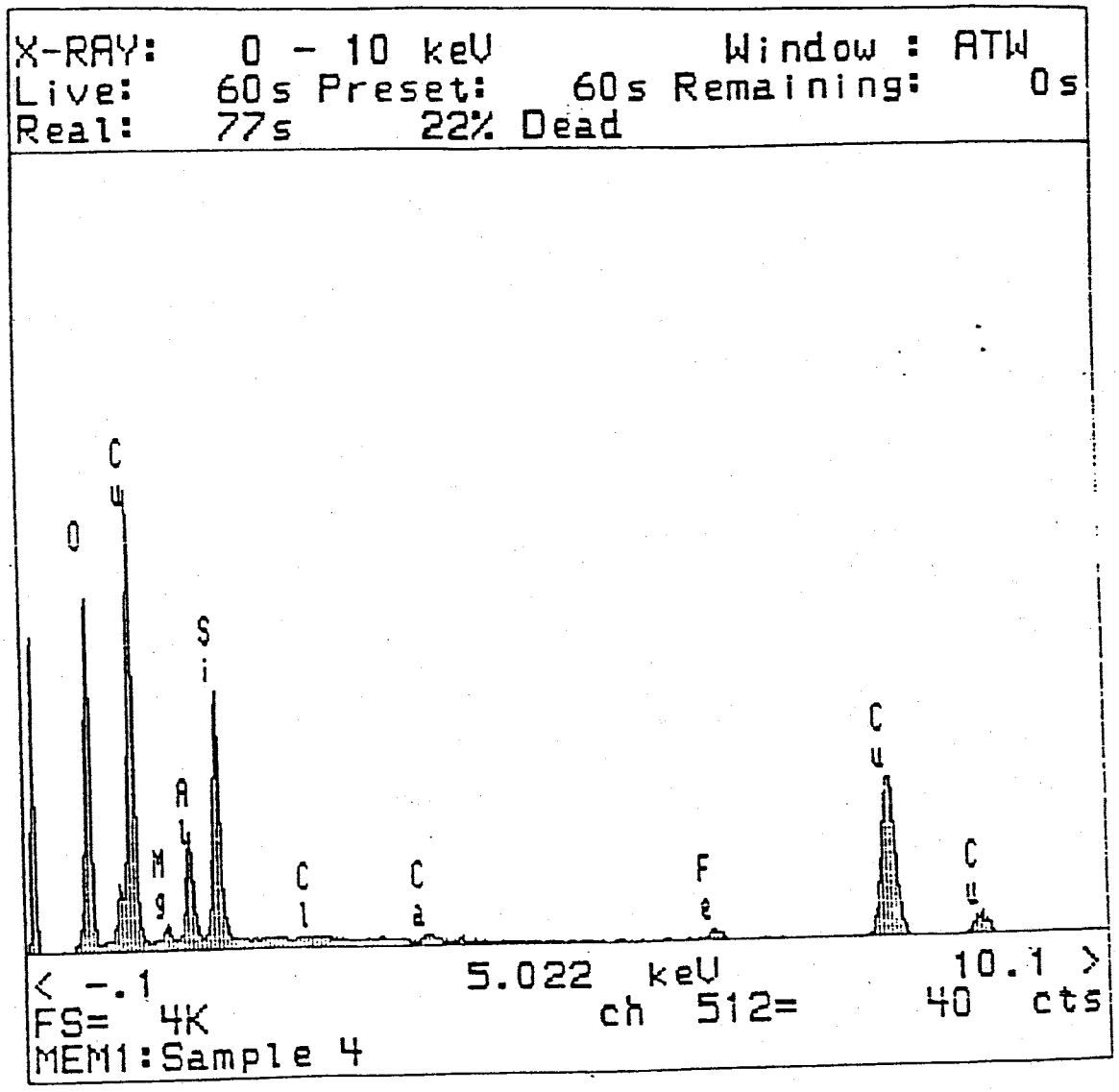

Figure 16. Energy dispersive spectra of elements present in the particle on the surface of the membrane after experiment WRRI-4.

Table 10a. Data for Experiment WRRI-7. All data for effluent samples, unless otherwise noted in the comment column.

Sample #	Sample Interval (hours)	Time Elapsed Total (hours)	Sample Volume (cm^3)	Pressure (bars)	pH	Comments
1	--	--	--	--	7.28	pump
2	6.60	6.60	89.02	8.16	4.33	
3	8.32	14.92	81.73	8.37	4.83	
4	7.68	22.60	77.02	8.57	5.11	
5	11.92	34.52	119.68	8.57	5.43	
6	12.05	46.57	118.67	4.15	5.71	
7	11.75	58.32	118.57	5.17	5.95	
8	11.83	70.15	116.71	5.31	5.52	
9	12.42	82.57	123.26	5.37	3.97	
10	12.05	94.62	120.68	5.92	6.09	
11	11.63	106.52	115.94	5.71	6.50	
12	12.02	118.27	119.45	5.92	6.70	
13	12.20	130.37	120.52	5.78	6.53	
14	12.75	143.12	130.40	6.12	6.94	
15	11.93	155.05	115.68	5.99	6.05	
16	11.13	166.18	110.98	6.19	5.63	
17	--		--	--	7.06	pump
18	--		--	--	5.76	cell

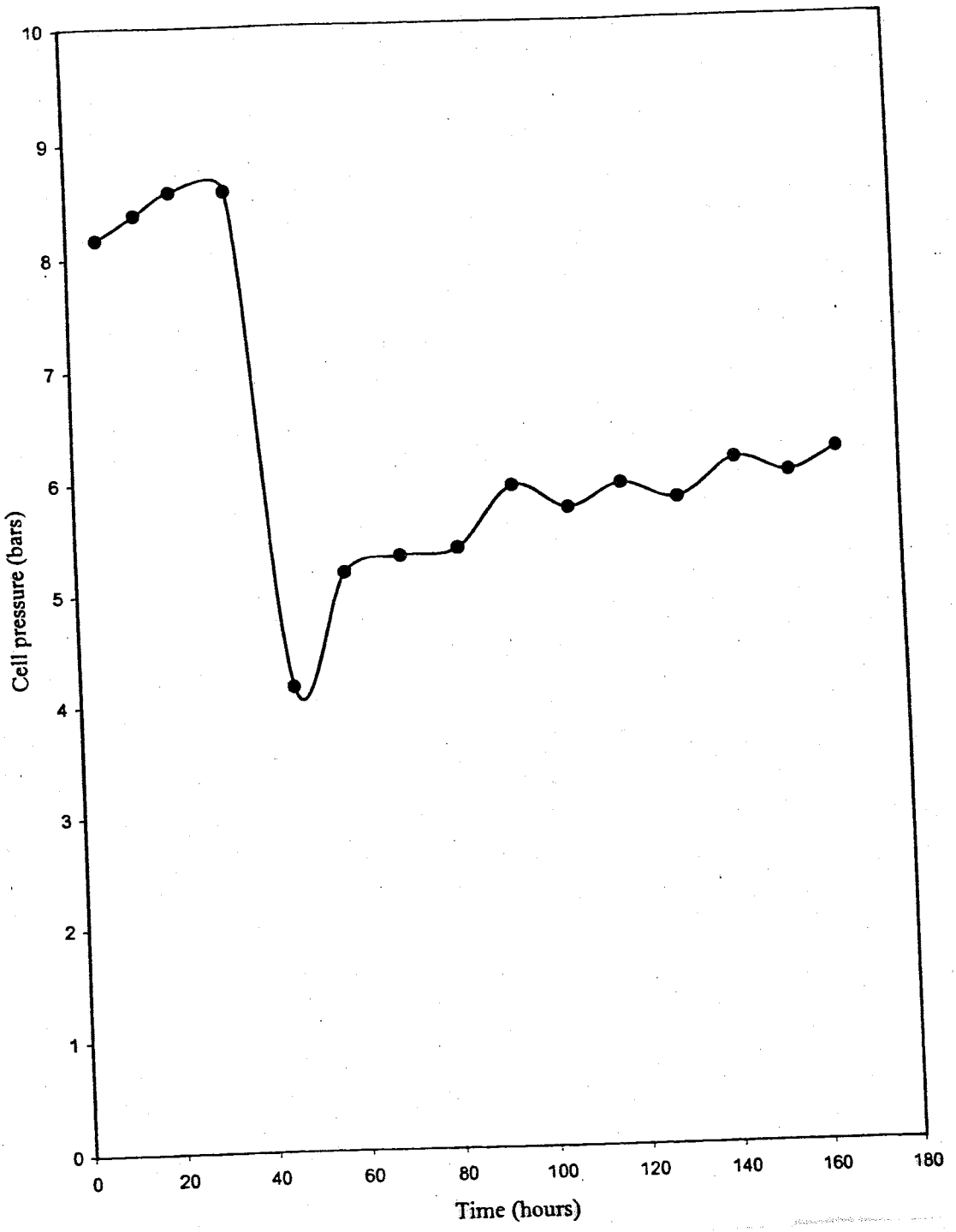

Figure 17. Time versus cell pressure for WRRI-7.

Table 10b. Chemical analysis for experiment WRRI-7. All data for effluent samples, unless otherwise noted in the comment column.

Sample #	HCO_3 (mN)	Cu (ppb)	Cr (ppb)	Ni (ppb)	Na (ppb)	Ca (ppb)	Comments
1	0.394	125	2.5	1.2	2730	4360	pump
2	0	3.2	5.3	4.9	859	3790	
3	0	3.5	3.3	2.6	1764	2360	
4	0	1.7	15.6	1.3	2340	1300	
5	0.046	2.3	9.9	0.9	2126	404	
6	0.083	1.5	2.4	0.8	2409	73	
7	0.071	1.4	16.6	4.1	2577	129	
8	0.071	2.7	4.6	1.2	2713	129	
9	0	2.4	6.9	0.9	2766	104	
10	0.109	2.7	1.0	0.4	2809	85	
11	0.135	3.7	0.3	0.8	2826	91	
12	0.141	6.8	0.9	0.7	2895	79	
13	0.098	5.8	0.4	0.6	2942	104	
14	0.098	5.9	0.3	0.7	2993	104	
15	0.095	7.6	0.4	0.6	3005	104	
16	0.048	8.6	0.8	1.6	3053	91	
17	0.078	124	0.8	1.8	2890	4619	pump solution
18	0.044	102	1.2	2.0	3172	408	cell solution

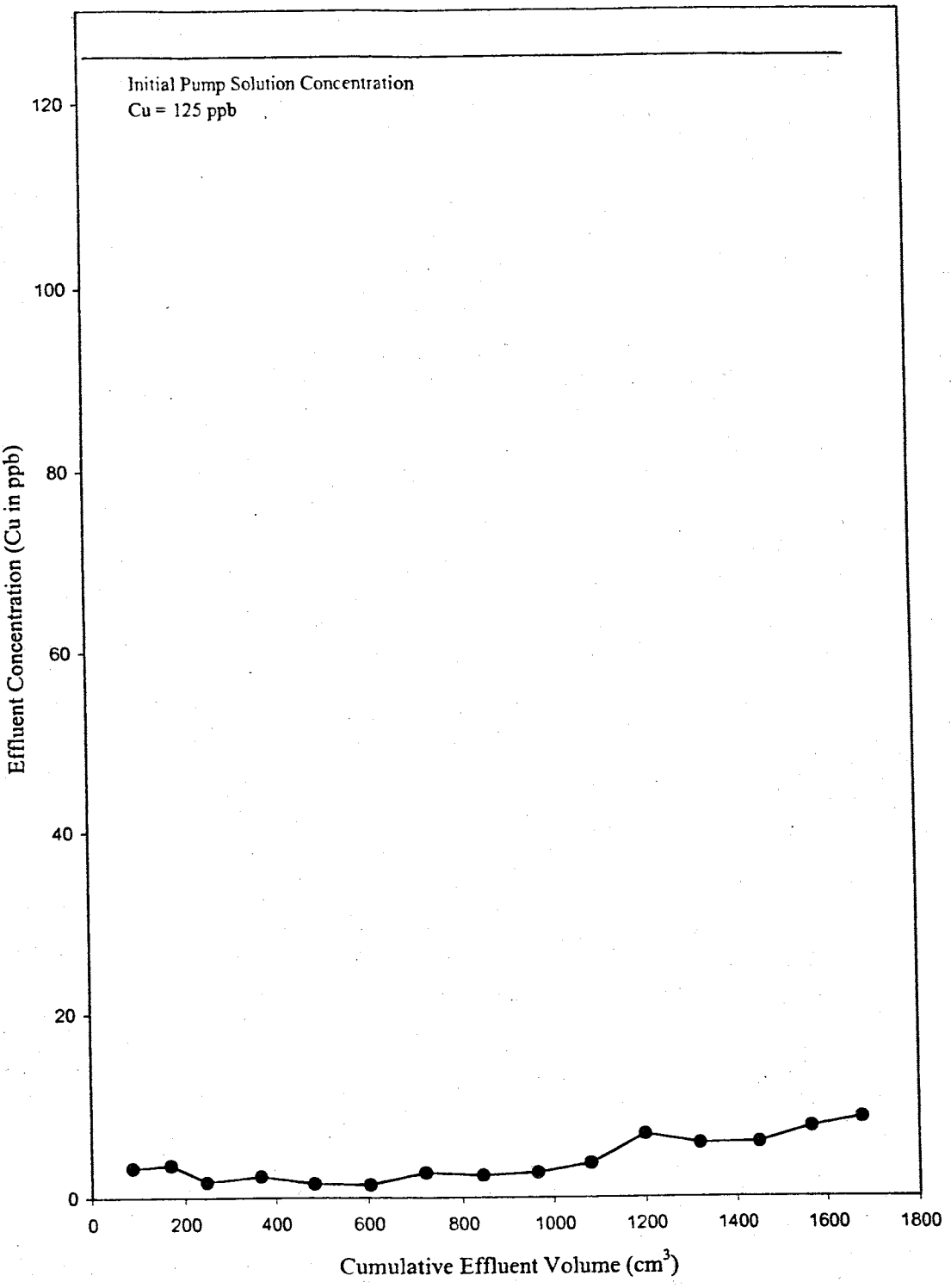

Figure 18. Cumulative effluent volume versus effluent sample copper concentration in ppb or WRRI-7.

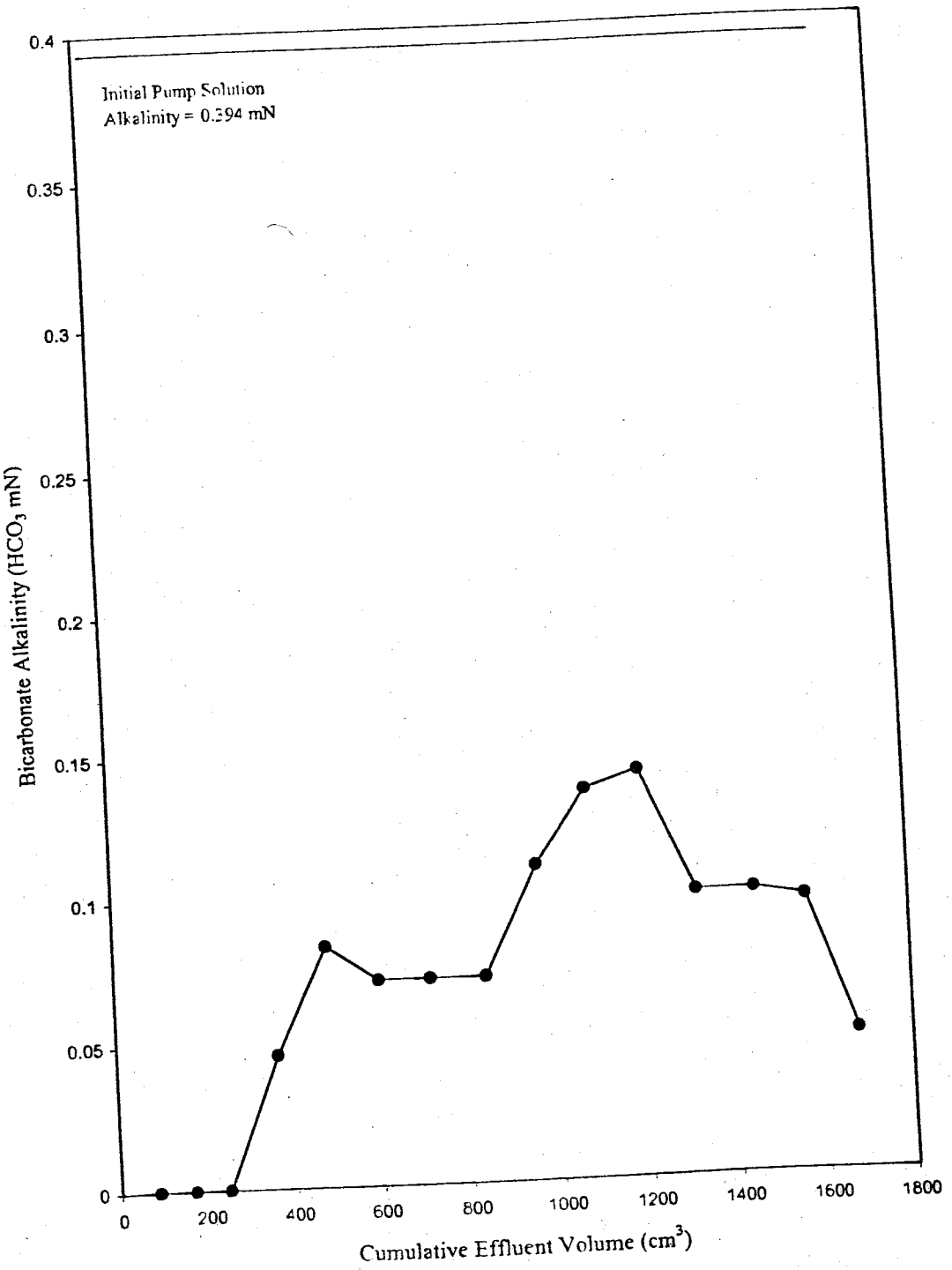

Figure 19. Cumulative effluent volume versus effluent sample alkalinity for WRRI-7.

storage container may have occurred during the experiment. The copper concentration in the pump solution remained steady, however, there were significant amounts of Na (2.7 ppm) and Ca (4.4 ppm) present in the make-up water used in this experiment due to problems with the deionization equipment. The concentration of Na in the effluent began lower than background, and slowly rose to just above background in the last half of the effluent samples collected. This probably occurred as a result of the exchange of copper and calcium ions for sodium cations attached to the clay membrane.

A scanning electron microscope analysis, as well as electron microprobe element mapping revealed that no particles were present on the surface of the membrane. It is speculated that CPL development was limited because sufficient time was not allotted for the experiment. Therefore, concentrations within the CPL did not exceed saturation so no precipitation occurred. Theoretically, however, precipitation should have occurred on this membrane. The only significant difference in this experiment, relative to the other experiments performed in this study, was that the solution flux was much lower in this run than in any of the other copper carbonate experiments. As described, one possibility might be that sufficient time was not allotted for CPL build-up, or the kinetics of the reaction may have been too slow for precipitation to form during this relatively low-flux experiment.

2.2.2.5 WRRI-8

The WRRI-8 experiment was the only copper experiment to make use of an undersaturated (≈80%) copper chloride solution in this study. The flow rate was set at 150 ml/hr for the duration of this experiment, and the final ΔP for this trial was 64.26 bars

or 932 psi (Table 11a, Figure 20). The chloride concentration of this effluent in this experiment remained consistently lower than the input concentration for the duration of the run (Table 11b, Figure 21). The copper concentrations displayed similar results (Figure 22). The most outstanding observation from the analyses of the effluent samples is that the cell solution concentration was significantly higher than the input solution; an indication that membrane processes were occurring. Approximately 10 hours into the experiment, a visible greenish-yellow precipitate began forming on the membrane. However, this was difficult to confirm before the end of the experiment because the copper chloride solution had a strong blue-green color, prohibiting a clear view of the surface of the clay through the experimental cell. At the completion of the experiment, as the hyperfiltration cell was being disassembled, visible precipitate was observed, and the suspicion that the membrane was coated with precipitate was confirmed. Subsequent energy dispersive analysis on the microprobe displayed that the membrane did indeed precipitate copper chloride minerals on the high pressure face (Figures 23, and 24). The observed mineralization appeared to be ubiquitous on the membrane surface. No other mineral phases were detected on this membrane. Furthermore, effluent analysis established that no Na or Ca ions were present in any of the aliquots.

2.2.3 Lead Experiments

2.2.3.1 WRRI-5

This was the first of two experiments to utilize an undersaturated (80%) lead chloride solution. This solution was hyperfiltrated through a clay membrane at 125 ml/hr that was constructed with 0.6 grams of smectite. The final ΔP in this experiment was

Table 11a. Data for Experiment WRRI-8. All data for effluent samples, unless otherwise noted in the comment column.

Sample #	Sample Interval (hours)	Time Elapsed Total (hours)	Sample Volume (cm3)	Pressure (bars)	pH	Comments
1	--	--	--	--	3.83	pump solution
2	0.500	0.500	67.48	19.0	3.19	
3	0.517	1.017	78.38	21.2	3.22	
4	0.833	1.850	138.66	24.1	3.27	
5	0.833	2.683	106.97	27.0	3.18	
6	0.717	3.400	109.52	30.2	3.15	
7	0.800	4.200	122.01	32.1	3.27	
8	0.800	5.000	125.17	33.9	3.18	
9	1.000	6.000	152.85	34.6	3.18	
20	1.083	7.083	170.69	38.1	3.25	
11	1.067	8.150	170.88	40.1	3.17	
12	1.633	9.783	244.09	45.9	3.10	
13	1.517	11.300	230.71	48.5	3.17	
14	2.567	13.867	380.72	56.1	3.12	
15	2.800	16.667	426.98	62.8	3.10	
16	1.400	18.067	220.96	66.3	3.14	
17	--	--	238.64	66.3	3.08	cell solution
18	--	--	--	--	3.15	pump solution

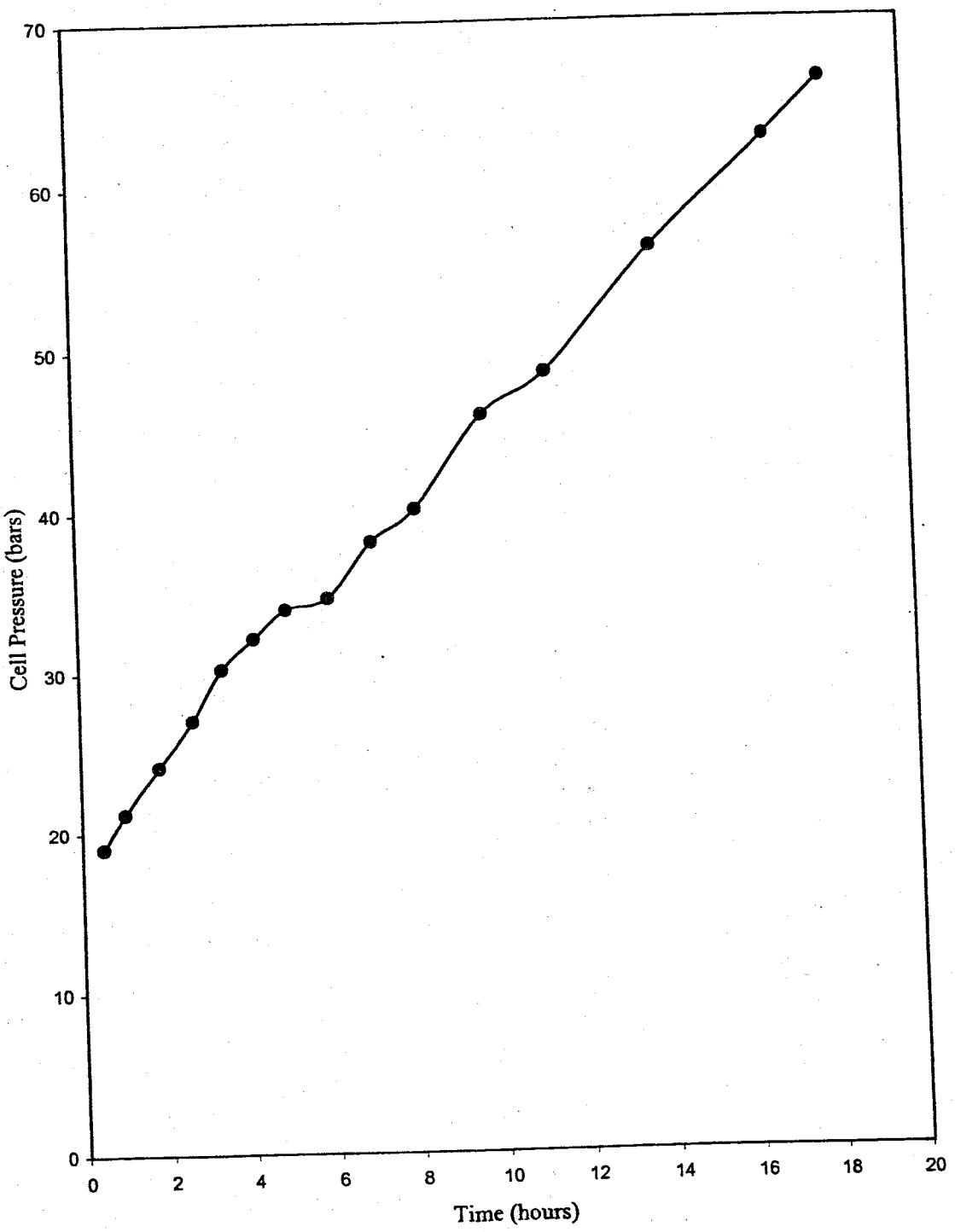

Figure 20. Time versus cell pressure in bars for WRRI-8.

Table 11b. Chemical Analysis for WRRI-8. All data for effluent samples, unless otherwise noted in the comment column.

Sample #	Cu (ppm)	Cl (ppm)	Na (ppm)	Ca (ppm)	Comments
1	1881	2309	0	0	pump solution
2	695	1978	0	0	
3	1762	1999	0	0	
4	1842	2194	0	0	
5	1825	2154	0	0	
6	1756	2203	0	0	
7	1768	2160	0	0	
8	1787	2193	0	0	
9	1704	1975	0	0	
10	1728	2242	0	0	
11	1666	1918	0	0	
12	1815	2202	0	0	
13	1833	1818	0	0	
14	1823	2244	0	0	
15	1859	2257	0	0	
16	1850	2271	0	0	
17	1953	2040	0	0	cell solution
18	1842	2195	0	0	pump solution

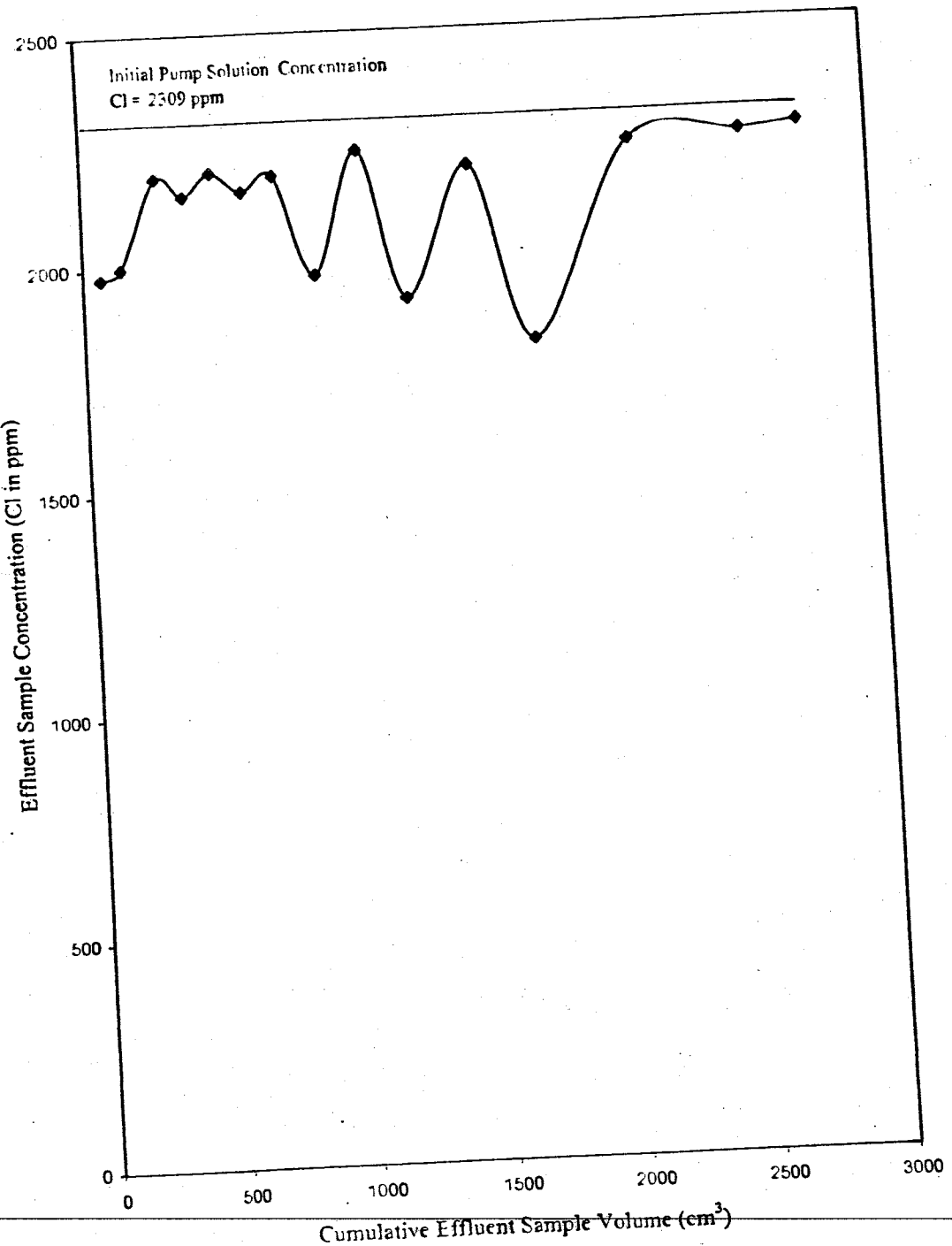

Figure 21. Cumulative effluent volume versus effluent sample chloride concentration in ppm for WRRI-8.

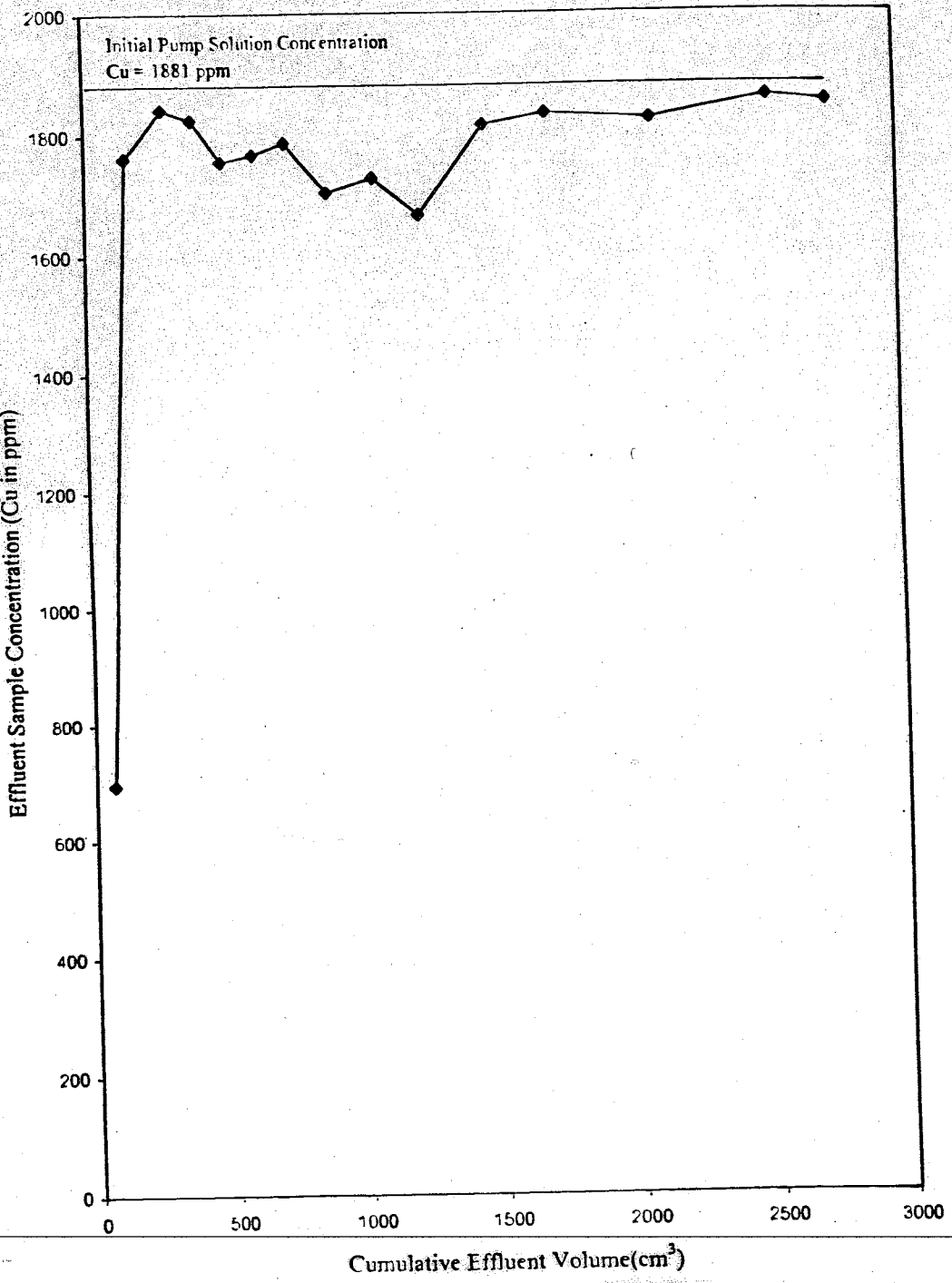

Figure 22. Cumulative effluent volume versus effluent sample copper concentration in ppm for WRRI-8.

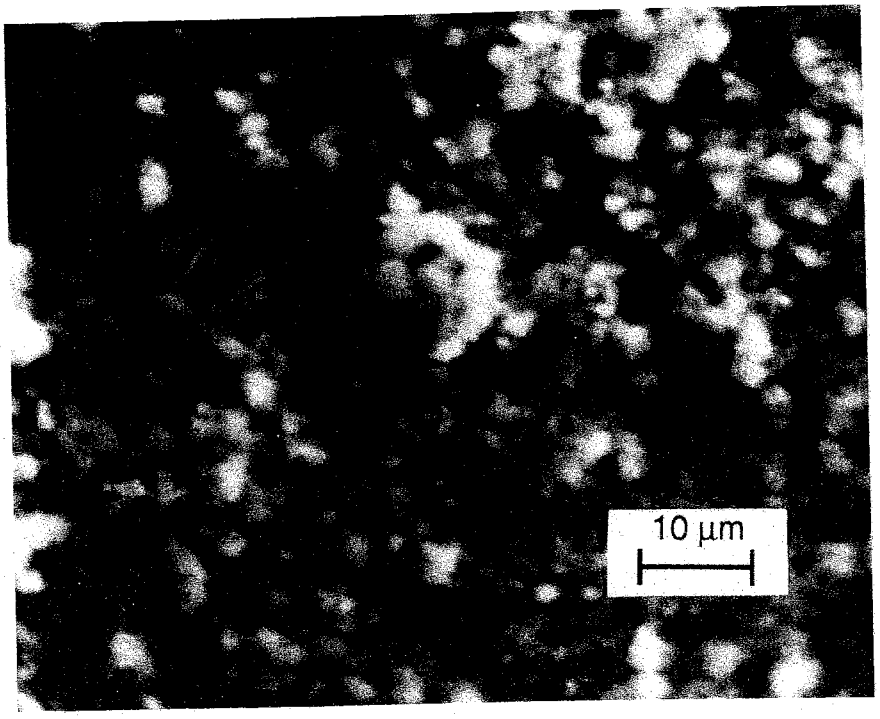

Figure 23. Scanning electron microprobe photograph of copper chloride precipitation on the surface of the membrane after experiment WRRI-8.

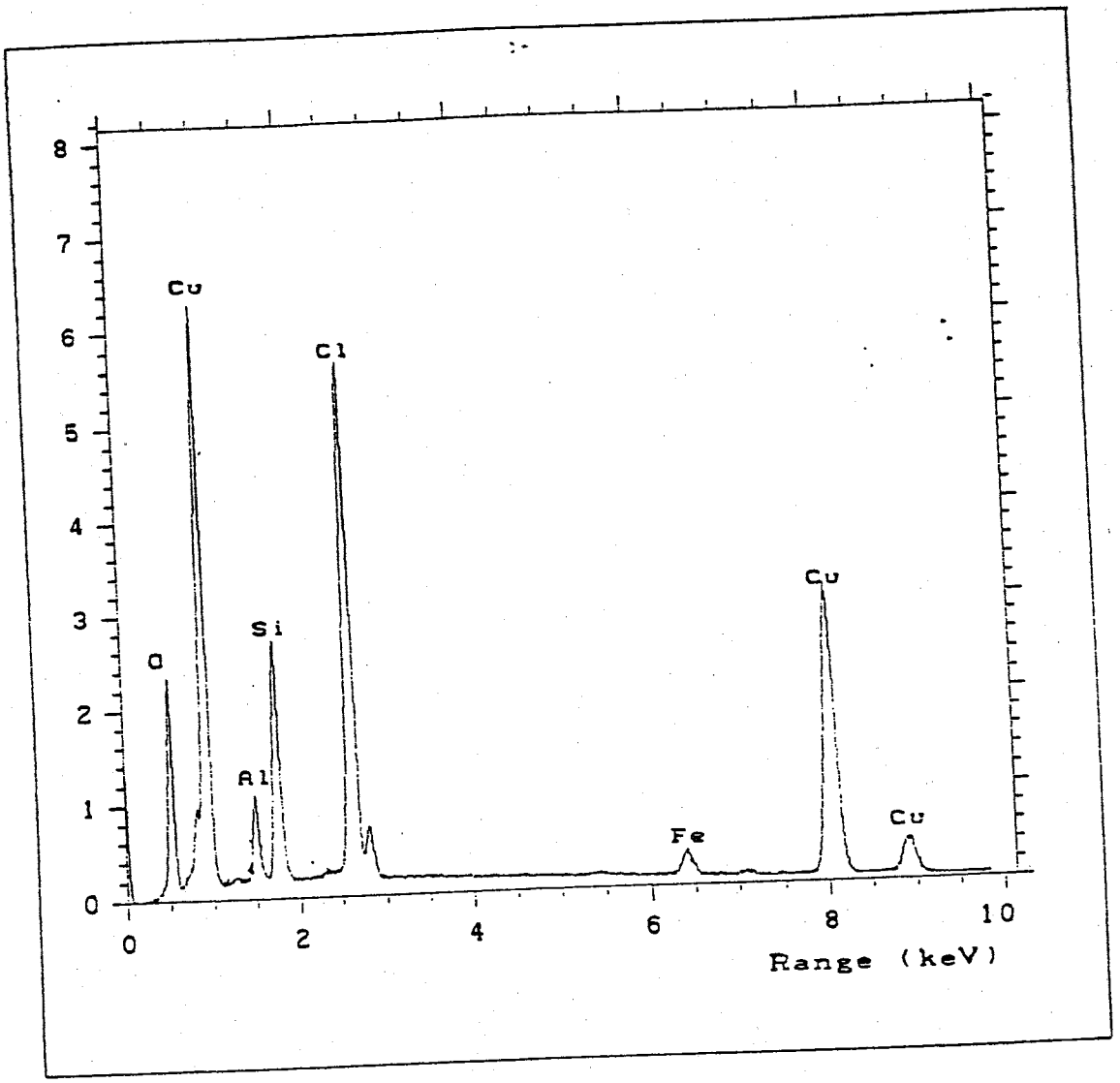

Figure 24. Energy dispersive spectra of mineralization on the surface of the membrane from experiment WRRI-8.

24.1 bars, or 355 psi (Table 12a, Figure 25). The concentration of the chloride in the effluent samples remained consistently lower than the input concentration for this ion (Table 12b, Figure 26). Moreover, the chloride concentration of the pump solution remained constant for the duration of the trial.

The chloride ion is conservative, and is not significantly involved in ion exchange processes. Therefore, the decrease in Cl concentration in the effluent minus any concentration increase in the CPL or the cell solution is the result of precipitation at the membrane face. However, this is difficult to quantify, because the cell solution showed no significant increase in chloride concentration. That is not to say that no CPL formed, on the contrary, the length of the CPL that may have formed during this experiment would have been quite small, approximately 0.008 cm. So a representative sample of the CPL would have been difficult to collect without disturbing the clay membrane. The measured concentrations of lead for this run were erratic, and do not appear reliable as they suggest more lead exited the experimental cell than was input (Figure 27). This is not possible. It is suspected that the poor results of the lead samples for this experiment may have been due to analytical error. The membrane parameters for both this experiment, as well as the next lead experiment were calculated from anion concentrations.

One of the most encouraging findings of this experiment was the presence of a greenish-yellow precipitate on the membrane face that could be seen through the clear acrylic cell 12 hours into the run. This experiment lasted 22.85 hours. Analysis of the membrane face on an electron microprobe revealed the presence of numerous dendritic

Table 12a. Data for Experiment WRRI-5. All data for effluent samples, unless otherwise noted in the comment column.

Sample #	Sample Interval (hours)	Time Elapsed Total (hours)	Sample Volume (cm^3)	Pressure (bars)	pH	Comment
1	--	--	--	--	3.01	pump solution
2	0.917	0.917	112.53	19.03	2.94	
3	1.000	1.917	124.90	19.44	2.96	
4	1.000	2.917	122.66	19.79	3.00	
5	0.917	3.834	121.33	20.06	2.97	
6	1.000	4.834	129.97	21.51	2.98	
7	1.000	5.834	126.31	21.37	2.96	
8	1.000	6.834	128.49	22.20	2.98	
9	1.000	7.834	120.63	22.27	2.95	
10	0.933	8.767	123.62	25.23	2.91	
11	0.983	9.750	126.17	25.51	2.99	
12	1.033	10.783	126.53	25.65	2.99	
13	0.933	11.716	117.82	25.72	3.09	
14	0.900	12.616	117.93	24.48	2.97	
15	0.883	13.499	111.16	24.55	3.00	
16	0.883	14.382	111.44	24.68	2.97	
17	0.967	15.349	120.20	24.68	3.04	
18	0.850	16.199	109.18	24.61	3.00	
19	0.917	17.116	115.23	24.75	2.99	
20	0.933	18.049	118.11	24.82	2.99	
21	0.917	18.966	112.97	24.82	2.97	
22	0.917	19.833	118.35	24.68	2.97	
23	1.067	20.950	133.08	24.68	3.02	
24	0.933	21.883	118.80	24.55	3.02	
25	0.967	22.850	123.11	24.48	2.97	
26	--	--	--	--	--	cell solution
27	--	--	--	--	3.04	pump solution

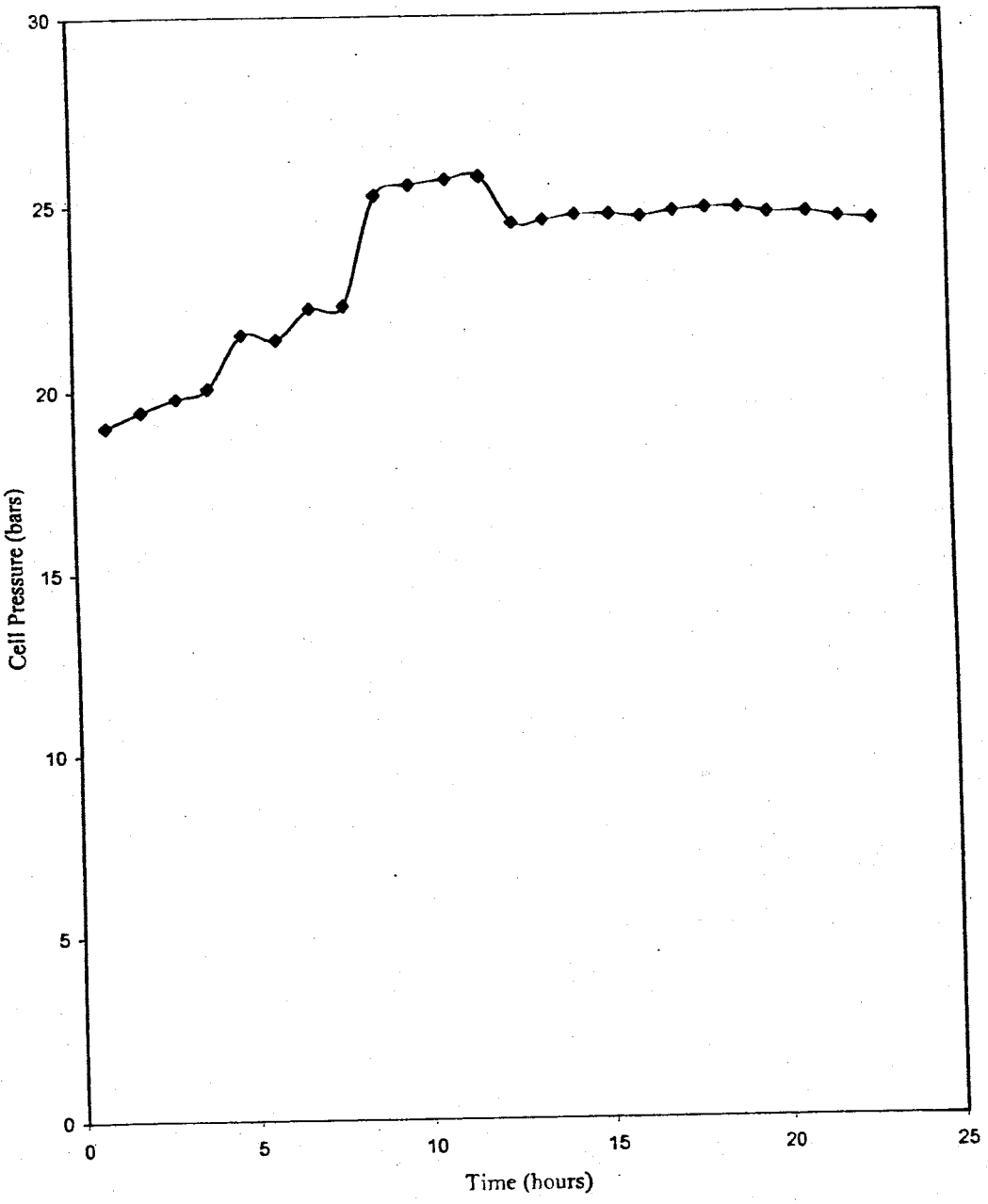

Figure 25. Time versus cell pressure in bars for WRRI-5.

Table 12b. Chemical analysis for WRRI-5. All data for effluent samples, unless otherwise noted in the comment column.

Sample #	Cl (ppm)	Pb (ppm)	Na (ppm)	Ca (ppm)	Comments
1	1931	4561	0	0	pump solution
2	1844	4159	0	15.7	
3	1901	4908	0	0	
4	1896	5897	0	0	
5	1852	5834	0	0	
6	1832	6012	0	0	
7	1965	5639	0	0	
8	1898	5769	0	0	
9	1944	5611	0	0	
10	1894	5686	0	0	
11	1873	5632	0	0	
12	1851	5583	0	0	
13	1840	5436	0	0	
14	1880	5901	0	0	
15	1871	5564	0	0	
16	1916	6181	0	0	
17	1716	5615	0	0	
18	1922	5679	0	0	
19	1889	4844	0	0	
20	1785	5334	0	0	
21	1807	5271	0	0	
22	1778	5072	0	0	
23	1777	4819	0	0	
24	1819	4778	0	0	
25	1837	5597	0	0	
26	1900	4883	0	0	cell solution
27	1927	4987	0	0	pump solution

Note: Chloride analysis performed by titration. Pb, Na, and Ca analysis performed by flame atomic adsorption.

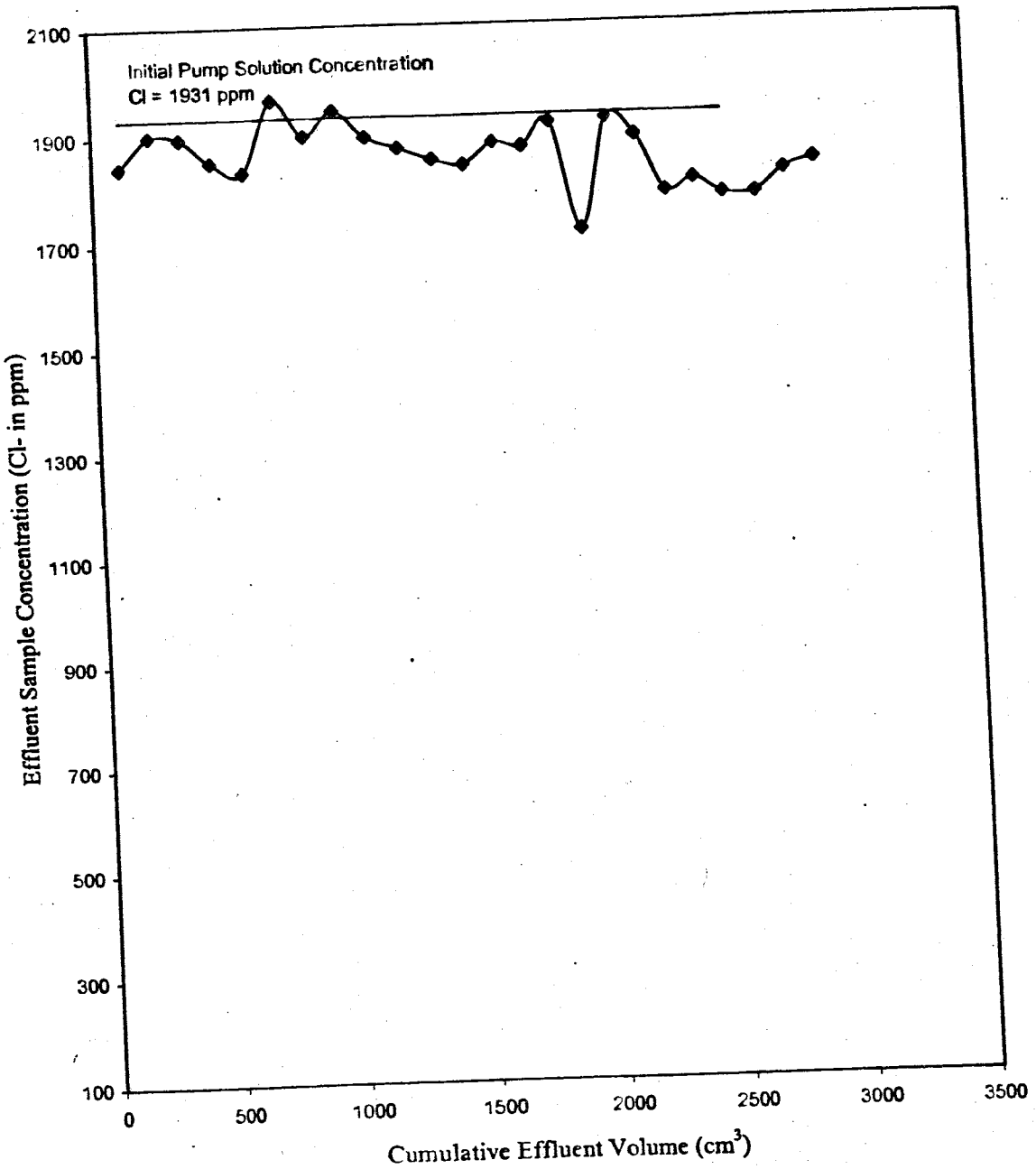

Figure 26. Cumulative effluent volume versus effluent sample chloride concentration for WRRI-5.

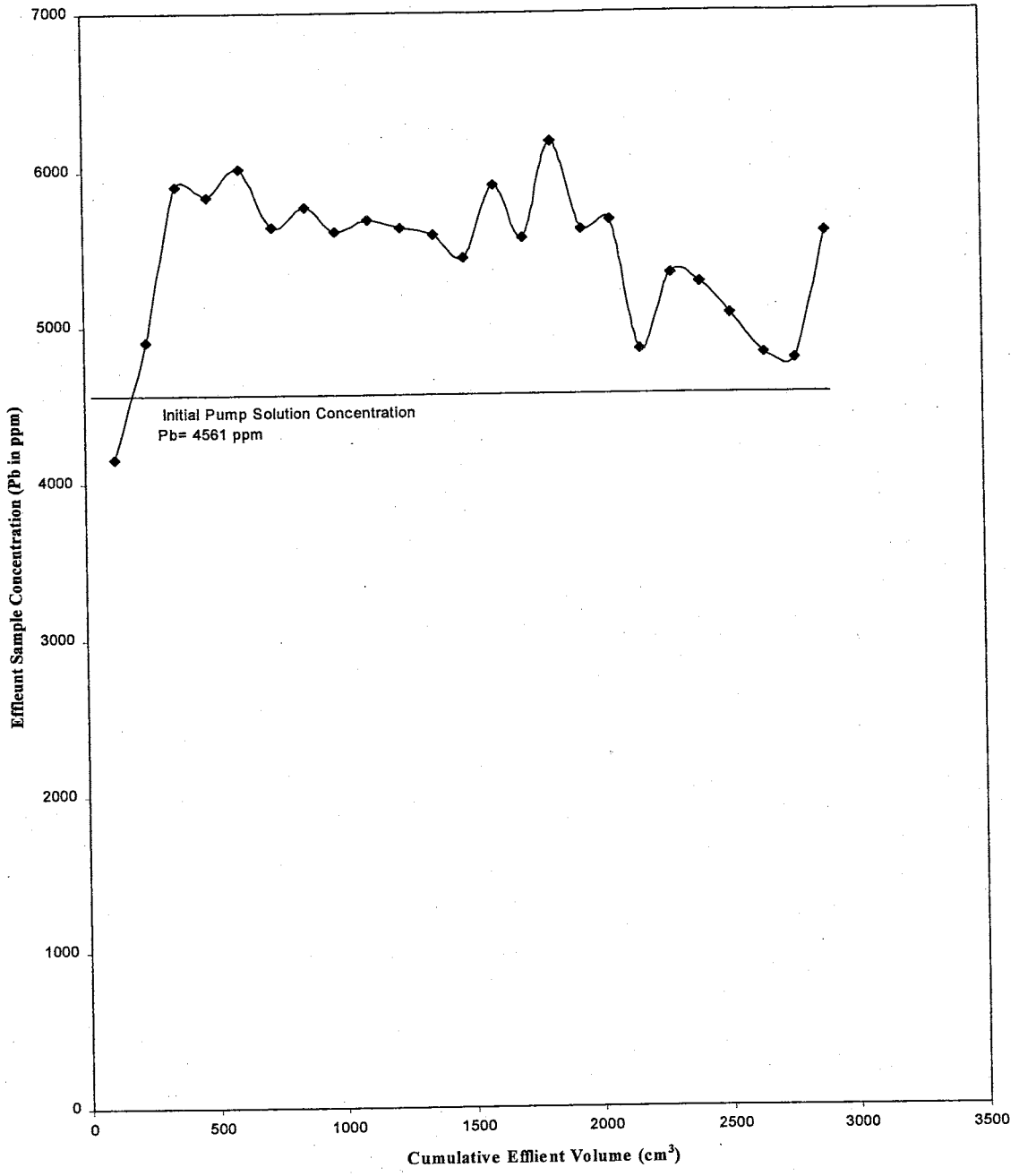

Figure 27. Cumulative effluent volume versus effluent sample lead concentration in ppm for WRRI-5.

crystalline particles on the surface of the membrane (Figures 28 and 29). Dendritic crystals are characteristic of rapid mineral formation. The electron microprobe energy dispersive analysis and X-ray fluorescence analysis revealed that these precipitates were in fact composed of lead chloride, and the mineral phase was consistent with that of cotunnite ($PbCl_2$).

2.2.3.2 WRRI-6

The second of the lead experiments made use of a 23% saturated lead chloride solution that was hyperfiltrated through a sedimented clay membrane, constructed with 0.06 grams of bentonite, at a flow rate of 75 ml/hr. The final ΔP for this trial was 16.4 bars, or 241 psi (Table 13a, Figure 30). The effluent chloride concentration of the first sample was low with subsequent concentrations rising towards the value of the input concentration (Table 13b, Figure 31). The lead analysis once again suggested the impossible; more lead exited the membrane than entered it (Figure 32). Once, again, analytical equipment malfunctions were suspected. No calcium was detected in the effluent, however, 40.6 ppm of sodium was present in the first effluent sample, suggesting that a significant amount of ion exchange was occurring early in the experiment. This Na concentration dropped quickly, and there was no trace of it by the time the eighth effluent sample was collected. As in WRRI-5, a greenish-yellow precipitate was visible on the membrane surface before the completion of the experiment, which lasted 25.28 hours in total. The scanning electron photomicrographs disclosed numerous dendritic crystal formations on the surface of the membrane, very much like those seen on the membrane of experiment WRRI-5. X-ray diffraction analysis

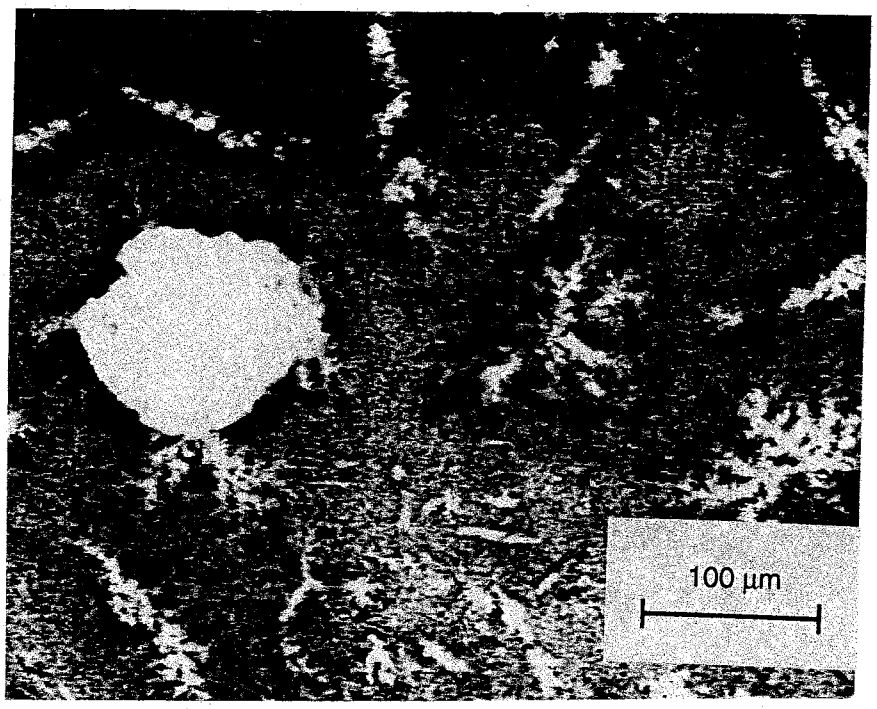

Figure 28. Scanning electron microphotograph of lead chloride particles on the surface of the membrane after experiment WRRI-5.

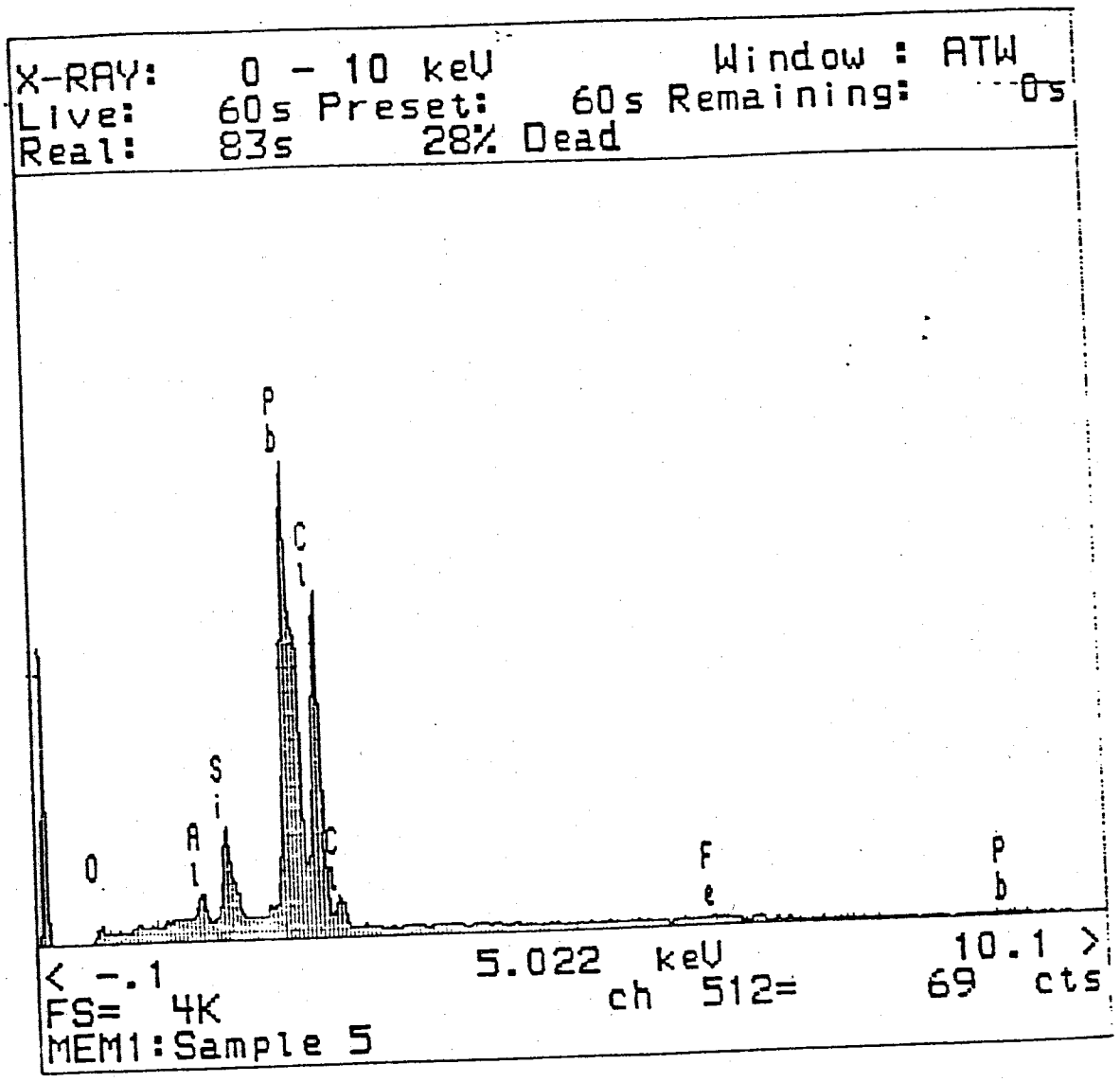

Figure 29. Energy dispersive spectra of elements present in the particle on the surface of the membrane after experiment WRRI-5.

Table 13a. Data for experiment WRRI-6. All data for effluent samples, unless otherwise noted in the comment column.

Sample #	Sample Interval (hours)	Time Elapsed Total (hours)	Sample Volume (cm^3)	Pressure (bars)	pH	Comments
1	--	--	--	--	4.17	pump solution
2	0.850	0.850	66.13	16.27	3.92	
3	1.167	2.017	87.69	16.20	4.00	
4	1.300	3.317	97.65	16.24	4.20	
5	1.250	4.567	93.59	16.13	4.20	
6	1.200	5.767	89.87	16.06	4.13	
7	1.350	7.117	102.49	15.65	4.15	
8	1.600	8.717	120.33	15.79	4.20	
9	1.733	10.450	129.79	16.00	4.20	
10	1.733	12.183	130.12	16.20	4.14	
11	1.767	13.950	134.59	16.20	4.19	
12	1.733	15.683	128.85	16.41	4.18	
13	1.367	17.050	102.41	16.48	4.22	
14	1.683	18.733	125.94	16.48	4.22	
15	1.583	20.316	121.96	16.69	4.20	
16	1.867	22.183	138.48	16.75	4.28	
17	1.417	23.600	105.77	16.55	4.27	
18	1.683	25.283	125.79	16.62	4.28	
19	--	--	--	--	4.23	pump solution
20	--	--	--	--	4.22	cell solution

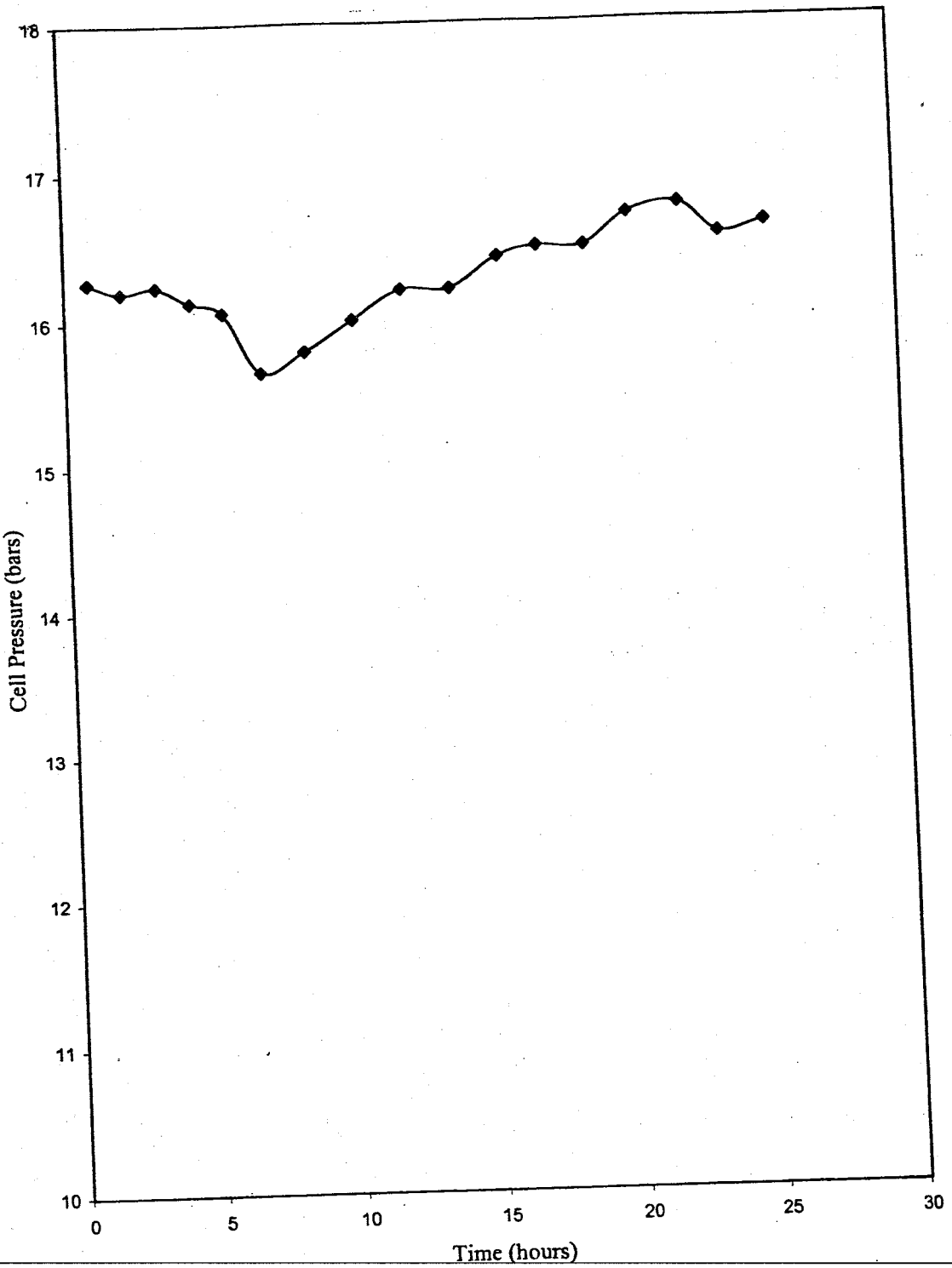

Figure 30. Time versus cell pressure in bars for WRRI-6.

Table 13b. Chemical analysis for WRRI-6. All data for effluent samples, unless otherwise noted in the comment column.

Sample #	Cl (ppm)	Pb (ppm)	Na (ppm)	Ca (ppm)	Comments
1	556	1569	0	0	pump solution
2	525	1393	40.6	0	
3	560	1532	0.82	0	
4	557	1497	0.23	0	
5	551	1601	0.29	0	
6	550	1660	0.28	0	
7	553	1493	0.17	0	
8	551	1601	0.05	0	
9	550	1605	0	0	
20	551	1662	0	0	
11	545	1719	0	0	
12	558	1652	0	0	
13	560	1627	0	0	
14	561	1556	0	0	
15	560	1595	0	0	
16	553	1612	0	0	
17	553	1811	0	0	
18	553	1679	0	0	
19	550	1487	0	0	pump solution
20	577	1696	0	0	cell solution

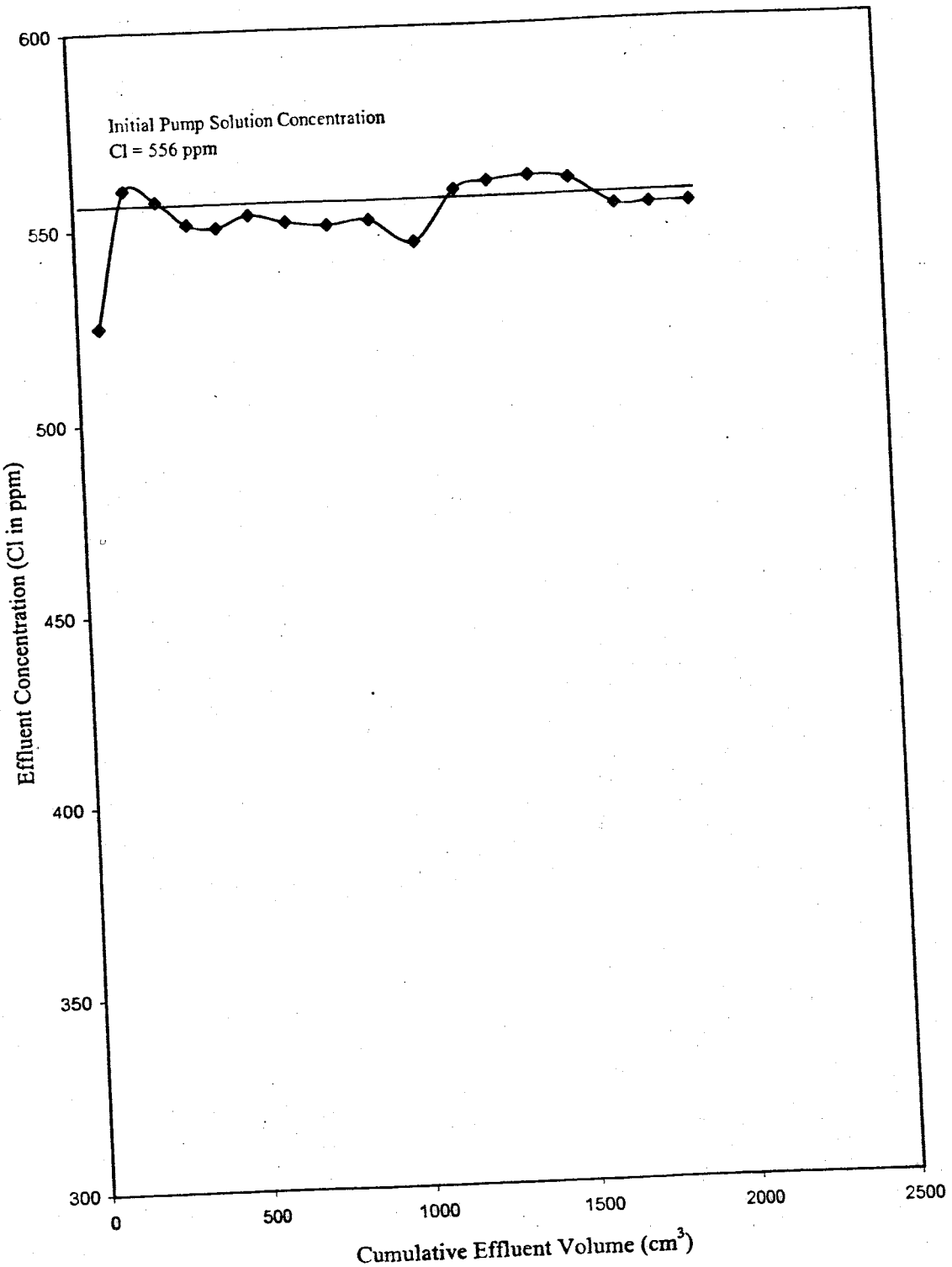

Figure 31. Cumulative effluent volume versus effluent sample chloride concentration in ppm for WRRI-6.

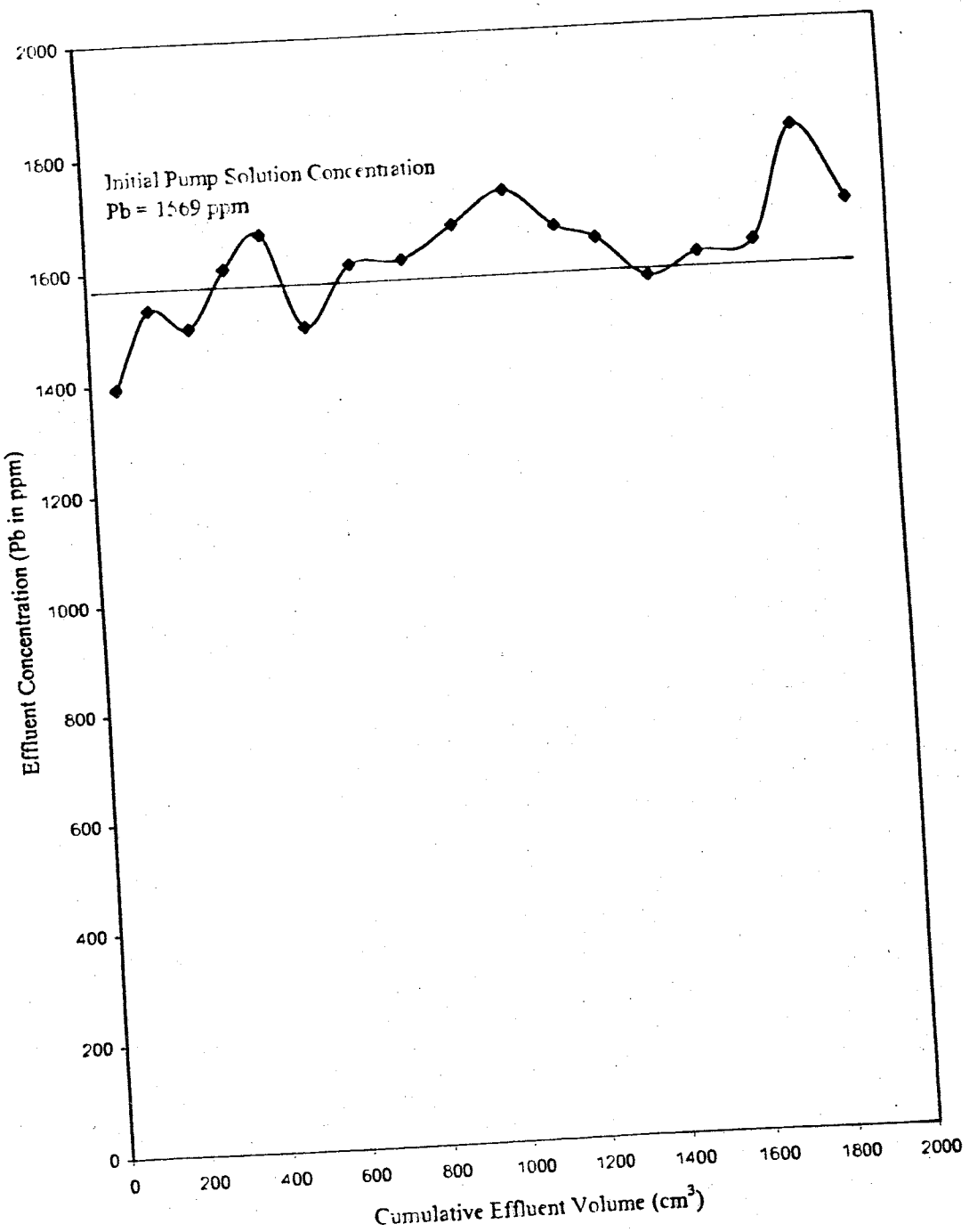

Figure 32. Cumulative effluent volume versus effluent sample lead concentration in ppm for WRRI-6.

confirmed that these crystals were lead chloride (Figures 33, and 34).

2.2.4 Cobalt Experiments

2.2.4.1 WRRI-9

This test hyperfiltrated an 80% saturated cobalt chloride solution through a sedimented clay membrane, constructed with 0.06 grams of bentonite, at a flow rate set at 100 ml/hr. The final ΔP for this test was 63 bars, or 926 psi (Table 14a, Figure 35). The first indication that the membrane was precipitating heavy metal came approximately 11 hours into the experiment, when it was suspected that the high pressure membrane surface was changing in color as a result of precipitation. This suspicion was difficult to confirm at the time, as the $CoCl_2$ solution that was being used had a distinct reddish color. However, when the experimental cell was disassembled, precipitate was visibly present on the membrane surface. Analysis of the cell solution revealed a significant build-up of Cl^- (Table 14b). Graphical representation of effluent sample analysis can be found in Figures 36 and 37. Scanning electron microprobe analysis of the membrane at the completion of the experiment revealed mineral precipitation on the high pressure face. It was determined that these minerals were $CoCl_2$ (Figures 38, and 39).

2.2.4.2 WRRI-10

This cobalt experiment differed from all other experiments performed in this study in three significant modes. First, the solution flux rate was set to only 10 ml/hr which was much lower than any of the previous experiments, second, the solution was 70% saturated, and finally, 2.0 grams of the Na-smectite was used to construct the membrane, more than used in any of the previous experiments. The final ΔP reached in

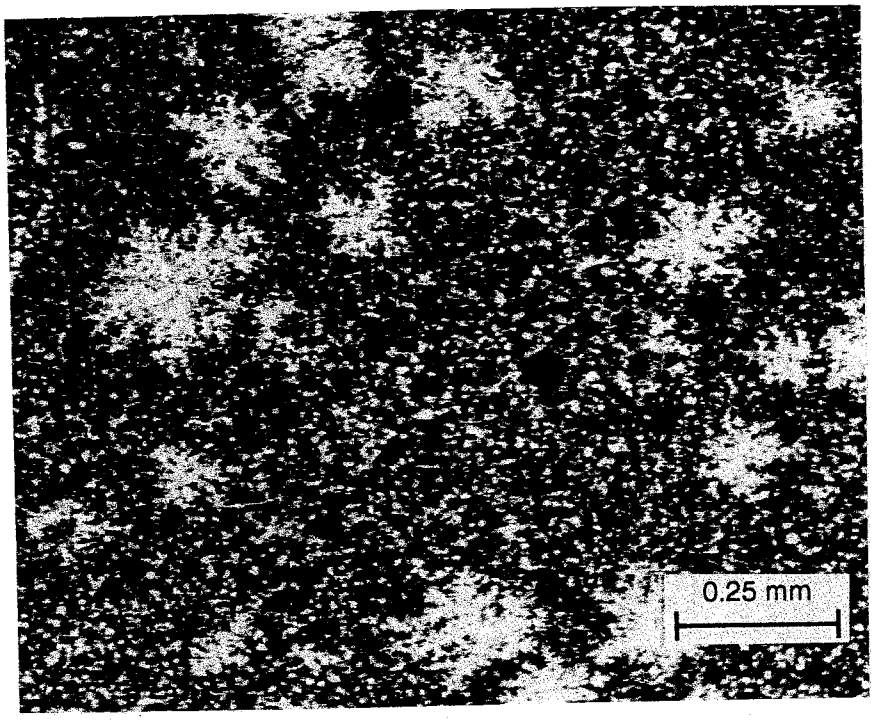

Figure 33. Scanning electron microphotograph of lead chloride particles on the surface of the membrane after experiment WRRI-6.

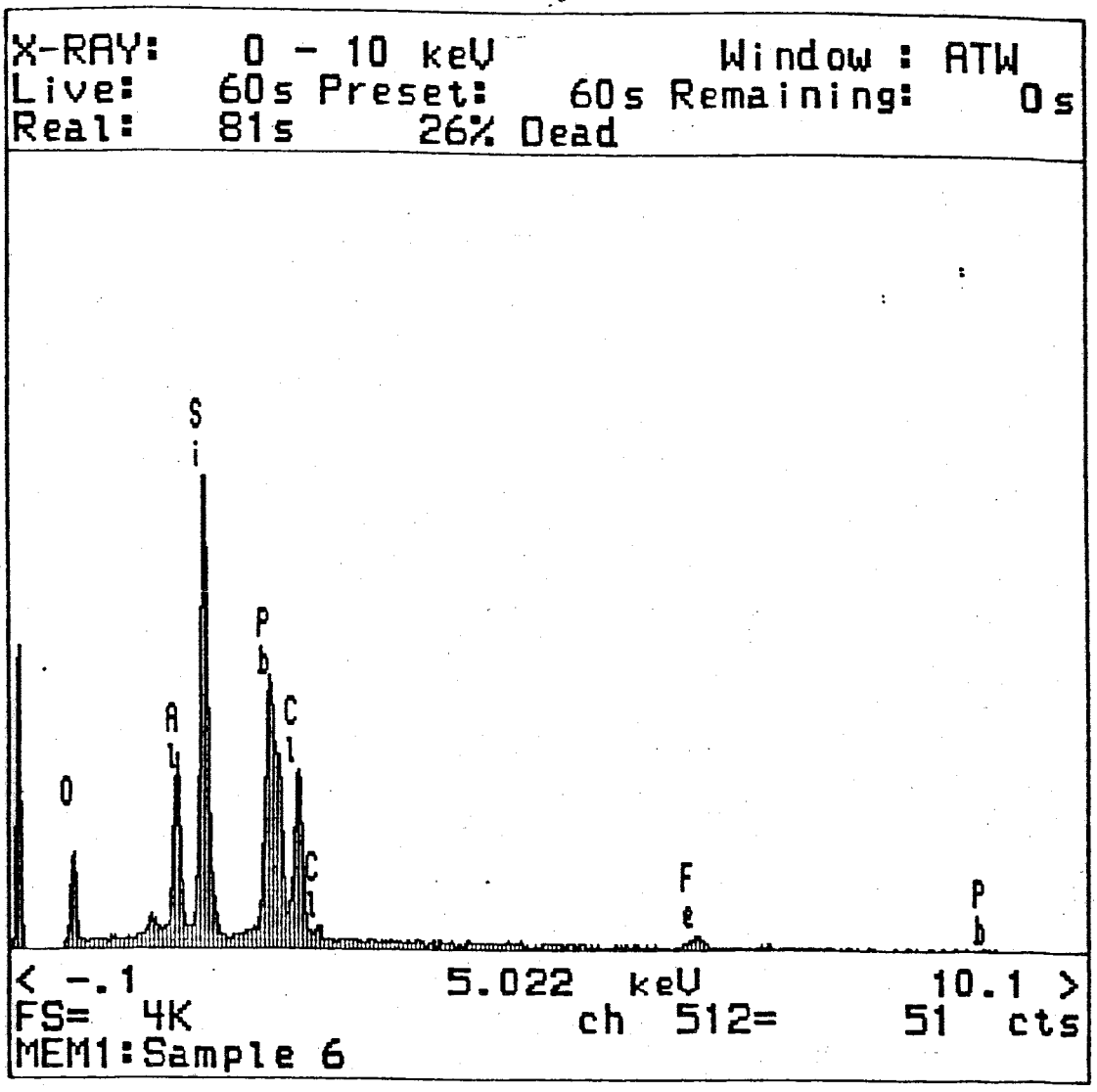

Figure 34. Energy dispersive spectra of elements present in the particle on the surface of the membrane after experiment WRRI-6.

Table 14a. Data for experiment WRRI-9. All data for effluent samples, unless otherwise noted in the comment column.

Sample #	Sample Interval (hours)	Total Elapsed time (hours)	Sample Volume (cm^3)	Pressure (bars)	pH	Comments
1	--	--	69.41	--	3.95	pump solution
2	0.700	0.700	67.40	16.6	4.42	
3	0.933	1.633	93.55	21.6	4.38	
4	0.867	2.500	85.33	25.9	4.19	
5	1.050	3.550	104.86	28.4	4.26	
6	1.317	4.867	114.18	31.9	4.32	
7	1.450	6.317	146.53	37.7	4.31	
8	1.717	8.033	173.17	41.3	4.23	
9	2.150	10.183	218.57	47.3	4.32	
10	2.250	12.433	224.71	50.7	4.29	
11	2.133	14.567	218.60	54.9	4.27	
12	2.150	16.717	215.02	56.8	4.26	
13	2.067	18.783	206.82	56.4	4.24	
14	2.100	20.883	211.12	58.8	4.25	
15	2.033	22.917	207.44	61.1	4.23	
16	2.250	25.167	226.24	63.0	4.25	
17	--	--	114.45	--	4.01	pump solution
18	--	--	--	--	4.28	cell solution

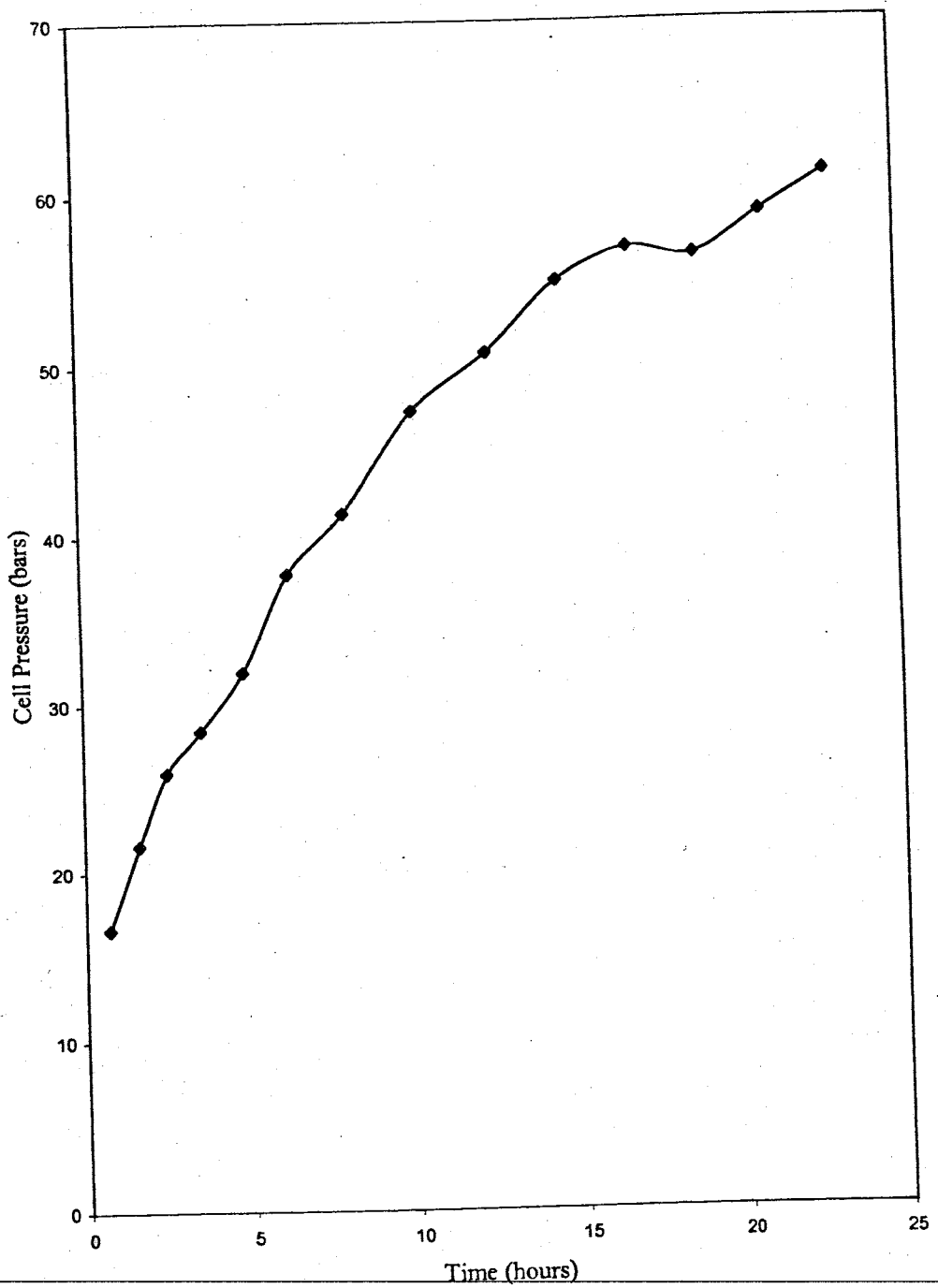

Figure 35. Time versus cell pressure in bars for WRRI-9.

Table 14b. Chemical analysis for WRRI-9. All data for effluent samples, unless otherwise noted in the comment column.

Sample #	Cl (ppm)	Co (ppm)	Comments
1	3028	4529	pump solution
2	3048	3562	
3	3119	3897	
4	3160	3911	
5	3245	3986	
6	3188	3192	
7	3074	4138	
8	3267	3787	
9	3117	3263	
10	3381	3535	
11	3658	3352	
12	3684	3473	
13	2684	3096	
14	3090	3109	
15	3238	3143	
16	4133	3198	
17	4167	3319	pump solution
18	6450	4526	cell solution

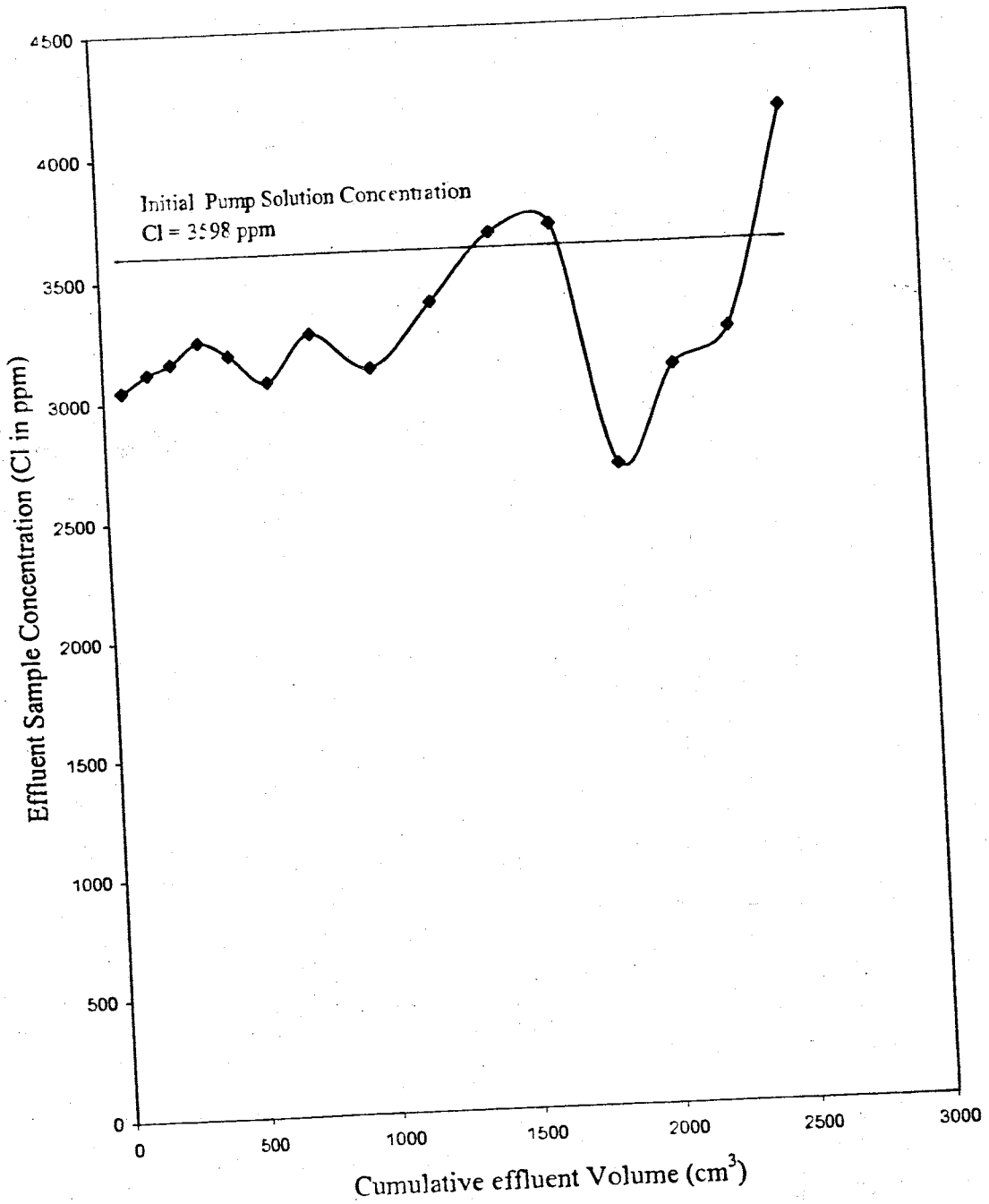

Figure 36. Cumulative effluent volume versus effluent sample chloride concentration in ppm for WRRI-9.

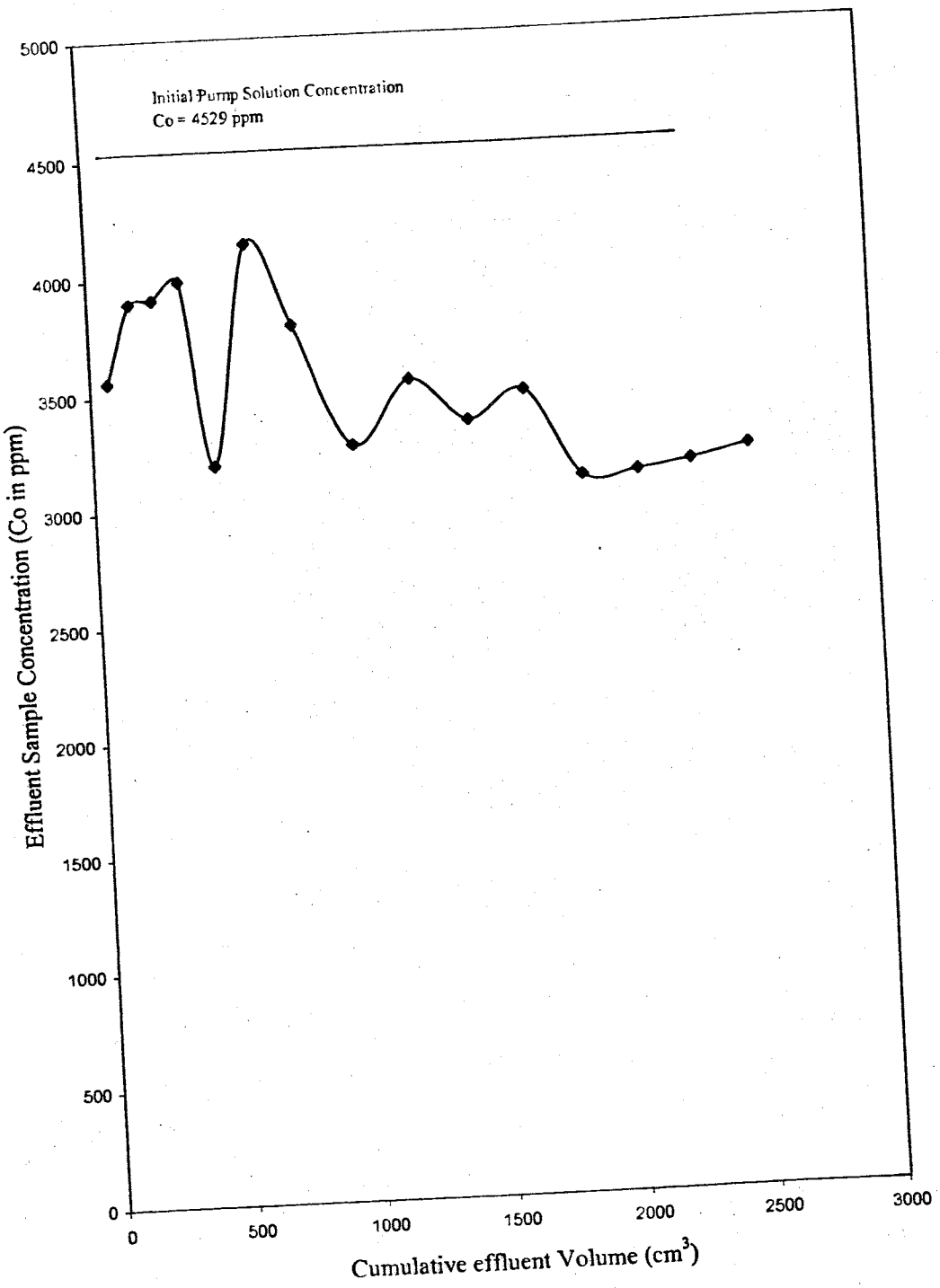

Figure 37. Cumulative effluent volume versus effluent sample cobalt concentration in ppm for WRRI-9.

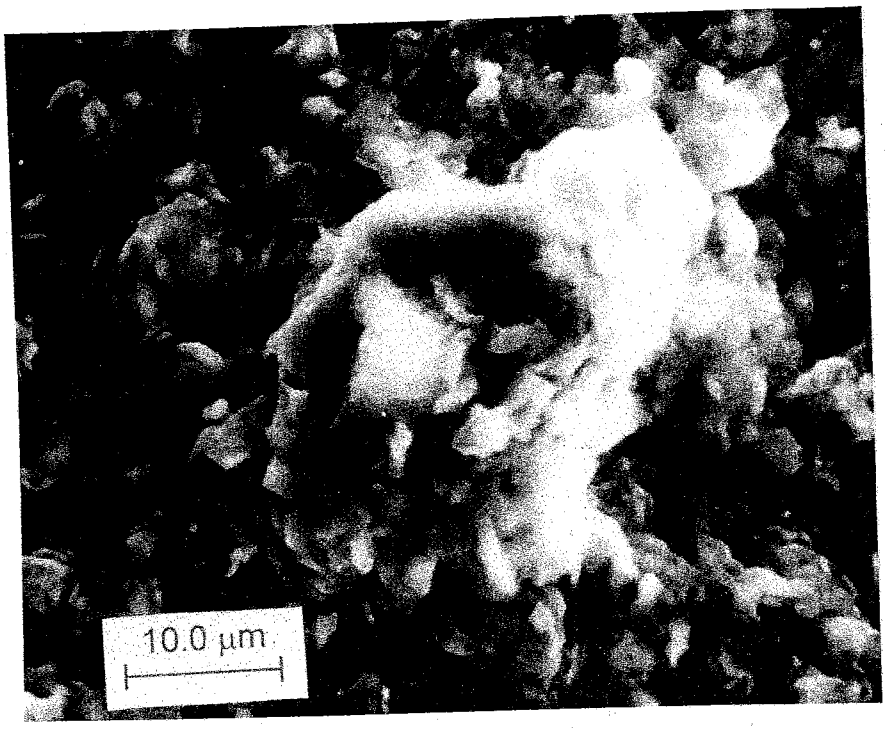

Figure 38. Scanning electron microphotograph of $CoCl_2$ particle on the surface of the membrane after experiment WRRI-9.

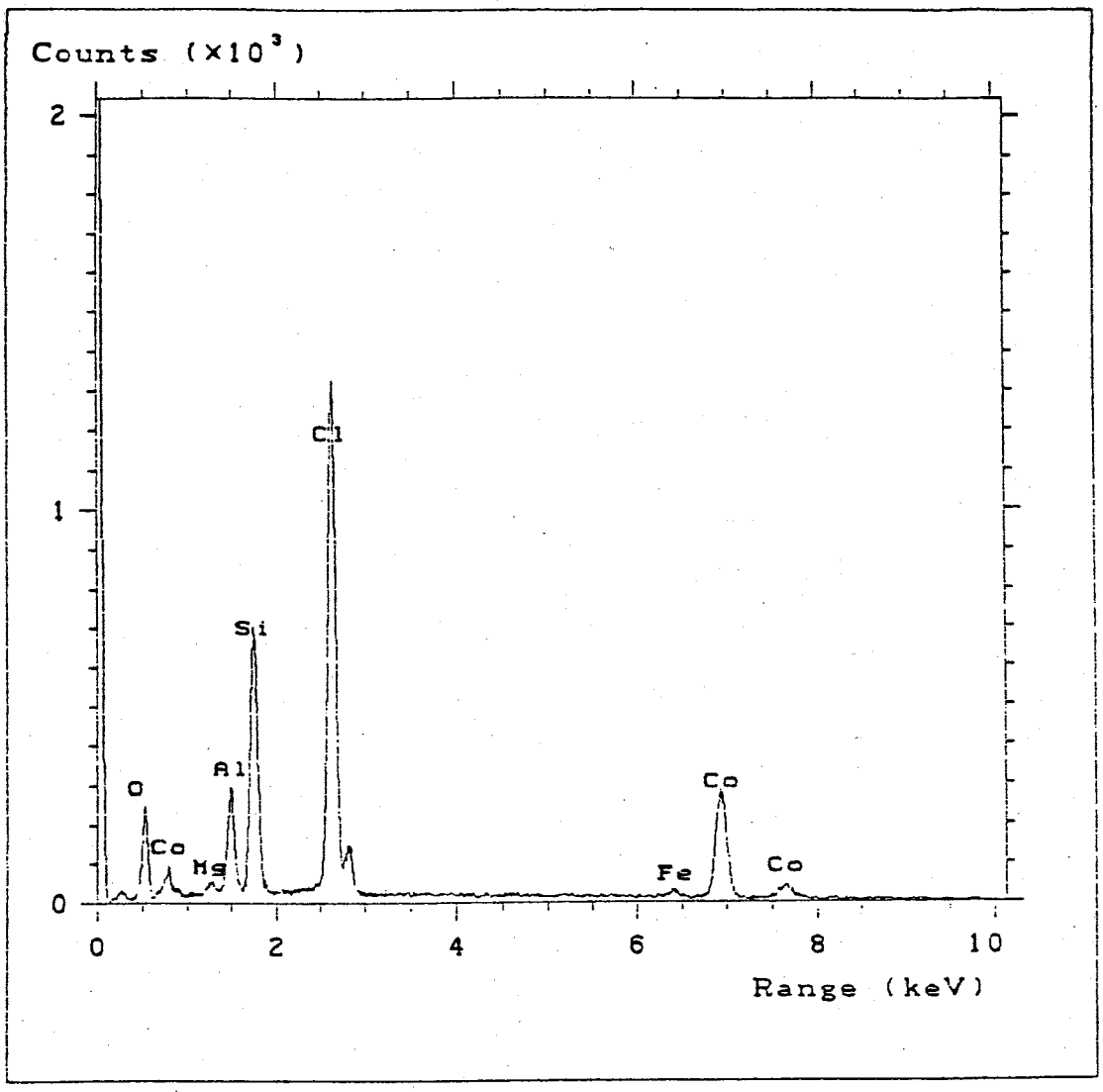

Figure 39. Energy dispersive spectra of elements from $CoCl_2$ particle on the surface of the membrane after experiment WRRI-9.

this system was 0.5 bars, or 8 psi (Table 15a, Figure 40). Effluent heavy metal concentrations did not change throughout the course of the experiment (Table 15b, Figure 41), and based on these analytical results, it was determined that no precipitation was present on the membrane face. As in experiment WRRI-7, the most probable explanation for the absence of heavy metal precipitation in this experiment is that perhaps the appropriate amount of time was not allotted for sufficient build-up of the CPL, and therefore precipitation did not occur. Because the flow rate was so low, and adequate pressure was not allowed to build in the membrane, the system most likely did not have time to develop.

2.2.5 Pyrophyllite Experiment

2.2.5.1 WRRI-11

All attempts to build a membrane composed of pyrophyllite clay failed. It is theorized that the grinding of the clay severely altered the structure of the clay, making the construction of a membrane impossible, as significant pressure could not be built inside the experimental cell. Because of the nature of the raw pyrophyllite, the grinding was a necessary step, and could not be avoided.

3.0 Discussion

3.1 Calculation of Membrane Coefficients

Mineral precipitation on the surface of, and ion exchange within the membranes, was expected and confirmed in this study. The use of the membrane equations as presented in Section 1, utilizing measured effluent concentrations in the calculation of steady-state values of σ, would be inaccurate as these equations do not correct for

Table 15a. Data for experiment WRRI-10. All data for effluent samples, unless otherwise noted in the comment column.

Sample #	Sample Interval (hours)	Time Elapsed Total (hours)	Sample Volume (cm3)	Pressure (bars)	pH	Comments
1	--	--	--	--	6.05	pump solution
2	3.78	3.78	51.10	0.41	3.69	
3	5.12	8.90	42.99	0.41	3.71	
4	3.98	12.88	122.58	0.41	4.05	
5	12.20	25.08	88.03	0.27	4.23	
6	8.73	33.81	116.80	0.34	4.38	
7	13.82	47.63	134.30	0.34	4.48	
8	13.00	60.63	122.29	0.48	4.60	
9	12.52	73.15	103.68	0.54	4.70	
10	10.32	83.47	119.28	0.54	4.92	
11	11.97	95.44	123.28	0.61	4.96	
12	12.22	107.66	123.43	0.54	4.98	
13	22.30	129.96	119.61	0.54	5.05	
14	11.85	141.81	119.49	0.54	5.09	
15	11.88	153.69	130.61	0.54	5.15	
16	13.00	166.69	119.81	0.54	5.19	
17	12.03	178.72	34.14	0.41	5.29	
18	--	--	--	0.54	5.87	cell solution
19	--	--	--	--	5.96	pump solution

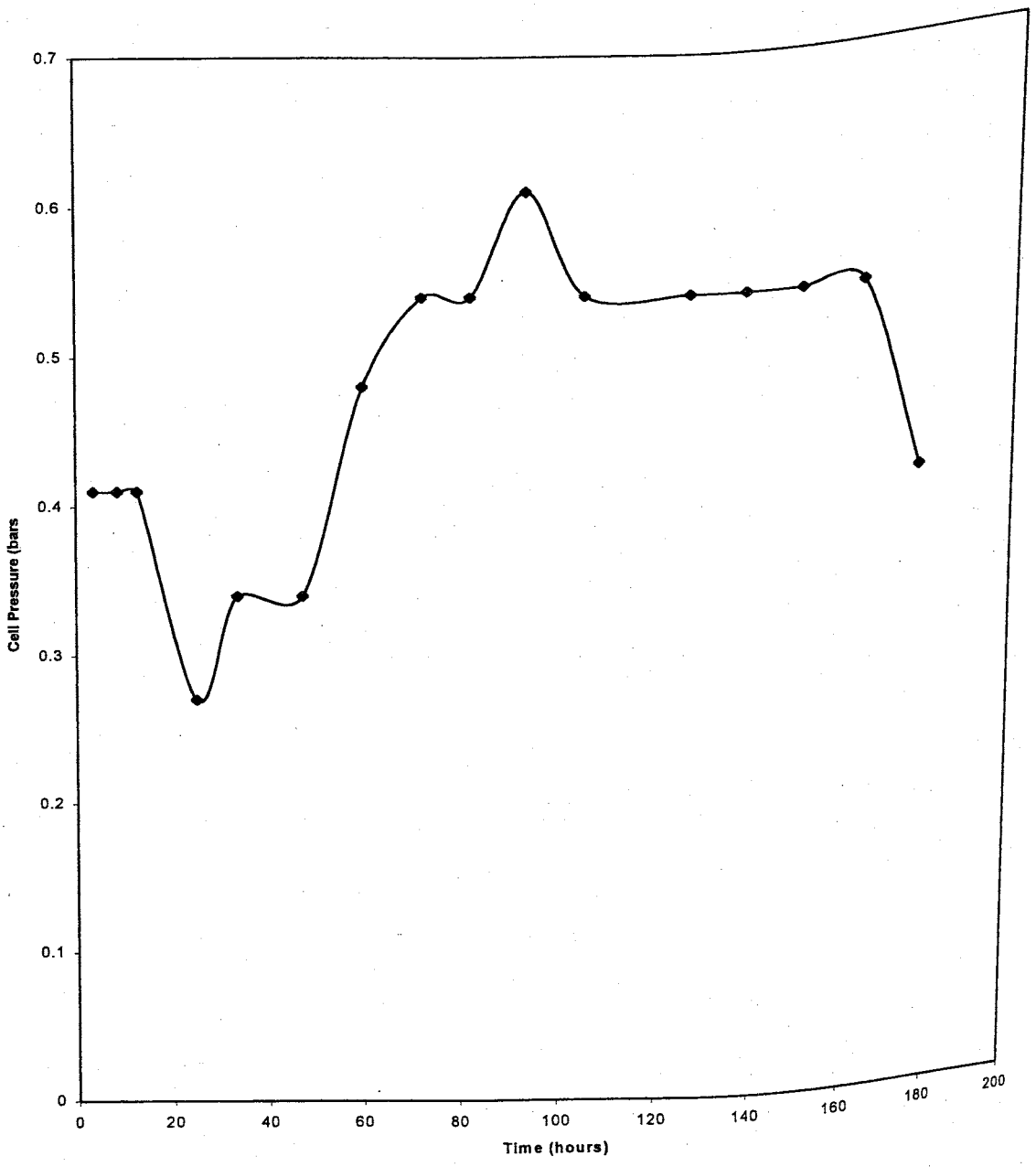

Figure 40. Time versus cell pressure in bars for WRRI-10.

Table 15b. Chemical data for WRRI-10. All data for effluent samples, unless otherwise noted in the comment column.

Sample #	Co (ppm)	Na (ppm)	Ca (ppm)	Comments
1	21340	0	0	pump solution
2	21337	0	0	
3	21337	0	0	
4	21338	0	0	
5	21337	0	0	
6	21337	0	0	
7	21338	0	0	
8	21338	0	0	
9	21338	0	0	
10	21337	0	0	
11	21340	0	0	
12	21339	0	0	
13	21339	0	0	
14	21338	0	0	
15	21338	0	0	
16	21337	0	0	
17	21337	0	0	
18	21337	0	0	cell solution
19	21338	0	0	pump solution

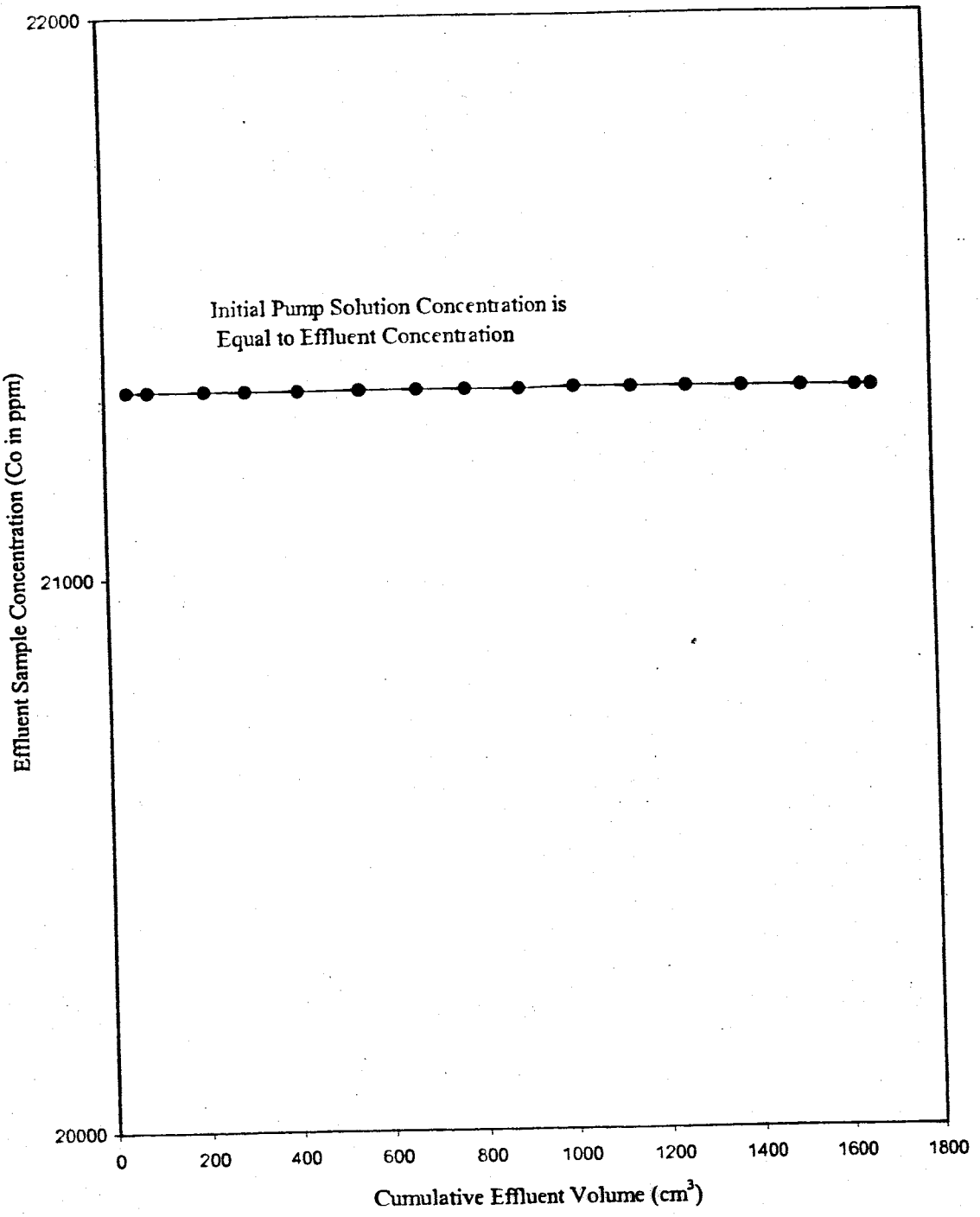

Figure 41. Cumulative effluent volume versus effluent sample cobalt concentration in ppm for WRRI-10.

situations in which precipitation is occurring. It is necessary, therefore, to derive a steady-state solution for σ that is not dependent on mass balance techniques as used by Fritz and Whitworth (1994). Recall at steady-state, $C_e = C_i$, and substituting Equation 4 into Equation 1, we obtain

$$J_v = L_p(\Delta P - \sigma v RT(C_o - C_e)) \tag{11}$$

and because $C_e = C_i$ at steady-state, equation 11 is equivalent to

$$J_v = L_p(\Delta P - \sigma v RT(C_o - C_i)) \tag{12}$$

Furthermore, Fritz and Marine (1983) defined

$$\omega = \frac{D}{RT\Delta x\zeta} \tag{13}$$

where Δx is the membrane thickness (cm), and ζ is the tortuosity of the flow path through the membrane, that is defined by the ratio of the actual length divided by the membrane thickness. By substituting Equation 4, Equation 13, and the steady-state relationship $J_s = J_v C_i$ into Equation 2, we obtain

$$J_v C_i = \frac{C_o + C_i}{2}(1-\sigma)J_v + \frac{D}{RT\Delta x\zeta} vRT(C_o - C_i) \tag{14}$$

Solving equations 12 and 14 for σ, and setting them equal we obtain

$$\frac{L_p\Delta P - J_v}{L_p vRT(C_o - C_i)} = \frac{\frac{2Dv(C_o - C_i)}{\Delta x\zeta} - J_v(C_i - C_o)}{J_v(C_o + C_i)} \tag{15}$$

Solving this equation for C_o yields a polynomial with one positive and one negative root. Since negative values have no meaning, the positive root (Equation 16) is chosen to calculate C_o not dependant on the solute mass balance.

$$C_O = \left(\frac{1}{2L_p vRT(J_v \Delta x - 2vD)}\right)\cdot\left(-2L_p vRTJ_v C_i \Delta x\zeta - 4L_p v^2 RTDC_i + \Delta x\zeta J_v L_p \Delta P - \Delta x^{1/2}\zeta^{1/2}\right)$$

$$\cdot\begin{pmatrix} -8\zeta\Delta x C_i J_v^3 TRvL_p + 8\zeta\Delta x C_i J_v^2 TRvL_p^2 + \zeta\Delta x J_v^4 - 2\zeta\Delta x\Delta P L_p J_v^3 + \zeta\Delta x\Delta P L_p^2 J_v^2 \\ -16J_v^2 C_i DTRv^2 L_p^2 \end{pmatrix}^{1/2} \quad (16)$$

The membrane mathematics section of this text provided a comprehensive overview of the equations used to solve for the various parameters. Table 16 summarizes the calculated coefficients for each experiment. Equation 13 was used to calculate ω, Equation 5 was used to calculate L_p, Equation 16 was used to calculate C_o (note that anion concentrations were used for the lead experiments), and Equation 9 was used to calculate σ.

Fritz and Whitworth (1994) state that the concept of an ideal membrane is a construct. They suggest that all membranes are non-ideal in that they allow the passage of some solute through their pores in response to gradients of both hydraulic pressure as well as chemical potential. The experimental data presented in this report tend to support this conclusion.

Examining the values of σ calculated for the theoretical steady-state presented in Table 16, we see that the values of the reflection coefficient and C_o are relatively high for two of the copper carbonate solutions (WRRI-2 and WRRI-4). However, the

Table 16. Summary of experimental parameters for successful hyperfiltration experiments.

Parameter	WRRI-2	WRRI-4	WRRI-5	WRRI-6	WRRI-7	WRRI-8	WRRI-9
Starting Solution	80% $CuCO_3$	80% $CuCO_3$	80% $PbCl_2$	23% $PbCl_2$	80% $CuCO_3$	80% $CuCl_2$	80% $CoCl_2$
Solubility in grams per 100 g water	$< 10^{-6}$	$< 10^{-6}$	1.10	1.10	$< 10^{-6}$	78.65	45
Final J_V (cm/s)	1.37×10^{-3}	1.37×10^{-3}	1.71×10^{-3}	1.03×10^{-3}	3.43×10^{-4}	2.06×10^{-3}	1.37×10^{-3}
Final ΔP (bars)	30.95	4.90	24.15	16.39	6.19	64.26	63
Clay Type	Na-Montmor-illonite	Na-Montmor-illonite	Na-Montmor-illonite	Na-Montmor-illonite	Na-Montmor-illonite	Na-Montmor-illonite	Na-Montmor-illonite
Mass of clay (grams)	0.60	0.60	0.60	0.60	0.60	0.60	0.60
L_p cm^3/dyne·s	4.97×10^{-11}	5.37×10^{-10}	9.00×10^{-11}	6.34×10^{-11}	2.21×10^{-11}	7.21×10^{-11}	6.69×10^{-11}
Membrane thickness	0.064 cm	0.064 cm	0.097 cm	0.094 cm	0.061 cm	0.064 cm	0.068 cm
Theoretical Steady State σ	0.90	0.95	0.74	0.49	0.59	0.96	0.88
Approximate Steady-state ω	7.25×10^{-16} mol/dyne·s	7.25×10^{-16} mol/dyne·s	8.32×10^{-16} mol/dyne·s	8.59×10^{-16} mol/dyne·s	7.60×10^{-16} mol/dyne·s	8.89×10^{-16} mol/dyne·s	7.83×10^{-16} mol/dyne·s
Theoretical steady-state C_o (mol/cm^3)	9.27×10^{-5}	5.45×10^{-5}	1.24×10^{-4}	1.88×10^{-5}	4.36×10^{-6}	5.78×10^{-4}	7.47×10^{-4}
$10D/J_V$	0.058 cm	0.058 cm	0.08 cm	0.135 cm	0.581 cm	0.070 cm	0.092 cm

Note: D calculated from Nernst Relation (Lide, 1990). D for copper carbonate = 7.963×10^{-6}, for lead chloride = 1.45×10^{-5}, for copper chloride = 1.177×10^{-5}, for cobalt chloride = 1.16×10^{-5}. Solubility data from Hem (1992) for $CuCO_3$; Lide (1990) for all others.

mathematics, as presented below, suggest that for a given set of conditions for a specific membrane (i.e., values of L_p, ΔP, ζ, and solution type) there will be a threshold input concentration below which σ must equal 1.0 (i.e. the membrane will be essentially perfect). This is further defined in the derivation of the membrane equations, as presented below.

Data from Kharaka and Barry's (1973) work indicates that selectivity of clay membranes for cations is directly proportional to atomic weight. Copper, lead and cobalt have higher atomic weights than any cations previously used in sedimented clay studies. It can be said then, that it is not surprising to find relatively high values for the reflection coefficient in this compilation of experiments.

The experiments performed in this study demonstrate that hyperfiltration-induced heavy metal precipitation by membranes is possible in the laboratory. Nevertheless, it is important to determine the theoretical limitations to these findings. To address these problems, a series of parameter maps were developed which delineate the theoretical conditions necessary for membrane-induced precipitation to occur. In the development of these maps, certain unnecessary parameters were eliminated. Equations 3, 4, 12, and the steady-state relationships $J_s = J_v C_e$ and $C_e = C_i$ are substituted into Equation 2, and solved for C_i.

$$C_i = C_o \cdot \frac{(\sigma - 1)(J_v \zeta \Delta x) - 2vD}{(\sigma + 1)(J_v \zeta \Delta x) - 2vD} \qquad (17)$$

This equation relates the system input concentration to seven parameters. J_v, C_o, Δx and σ are considered variables, while v and D are constants in the development of the parameter maps.

To solve this equation a value of 7.2 is used for tortuosity (average value reported for clays by Barone et al, 1992, and Barone et al, 1990), while C_o is fixed at saturation for the mineral of interest for the calculations. Since pH plays a significant role in heavy metal solubility, it would be necessary to recalculate the results of these plots for systems substantially different than neutrality. To develop the parameter maps (Figures 42-49), J_v was iterated in Equation 17 for fixed values of Δx and σ, and the C_i necessary to produce saturation at the membrane face was calculated. The plot of these values for a given Δx and σ produces the boundary between values of J_v and C_i which will or will not produce saturation, and thus potentially produce mineralization at the sand/shale interface.

The individual boundary lines for specific values of σ join as J_v decreases to the left in the boundary maps. This occurs when the solution flux through the membrane becomes too slow to prevent of the solute from diffusing away from the membrane. As a result, there is no CPL development, and precipitation can occur only at or above saturation. Notice that in the region of the map where CPL development is possible, as σ increases, lower and lower input concentrations can result in the development of saturation at the membrane.

Determination of a reasonable estimation of the total solution flux through the membrane at any particular site can be difficult, and will usually prove more complicated than a simple application of Darcy's Law. Equation 1 states that the total solution flux

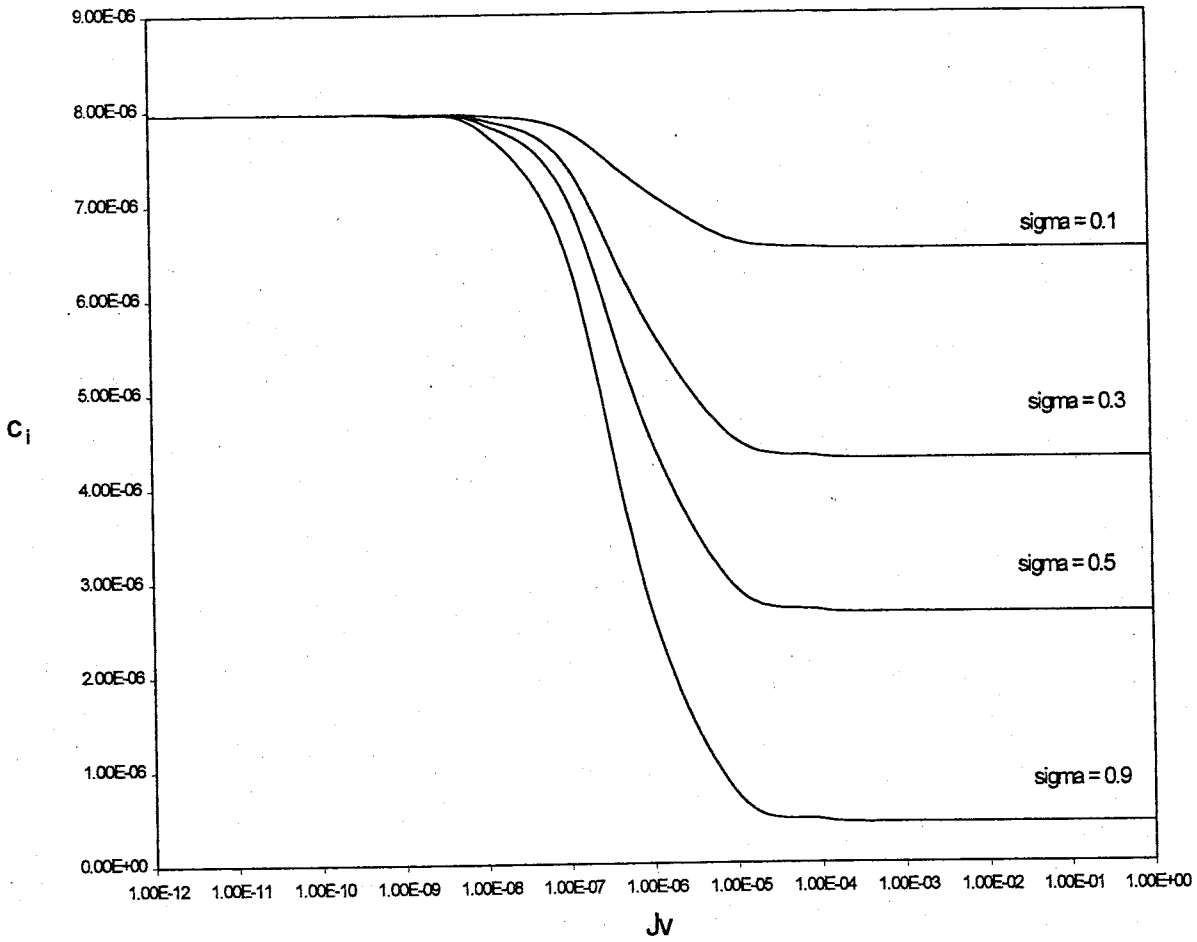

Figure 42. Membrane parameter map for copper carbonate, membrane thickness 10 cm (0.1 m). Each line (or boundary) on the map is for a different value of σ. Along the right hand side going downward, the lines have the following values of σ: 0.1, 0.3, 0.5, and 0.9.

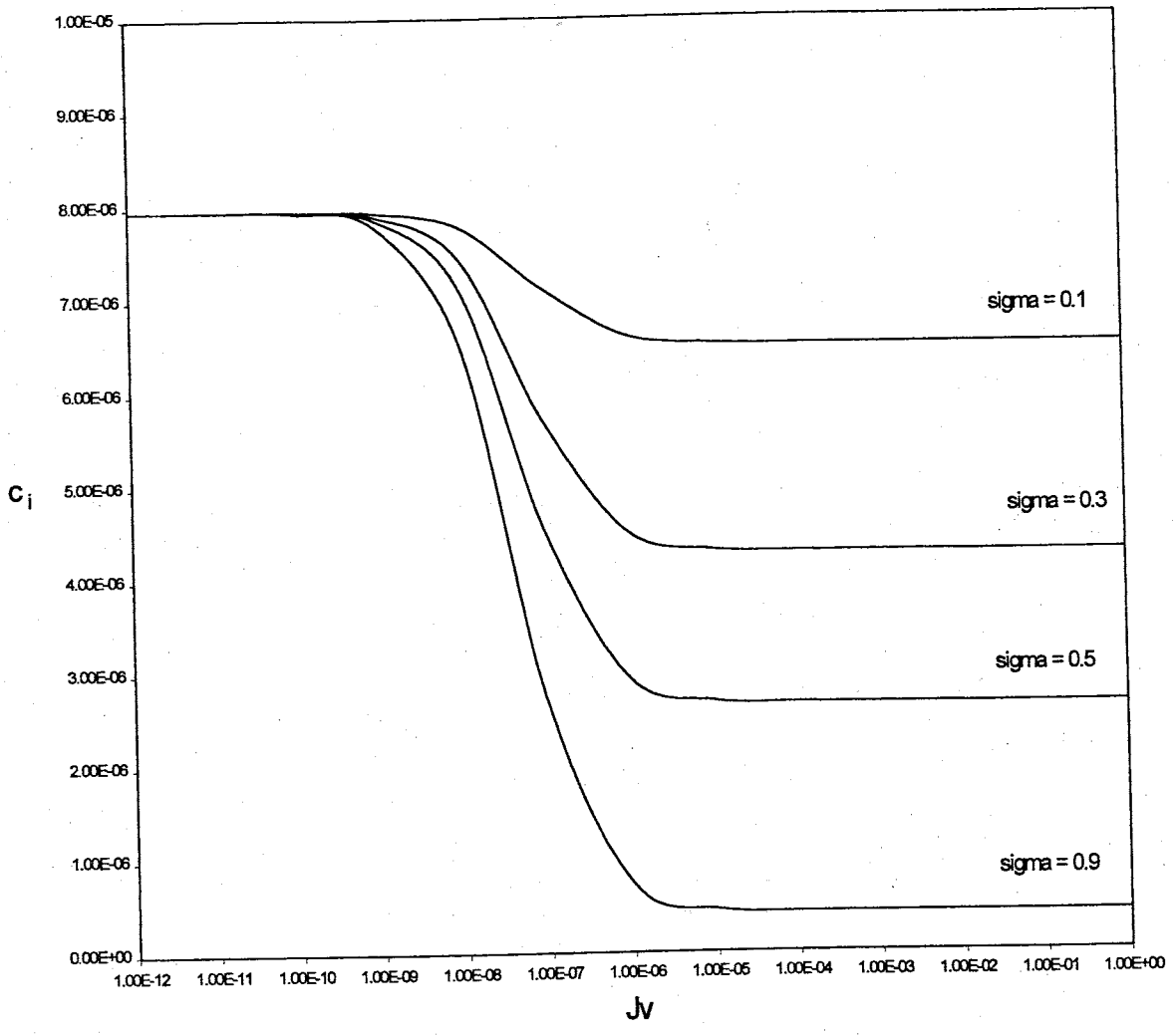

Figure 43. Membrane parameter map for copper carbonate, membrane thickness 1 m. Each line (or boundary) on the map is for a different value of σ. Along the right hand side going downward, the lines have the following values of σ: 0.1, 0.3, 0.5, and 0.9.

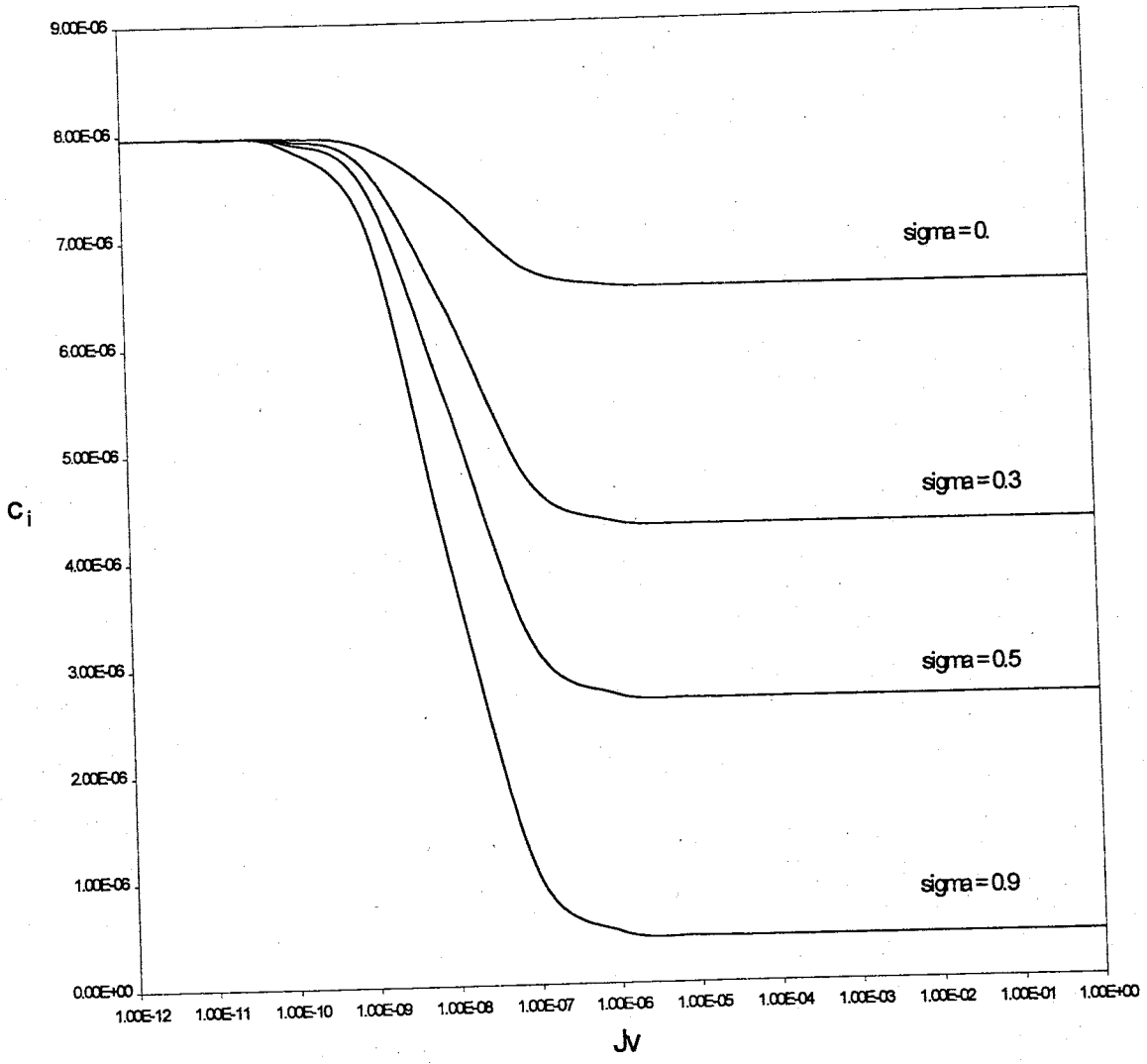

Figure 44. Membrane parameter map for copper carbonate, membrane thickness 5 m. Each line (or boundary) on the map is for a different value of σ. Along the right hand side going downward, the lines have the following values of σ: 0.1, 0.3, 0.5, and 0.9.

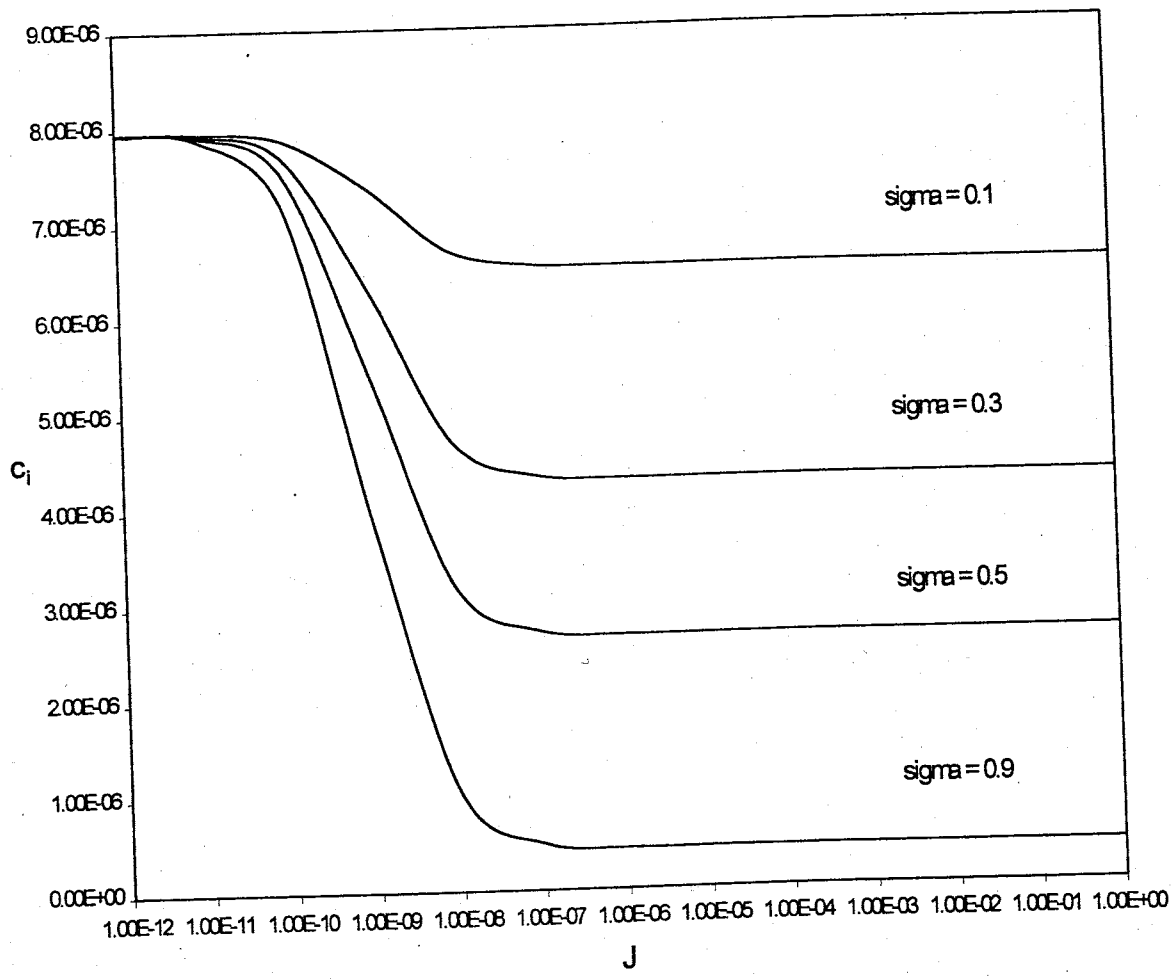

Figure 45. Membrane parameter map for copper carbonate, membrane thickness 50 m. Each line (or boundary) on the map is for a different value of σ. Along the right hand side going downward, the lines have the following values of σ: 0.1, 0.3, 0.5, and 0.9.

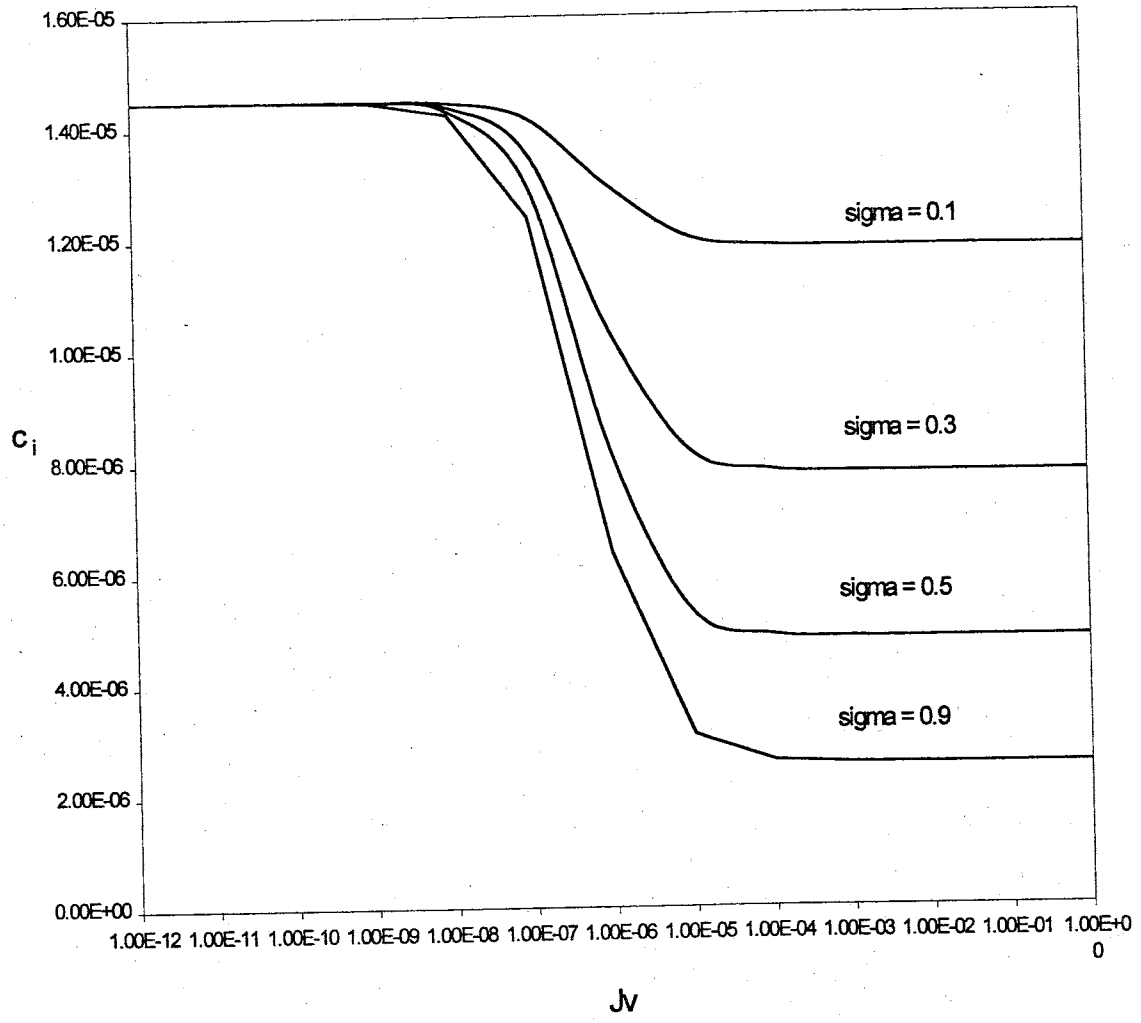

Figure 46. Membrane parameter map for lead chloride, membrane thickness 10 cm (0.1 m). Each line (or boundary) on the map is for a different value of σ. Along the right hand side going downward, the lines have the following values of σ: 0.1, 0.3, 0.5, and 0.9.

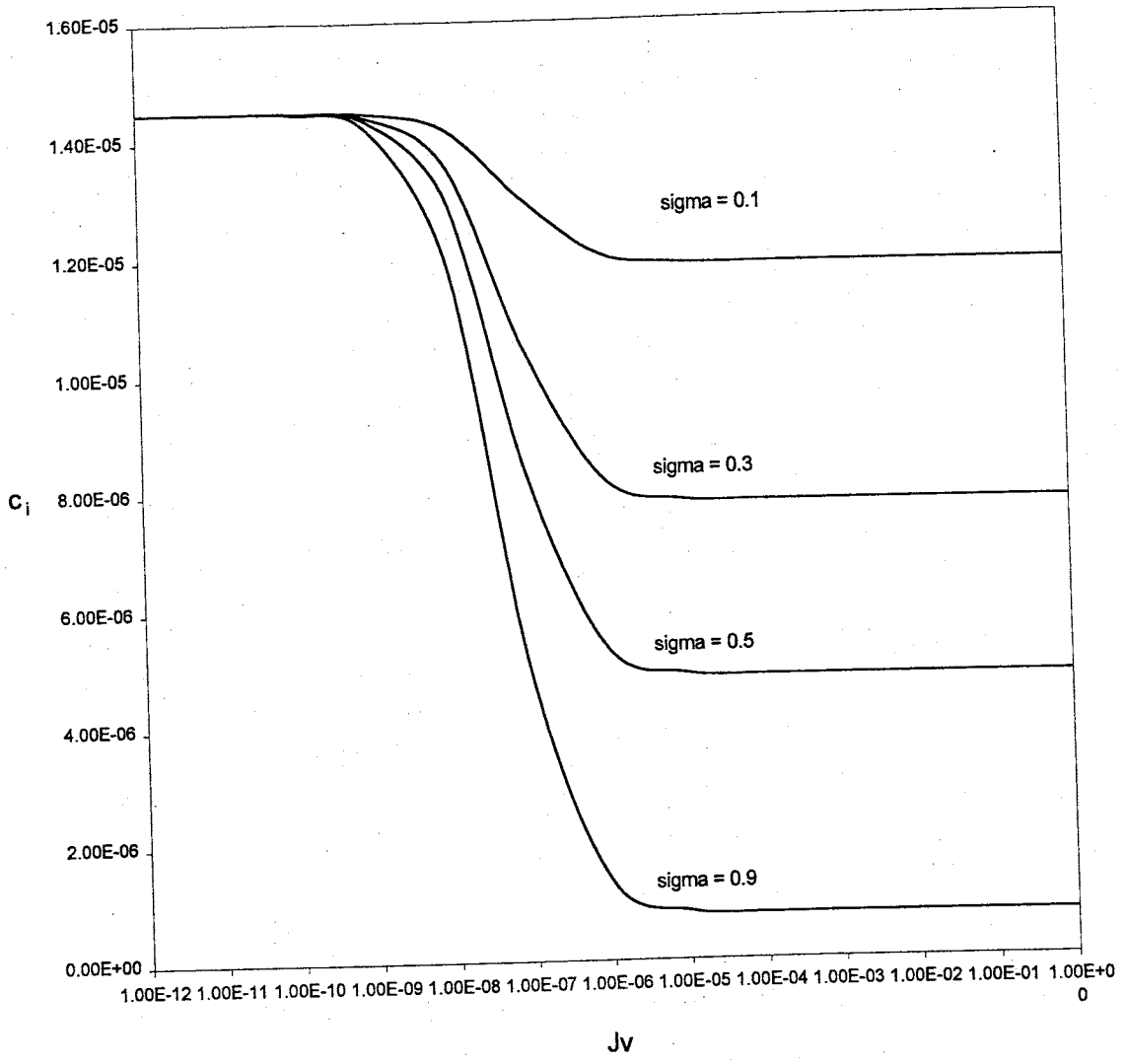

Figure 47. Membrane parameter map for lead chloride, membrane thickness 1 m. Each line (or boundary) on the map is for a different value of σ. Along the right hand side going downward, the lines have the following values of σ: 0.1, 0.3, 0.5, and 0.9.

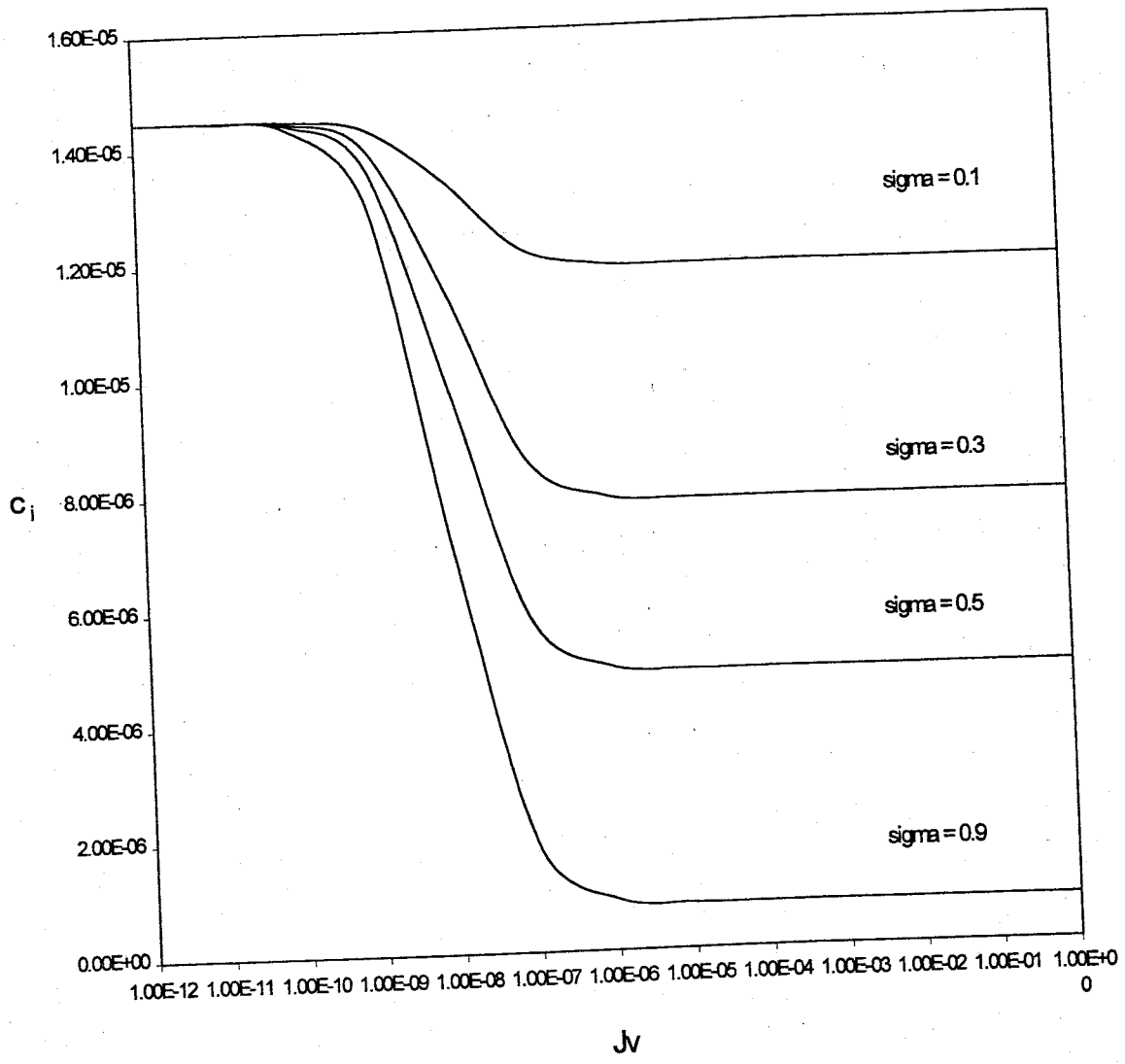

Figure 48. Membrane parameter map for lead chloride, membrane thickness 5 m. Each line (or boundary) on the map is for a different value of σ. Along the right hand side going downward, the lines have the following values of σ: 0.1, 0.3, 0.5, and 0.9.

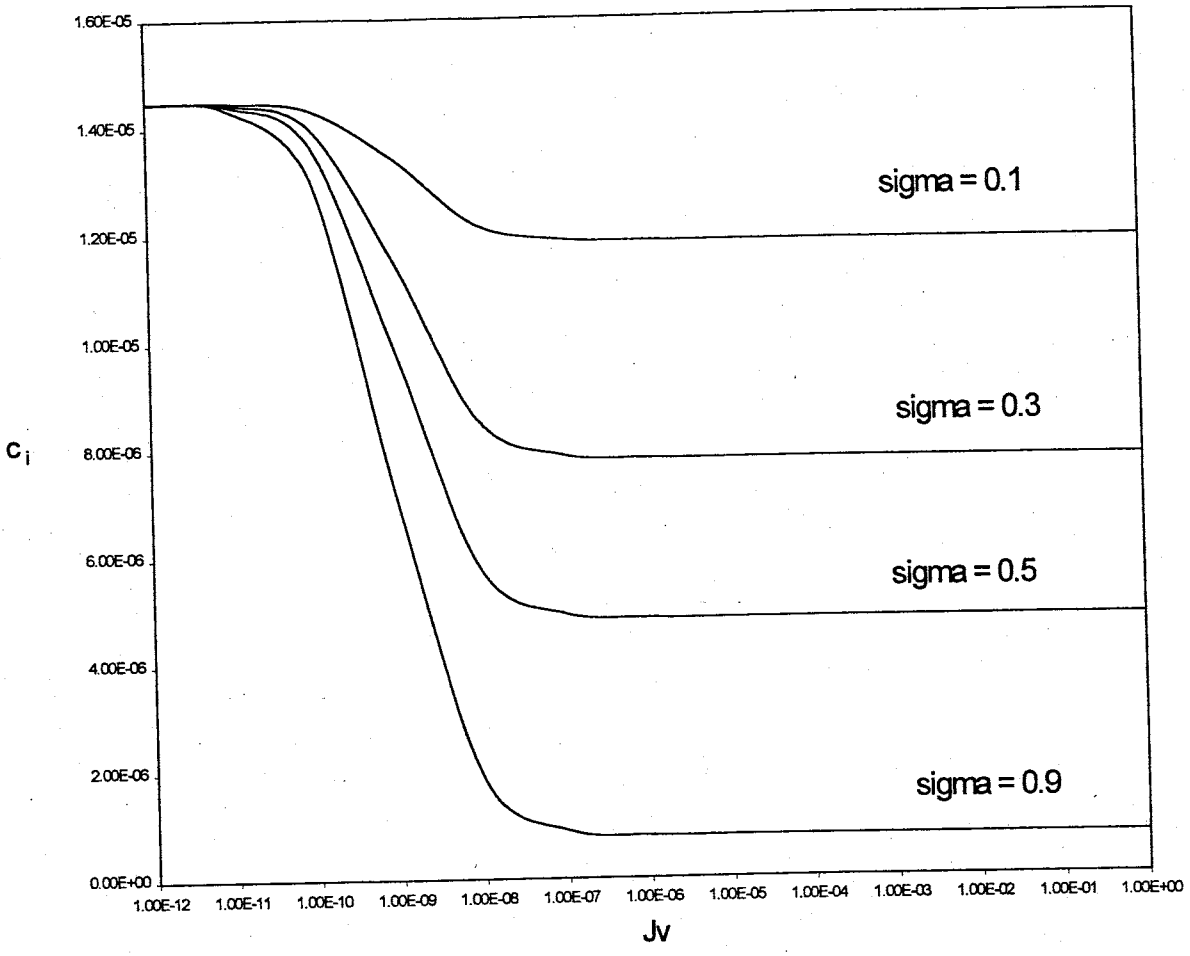

Figure 49. Membrane parameter map for lead chloride, membrane thickness 50 m. Each line (or boundary) on the map is for a different value of σ. Along the right hand side going downward, the lines have the following values of σ: 0.1, 0.3, 0.5, and 0.9.

through the membrane increases as the differential pressure across the membrane increases, and decreases with increasing osmotic pressure. If the osmotic pressure is equal to zero, then Equation 1 reduces to Darcy's Law:

$$J_v = \frac{K\Delta P}{\rho g \Delta x} \tag{18}$$

On the other hand, if the osmotic pressure is significant, J_v would be less than that predicted by Darcy's Law. An approximate equation is derived from Equation 1 that will incorporate osmotic pressure in the calculation of J_v. Substituting Equations 3 and 4 into Equation 1 yields

$$J_v = \frac{K}{\rho g \Delta x}\left(\Delta P - \sigma v R T\left(C_o - C_e\right)\right) \tag{19}$$

Fritz and Marine (1983) derived an approximate expression for Co, the only unknown parameter in this equation, in terms of Ci and σ. Recall, their expression:

$$\sigma = \frac{C_o - C_e}{C_o + C_e} \tag{20}$$

Solving this for C_o and substituting the steady-state relationship $C_e = C_I$ yields

$$C_O = \frac{-\left(\sigma C_i + C_i\right)}{\sigma - 1} \tag{21}$$

Substituting this into Equation 19 yields

$$J_v = \frac{K}{\rho g \Delta x}\left(\Delta P - \sigma v R T \frac{\left(-\left(\sigma C_i + C_i\right) - C_i\right)}{\sigma - 1}\right) \tag{22}$$

where all parameters other than J_v are known for a given system, or reasonable values can be assumed. This results in the ability to calculate the effects of osmotic pressure on a single solute system. As an example, consider a 0.01 M (230 mg/l) NaCl system in which $\Delta x = 10$ cm, $\sigma = 0.6$, $v = 2$, $D = 1.545 \times 10^{-5}$ s/cm^2, $\Delta P = 1{,}861{,}585$ dynes/cm^2 (27 psi), $K = 1 \times 10^{-9}$ cm/s, $T = 298.15°$ K, $g = 980$ cm/s^2, $R = 8.314 \times 10^{-7}$ dyne-cm/mole-°K, and $\rho = 1.0$ g/cm^3. J_v as calculated from Darcy's Law (Equation 18) is 1.9×10^{-7} cm/s, while Equation 22 yields a J_v of 9.9×10^{-8} cm/s. It can now be seen that in this simple system, Darcy's Law has underestimated J_v by 92%. To use Equation 22, the value of σ must either be measured or approximated.

Since groundwaters are multi-component systems, Equation 22 can be re-written as follows:

$$J_v = \frac{K}{\rho g \Delta x}\left(\Delta P - \sum_{0 \rightarrow j} \sigma v R T \frac{\left(-\left(\sigma C_{i,j} + C_{i,j}\right)\right)}{\sigma - 1} - C_{i,j}\right) \qquad (23)$$

where the second term is summed over all of the specified solution components. Because the reflection coefficient is solute-specific, each solution component will have a different value of σ, and these values can be measured in the laboratory.

The boundary maps presented in this report were constructed for copper carbonate and lead chloride. To use the maps for either compound, first select the boundary map drawn specific to the thickness of shale of interest. Next, calculate the expected J_v from either Equation 22 or 23, and draw a vertical line perpendicular to this value on the x-axis. Next, draw a horizontal line perpendicular to the value of C_i on the y-axis. Note the

intersection of these two lines. If the intersection is 1) below all of the boundary lines, no precipitation will occur as the concentration at the membrane will not reach saturation, 2) between a pair of boundary lines for differing values of the reflection coefficient, then in order for precipitation to occur, the σ of the shale must exceed the value for σ on the lowermost adjacent boundary line, or 3) above all of the boundary lines, then precipitation is possible with a relatively inefficient membrane in which σ is less than 0.1.

For situations in which precipitation is occurring, the magnitude of the solution flux directed toward the membrane within the aquifer must be somewhat greater than the solution flux which actually passes through the membrane. However, because of the low concentrations involved, we can assume, for purposes of illustration, that even with precipitation occurring, that the solution flux through the membrane is essentially equal to that toward the membrane within the aquifer. When there is no precipitation occurring, the two solute flux terms are exactly equal at steady-state.

Repeated laboratory experiments presented in this study have confirmed that membrane-induced precipitation of heavy metals is possible. This data demonstrates that membrane-induced precipitation of heavy metals may be important in the assessment of heavy metal contaminated zones in the subsurface. Several factors, however, are crucial in the determination of how a membrane in the subsurface will affect the transport of heavy metals, including contaminant concentration, membrane thickness, and the rate of flux that is being imposed on the membrane.

Dissolved lead concentrations in natural waters containing bicarbonate and carbonate alkalinity should be limited by the solubility of lead carbonate (approximately 0.065 mg/l) (Hem, 1959). Lead concentrations in groundwaters seldom reach saturation for lead carbonate, however, concentrations in contaminant plumes are often elevated over those encountered in pure waters. Therefore, precipitation of lead minerals due to hyperfiltration through clay membranes is even more likely in polluted versus undisturbed systems.

Important factors in the consideration of membrane-induced precipitation at heavy metal contaminated sites is the thickness of the clay membrane, and the hydraulic conductivity of the clay. These parameters play a critical role in the time scale required for a system to reach steady-state. Fritz and Whitworth (1994) determined that a 0.3 cm thick clay membrane with a hydraulic conductivity of 2.03×10^{-10} cm/s required a little more than 19 days to reach steady-state in a system with a solution flux of 1.370×10^{-5} cm/s. Moreover, Whitworth and Fritz (1994) found that a 0.274 cm thick clay membrane with a hydraulic conductivity of 1.83×10^{-16} cm/s required only about 20 days to closely approach steady-state at a solution flux of approximately 8.83×10^{-6} cm/s, while a 0.810 cm thick clay membrane with a hydraulic conductivity of 1.15×10^{-17} cm/s required approximately 90 days to reach steady-state. These experiments indicate that it should be possible for thin clay membranes to form a CPL and precipitate heavy metals from solution in geologically and environmentally significant time frames.

A few assumptions are required to make the initial estimations of the relative importance of membrane-induced precipitation on heavy metal transport in contaminated systems. For example, consider a 1 cm thick clay with a hydraulic conductivity of

1×10^{-7} cm/s under a gradient of 1.0 in which 0.001 cm^3 of solution will pass through 1 m^2 in 1 second. If an aquifer porosity of 25% is assumed, then the fluid that passes through 1 m^2 of this membrane in 1 year would occupy 0.126 m^3 of the aquifer material. Ten years would see fluid from 1.26 m^3, and 100 years would see fluid from 12.6 m^3 of aquifer material. We see that over a period of 100 years, a thin bounding clay membrane can remove much of the heavy metal from an aquifer almost 13 m thick both by precipitation due to solute-sieving effects and ion-exchange of the contaminant ions with the exchangeable ions in the shale. The conclusion is then that with qualifying conditions (i.e. appropriate solution flux, adequate hydraulic conductivity, sufficient time) aquifers with bounding shales may ultimately be self-cleansing of heavy metal contamination. Thicker clays will be just as effective in inducing precipitation, as long as the flux toward the membrane exceeds the ability of the solute to diffuse away from the membrane, however, longer periods of time will be required.

In addition to the considerations presented thus far, the pressure/solubility relationship as related to these experiments must be addressed. Appelo and Postma (1994) present a clear explanation of the pressure/solubility relationship in terms of thermodynamic properties. The following reaction is provided as an example because of the relatively large volume change with respect to the reactants and the products:

$$CaCO_3 \leftrightarrow Ca^{2+} + CO_3^{2-}$$

Thermodynamic analysis of the reaction reveals that for every 1 atmosphere increase in pressure, the log of the solubility product is increased by ≈ 0.001. Thus despite the relatively large volume change of this reaction, the effect of pressure on

equilibrium is rather small. It is an important note that an increase in pressure increases the solubility. Appello and Postma (1994) go on to indicate that pressure effects as related to solubility are normally neglected in consideration of hydrochemistry. As related to these experiments, cell pressure ranged from 4.8 to 64 atmospheres. Considering the relatively low pressures induced on the experimental system, it is reasonable to disregard the pressure effects as related to solubility for this study.

Other geochemical considerations, however, should be addressed. The following reactions can be considered in this discussion:

$$CuCO_3 + H^+ \leftrightarrow HCO_3^- + Cu \quad (A)$$

$$HCO_3^- + H^+ \leftrightarrow H_2CO_{3(aq)} \quad (B)$$

$$H_2CO_{3\,(aq)} \leftrightarrow CO_{2(g)} + H_2O \quad (C)$$

The alkalinity trend for the carbonate experiments varied for each trial. In experiment WRRI-2 there was a noted decrease in bicarbonate alkalinity of the effluent samples with time, while the pH of the system varied between 5.33 and 6.00. It is postulated that the clay membrane had an effect on alkalinity, which is described by the alkalinity decrease in the effluent. However, there should be a note to explain the decrease in bicarbonate alkalinity between the initial pump solution, and the alkalinity of the pump solution collected at the end of the experimental run. This decrease in bicarbonate alkalinity is coupled with a decrease in pH. This data can be explained by the reactions above. The copper carbonate dissociated in solution to copper ions and bicarbonate (reaction A). The bicarbonate reacted with the H^+ ions in solution to form carbonic acid (reaction B), which is the predominant species in solutions with pH less than 6.3; recall the pH for the initial

pump solution is 5.95. This reaction may have driven further, resulting in the formation of gaseous CO_2 and water (reaction C).

Experiment WRRI-7 was similar to experiment WRRI-2 in that the alkalinity of the final collected pump solution was significantly less than that of the initial pump solution alkalinity. As described in the text, it is suspected that the stock solution may have been poorly buffered, and interaction with atmospheric CO_2 may have occurred. This is data can be described in the manner as described for experiment WRRI-2 above.

4.0 Summary and Conclusions

Eight hyperfiltration experiments were performed in this study. Of the eight experiments, six succeeded in precipitating heavy metals on the high pressure side of the membrane face. These experimental results demonstrate that hyperfiltration-induced precipitation of heavy metals by geologic membranes is possible.

To address the ultimate question concerning the significance of membrane-induced precipitation on heavy metal contaminated plumes in the subsurface, the research presented herein suggest, the following:

- The experiments denote that when heavy metal concentrations are high, the value of the reflection coefficient may be relatively high, resulting in easily attainable precipitation conditions within the CPL. However, it should be noted that, under these conditions, more of the heavy metals will enter the shales. For this reason, the ion exchange capacity of the shale is more likely to be exceeded when heavy metal concentrations in the aquifer are high. The assumption can be made that for a given site, any heavy metals which do not take part in precipitation and are not retained in

the CPL will ultimately enter the shale and be available to participate in ion exchange. The rate at which the heavy metals will enter the bounding shales is a function of the membrane properties of the shale, the vertical head conditions, and solution concentrations which determine J_v.

- Analysis of the data collected from this study indicates that heavy metals can be concentrated as much as 100 times or more in the CPL when σ approaches 1.0. If, however, steady-state C_o is not greater than solubility, the result will be an increase in the concentration within the CPL, with no precipitation occurring. In any case, any heavy metals entering the shale will be subject to ion exchange and will likely be tied up in the shale until the ion exchange capacity of the shale is exceeded.
- Two of the experiments in this study failed to precipitate heavy metals as hypothesized. It is theorized that CPL development was limited because adequate time was not allotted for these experiments, and the concentrations within the CPL did not exceed saturation. This is an important finding in itself, that different systems require different times to reach achieve the state that is necessary to result in hyperfiltration induced precipitation of heavy metals. This has serious implications when extrapolating the finding of this study to the natural environment. It can be said that systems with very low flow rates might require longer time periods to see the pressure build and subsequent CPL development that is necessary to precipitate heavy metals.
- The mathematical equation presented in this study (Equation 16) is capable of calculating values of σ from a knowledge of the permeability coefficient L_p, the

temperature T, the total solution flux J_v, the membrane thickness Δx, tortuosity ζ, and the diffusion coefficient D. All of these values can be obtained from laboratory or field measurements. However, further work is needed to develop a routine method to determine values of the reflection coefficient for natural shales in order to independently verify the model developed in this study.

- The six successful experiments presented in this study demonstrate that it is possible for geologic membranes to attain values of σ which approach 1.0. Furthermore, mathematical analysis coupled with the experimental finding of this study suggest that hyperfiltration-induced heavy metal precipitation may be possible in the subsurface where contaminated aquifers are bounded by membrane-functioning shales. Membrane parameter maps were prepared for copper carbonate and lead chloride solutions and specified membrane thickness that predict the possibility of copper carbonate or lead chloride mineral precipitation due to solute sieving for site specific conditions when the total solution flux, the value for the reflection coefficient for the shale of interest, and the input (or background) solute concentrations are known.

5. References Cited

Alexander, J. 1990, A review of osmotic processes in sedimentary basins, British Geologic Survey Technical Report, WE/90/12.

Appelo, C.A. and Postma, D., 1994, *Geochemistry and Groundwater Pollution,* AA.Balkema/Rotterdam/Brookfield, 536 P.

Barone, F. S., R. K. Rowe, and R. M. Quigley 1992, Estimation of chloride diffusion coefficient and tortuosity factor for mudstone, Journal of Geotechnical Engineering. v. 118, p. 1031-1047.

Barone, F. S., R. K. Rowe, and R. M. Quigley 1990, Laboratory determination of chloride diffusion coefficient in intact shale, Canadian Geotechnical Journal, v. 27, p. 177-184.

Bernstein, F., 1960, Distribution of water and electrolyte between homoionic clays and saturating NaCI solutions, in Clays and Clay Minerals: Proceedings 8th National Clay Conference, p.122-1149, Pergamon Press.

Benzel, W.M. and Graf, D.L., 1984, Studies of smectite membrane behavior: Importance of layer thickness and fabric experiments at 20_C, Geochimica et Cosmochimica Acta, v. 48, p.1769-1778.

Berner, R.A., 1971, *Principles of Chemical Sedimentology,* McGraw-Hill, N.Y., 240 p.

Berry, F.A.F., 1959, Hydrodynamics and geochemistry of the Jurassic and Cretaceous systems in the San Juan Basin, northeastern New Mexico and southwestern Colorado, Ph.D. dissertation, Stanford University, 192 p.

Berry, F.A.F., 1960, Geologic field evidence suggesting membrane properties of shales, American Society of Petroleum Geologists Bulletin, v. 44, p. 953-954.

Berry, F.A.F., 1966, Proposed origin of subsurface thermal brines, Imperial Valley, California (abstract), American Society of petroleum Geologists Bulletin, v. 50, p. 644-645.

Berry, F.A.F., 1967, Role of membrane hyperfiltration on origin of thermal brines, Imperial Valley, California, American Society of Petroleum Geologists Bulletin, v. 51, 454-455.

Bredehoeft, J.D., Blyth, C.R., White, W.A., and Maxey, G.B., 1963, Possible mechanism for concentration of brine in subsurface formations, American Association Petroleum Geologists Bulletin, v. 42, no. 2, p. 257-269.

Bredehoeft, J.D., and Hanshaw, B., 1968, On the maintenance of anomalous fluid pressures, 1. thick sedimentary sequences, Geological Society of America Bulletin, No. 79, p. 1097-1106.

Briggs, L.J., 1902, Filtration of suspended clay from solutions, U.S. Bureau of Soils Bulletin, No. 19, p. 31-39.

Coplen, T.B., and Hanshaw, B.B., 1973, Ultrafiltration by a compacted membrane-I. Oxygen and hydrogen isotope fractionation, Geochimica et Cosmochimica Acta, v. 37, p. 2205-23 10.

De Groot, S.R. and Mazur, P., 1962, Non-equilibrium thermodynamics, North Holland Publishing Company, Holland. Also by Dover Publications, Inc., New York, 1984, 510p.

Elrick, D.E., Smiles, D.E., Baumgartner, N., and Groenvelt, P.H., 1976, Coupling phenomena in saturated homo-ionic montmorillionite: 1. Experimental, Soil Science Society of America Journal, v. 40, p. 490-491.

Fetter, C. W., 198 8, *Applied Hydrogeology,* Merrill, Columbus Ohio, 5 92 p.

Freeze, R.A., and Cherry, J.A., 1988, *Groundwater,* Prentice-Hall, Englewood Cliffs, N.J., 604 p.

Fritz, S.J., 1986, Ideality of clay membranes in osmotic processes: a review, Clays and Clay Minerals, v. 34, p. 214-223.

Fritz, S.J., 1992, Measuring the ratio of aqueous diffusion coefficients between _Li_Cl_ by osmometry, Geochimica et. Cosmochimica Acta, v. 556, p.3781-3789.

Fritz S.J., and Eady, C.D., 1985, Hyperfiltration-induced precipitation of calcite, Geochimica et. Cosmochimica Acta, v. 49, p. 761-768.

Fritz, S.J., Hinz, D.L., and Grossman, E.L., 1987, Hyperfiltration-induced fractionation of carbon isotopes, Geochimica et. Cosmochimica Acta, v. 5 1, p. 1121-1134.

Fritz, S.J., and Marine, I.W., 1983, Experimental Support for a predictive osmotic model of clay membranes, Geochimica et Cosmochimica Acta, v.46, p. 1431-1448.

Fritz, S.J., and Whitworth, T.M., 1993, Measuring phenomenological coefficients of membranes for use in predicting osmotically-induced hydraulic pressures, Hydrological Sci. and Tech., v. 8, p. 1-10.

Fritz, S.J., and Whitworth, T.M., 1994, Hyperfiltration-induced fractionation of lithium isotopes: ramifications relating to representativeness of aquifer sampling, Water Resources Research, v. 30, p. 225-235.

Graf, D.L., 1982, Chemical osmosis, reverse chemical osmosis, and the origin of subsurface brines, Geochimica et Cosmochimica Acta, v.46, p. 1431-1448.

Greenberg, J.A., Mitchell, J.K., and Witherspoon, P.A., 1973, Coupled salt and water flows in a groundwater basin, Journal of Geophysical research, v. 78, p. 6341 6353.

Gregor, H.P., and Gregor, C.D., 1978, Synthetic membrane technology, Sci. Amer., v. 239, p. 112-128.

Grim, R.E., 1968, *Clay Mineralogy,* McGraw-Hill, Inc., New York, 596 p.

Hanshaw, B.B., and Hill, G.A., 1969, Geochemistry and hydrodynamics of the Paradox Basin Region, Utah, Colorado, and New Mexico, Chemical Geology, v. 4, p. 263294.

Harris, F.L., Humphreys, G.B., and Spiegler, K.S., 1976, Reverse osmosis (hyperfiltration) in water desalination, in P. Meares, ed., Membrane Separation Processes, Elsevier, Amsterdam, Chapter 4.

Hem, J., 1959, Study and interpretation of chemical characteristics of natural waters, U.S. Geological Survey Water-Supply Paper 1473.

Hem, J., 1992, Study and interpretation of chemical characteristics of natural waters, U.S. Geological Survey Water-Supply Paper 2254.

Horseman, S., Hobbs, P., McEwen, T.S., Avery, L., and Foster, A., 1982, Basic geotechnical properties of core from the Harwell boreholes, Report Institute Geological Sciences, ENPU 82-7.

Jones, P.H., 1968, Geochemical hydrodynamics, a possible key to the hydrology of certain aquifer systems in the northern part of the gulf of Mexico basin, International Geological Congress, v. 17, p. 113-125.

Katchalsky, A., and Curran, P.F., 1965, *Biophysics,* Harvard University Press, Cambridge, 248 p.

Kedem, 0., and Katchalsky, A., 1962, A physical interpretation of the phenomenological coefficients of membrane permeability, Journal of General Physiology, v. 45., p. 143-179.

Kemper, W.D., 1960, Water and ion movement in thin films as influenced by the electrostatic charge and diffuse layer of cations associated with clay mineral surfaces, Soil Science Society Proceedings, p. 10- 16.

Kemper, W.D., 1961, Movement of water as effected by free energy and pressure gradients. I., Application of classic equations for viscous and diffusive movements to the liquid phase in finely porous media. 11. Experimental analysis of porous systems in which free energy and pressure gradients act in opposite directions, Proceedings, Soil Science Society of America, v. 25, p. 255-265.

Kharaka, Y.K., and Berry, F.A.F., 1973, Simultaneous flow of water and solutes through geologic membranes, 1. Experimental investigation, Geochimica et Cosmochimica Acta, v. 37, p. 2577-2603.

Kharaka, Y.K., Berry, F.A.F., and Friedman, L, 1973, Isotopic compositions of oil-field brines from Kettleman North Dome, California, and their geologic implications, Geochimica et Cosmochimica Acta, v. 37, p. 1899-1908.

Lakshminarayanaiah, N.L., 1984, *Equations of membrane biophysics,* Academic Press Inc., New York, 426 p.

Lide, D., and Kehiaian, H. (Ed.), 1990, CRC handbook of thermophysical and thermochemical data, Boca Raton: CRC Press, c. 1994.

Lueth, VW., and Whitworth, T.M., 1994a, Geologic membrane effects and the origin of red bed copper deposits in New Mexico (abstract), Geological Society of America, Annual Meeting, Seattle, Abstracts and Programs, p. A3 10.

Lueth, VW., and Whitworth, T.M., 1994b, Evidence of geologic membrane effects at two New Mexico red bed copper deposits (abstract), NMGS spring meeting, Socorro, New Mexico.

Mariflas, B.J., and Selleck, R.E., 1992, Reverse osmosis treatment of multicomponent electrolyte solutions, Journal of Membrane Science, v. 72, p.211-229.

Marine, W.I., 1974, Geohydrology of the buried Triasic basin at Savahnah river plant, South Carolina, Bulletin American Association Petroleum Geology, v. 58, no. 9, p. 1825-1837.

Marine, W.I., and Fritz, S.J., 198 1, Osmotic model to explain anomalous hydraulic heads, Water Resources Research, v. 17, no. 1, p. 73-82.

Marshall, C.E., 1948, The electrochemical properties of mineral membranes 111, Journal of Physical Chemistry, v. 52, p. 1284-1295.

McKelvey, J.G., and Milne, I.H., 1963, Permeability and salt-filtering properties of compacted clays, Clays and Clay Minerals (extended abstract, Monograph No. 13, p. 250-251.

Merian, E., 1990, Metals and Their Compounds in the Environment: Occurance, Analysis, and Biological Relevance. Weinheim, New York, 1438 pages.

MIT, 1998, Massachusetts Institute of Technology, Chemistry Department Homepage at www.mit.edu, data collected January, 1998.

Noggle, J. H. 1984. *Physical Chemistry.* Little, Brown & Company Limited, 953 p.

Oberg, E., F. D. Jones, H. L. Horton, and H. H. Ryffel 1992, *Machinery's Handbook,* 24th edition. Industrial Press, Inc., New York. 2543 p.

OSU, 1998, Ohio State University, Chemistry Department Home Page, at www.osu.edu, data collected January 1998.

Paulsen, C.G., 1949, Water levels and artesian pressures in observation wells in the United States in 1946, Part 6, Southwestern States and Territory of Hawaii, United States Geological Survey Water Supply Paper 1076, 316 p.

Phillips, F.M., Bentley, H.M., Davis, S.N., Elmore, D. and Swanick, G.H., 1986, Chlorine 36 dating of very old groundwater 2. Milk River Aquifer, Alberta, Canada. Water Resources Research, v. 22, p. 2003-2016.

Phillips F.M., 1983. Comment on "Chemical osmosis, reverse chemical osmosis, and the origin of subsurface brines" by Graf, D.L.. Geochimica et Cosmochimica Acta, v. 47, p. 13 3 1.

Plumley, W.J., 1980, Abnormally high fluid pressure; survey of some basic principles, American Association of Petroleum Geologists, v. 64, p. 414-430.

Seiver, C.S., Uchrin, C.G., and Ahlert, R.C., 1965, Composition of interstitial waters of modern sediments, Journal of Geology, v. 72, no 1, p. 39-73.

Spiegler, K. S. and 0. Kedem 1966, Thermodynamics of hyperfiltration (reverse osmosis): criteria for efficient membranes, Desalination, v. 1, p.311-326.

Staverman, A.J., 1952, Non-equilibrium thermodynamics of membrane processes, Trans. Faraday Society, v. 48, p. 176-185.

Tolman, C.F., 1937, *Ground Water,* McGraw-Hill Book Company, Inc., New York, 593 P.

Toth, J., and Millar, R.F., 1983, Possible effects of erosional changes of the topographic relief on pore pressures at depth, Water Resources Research, v. 19, no. 6, p. 1585 -1597.

Whitworth, T.M., 1998, Steady-state mathematical modeling of geologic membrane processes in aquifer systems, WERC/WRHSRC/NMHWMS Joint Conference on the Environment, Proceedings, Albuquerque, NM, March 31 - April 2, 1998, p. 37-41.

Whitworth, T.M., Gamblin, G.B., and Fritz, S.J., 1993, A simple air-stream clay separator, Journal of Sedimentary Petrology, v. 66, p. 716-718.

Whitworth, T.M., and Fritz, S.J., 1994, Electrolyte-induced solute permeability effects in compacted smectite membranes, Applied Geochemistry, v. 9, p. 533-546.

Whitworth, T.M., and Lueth, VW., 1994 A geologic membrane mechanism for the origin of sedimentary copper deposits (abstract), New Mexico Geology, v. 16, p.36.

Whitworth, T.M., MariAas, B.J., and Fritz, S.J., 1994, Isotopic fractionation and overall permeation of lithium by a thin-film composite polyamide reverse osmosis membrane, Journal of Membrane Science, v. 88, p. 231-241.

Wood, W.W., 1976, A hypothesis of ion filtration in a potable-water aquifer system, Ground Water, v. 14, p.23 3 -244.

Wyllie, M.R.J., 1948, Some electrochemical properties of shales, Science, v. 108, p. 684 685.

Wyllie, M.R.J., 1949, A quantitative analysis of the electrochemical component of the S.P. curve, Journal of Petroleum Technology, v.1, p. 17-26.

Wyo-Ben, 1998. Technical Information Sheet on powdered pure sodium bentonite, located in Billings, Montana.

Young, A. and Low, P.F., 1965, Osmosis in argillaceous rocks, American Association of Petroleum Geologists Bulletin, v. 49, p. 1004-1008.

This thesis is accepted on behalf of the faculty

of the institute by the following committee:

J M Phillips

Advisor

Robert L. Bowman

18 August 95

Date